Università degli Studi di Ferrara

Dottorato di Ricerca in

"Scienze Biomediche e Biotecnologiche"

Ciclo XXXI

Coordinatore Prof. Paolo Pinton

Coupling AAV-mediated promoterless gene-targeting to *Sa*Cas9 nuclease to efficiently correct liver metabolic diseases

Settore Scientifico Disciplinare BIO/10

Dottoranda

Dott.ssa Alessia De Caneva

Tutore

Dott. Andrés Fernando Muro

Anni 2015/2018

ACKNOWLEDGEMENTS

First, I would like to thank Dr. Andrés Muro for giving me the opportunity to work on this project, to trust me and my skills. Being my studies director, he provided constant guidance during these years and he was available every time I needed help. Without his contribution this amazing work would not have been possible. I am very grateful for entering in his science world doing my PhD in his group. I would also like to thank Dr. Fabiola Porro and Dr. Giulia Bortolussi, for their experimental and critical contribution to my project.

Next, my gratitude goes to all the present and past members of the Mouse Molecular Genetics Group, Luka Bockor, Luisa Costessi, Simone Vodret, Riccardo Sola, Fabiola Porro, Vipin Singh Rawat, Alessandra Iaconcig, Joseph Olajide Olayemi, Giulia De Sabbata, Michela Lisjak and Filippo Ferrucci.

I would like to thank Fabi and her wonderful Family, Fredi, Gio, Tommy and Ghita, for helping me in science and life since my first day in Trieste.

My gratitude goes also to Simo for introducing me to the mice world. I will never forget time spent laughing with him and Fabi. I am lucky to share with them my PhD story.

I would like to thank Lucia for teaching me how PhD life can be lived much easier and for our free-time spent running, cooking, going out, tasting wine, watching movies, talking about men.

I would like to thank all my friends, Paola, Simona, Marina, Ramiro, Lella, Giulia, Lalla, Beatrice, for all the joy and pain shared through these years.

I would like to thank Michela who arrived as a present for my third PhD year.

Last, but not least, I would like to thank all my Family. My gratitude goes to my mom and my dad for supporting me since the day I was born and for giving me life opportunities that they could not have. I would like to thank my sisters Ambra and Gessica for making me aunt of Carlos Maria and Giorgia, they are the sun of my days.

1. INTRODUCTION

1.1 Rare monogenic diseases

A rare monogenic disease is defined as a disorder caused by the modification of a single gene affecting less than 1 in 2000 individuals. It has been estimated that over 10.000 human disorders are rare and of monogenic nature. Despite the single prevalence of each of these diseases is very low, their overall global prevalence at birth is 10/1000, affecting millions of people worldwide, according to the World Health Organization (Genes and human disease. Monogenic diseases; WHO, 2012, http://www.who.int/genomics/public/geneticdiseases/en/index2.html). Moreover, monogenic disorders represent a frequent cause of mortality in pediatric populations (Cunniff, Carmack et al., 1995, Stevenson & Carey, 2004). All these considerations highlight the clinical need to develop new curative and safe therapeutic treatments for monogenic inherited diseases.

1.2 Inherited liver diseases

The liver plays an important role in several vital functions, being involved in the metabolism of proteins, carbohydrates and lipids, in the synthesis of plasma proteins, such as albumin and clotting factors, and in the detoxification of several metabolites, such as ammonia and bilirubin (Hansen & Horslen, 2008). Any genetic defect that occurs in genes that take part into these fundamental functions can result into liver diseases grouped as "inborn errors of metabolism" (IEMs) (Brunetti-Pierri & Lee, 2005). IEMs are a heterogeneous class of genetic disorders caused by a defective protein, usually an enzyme or a transporter (Lanpher, Brunetti-Pierri et al., 2006), involved in the synthesis or catabolism of proteins, carbohydrates or fats (Hansen & Horslen, 2008). The alteration of one or more of these chemical reactions involved in metabolism lead to the subsequent deregulation of one or more metabolite fluxes, affecting the quantity of produced or eliminated metabolites. According to that, IEMs can be classified as classic, in which one metabolic flux is altered, or as complex, in which a network of metabolite fluxes is involved (Lanpher et al., 2006). According to the condition and involvement of the liver and other tissues, liver monogenic diseases can be characterized by 1) a predominant liver parenchymal damage, 2) an architecturally near-normal liver, 3) a systemic damage with a marginal liver involvement (Tab. 1) (Fagiuoli, Daina et al., 2013). Despite the single prevalence of each of these disorders is very low, their overall global prevalence accounts for a significant proportion of

illness, particularly in the childhood period (Lanpher et al., 2006), representing approximately 10% of pediatric liver transplants (Hansen & Horslen, 2008).

Monogenic diseases with primary hepatic expression and parenchymal damage
Genetic cholestasis (Alagille syndrome) Wilson's disease Hereditary hemochromatosis Tyrosinemia type 1 α-1-antitrypsin deficiency Argininosuccinic aciduria (ASL) Glycogen storage disease (GSD) type I (adenoma/hepatocellular carcinoma)
Monogenic diseases with primary hepatic expression without significant parenchymal damage
Urea cycle disorders (excepted ASL) Crigler-Najjar syndrome Familial amyloid polyneuropathy Atypical haemolytic uremic syndrome-1 Primary hyperoxaluria type 1 Maple syrup urine disease (MSUD) Acute intermittent porphyria Coagulation defects GSD type Ia (in metabolic control) Homozygous familial hypercholesterolemia
Monogenic diseases with both hepatic and extrahepatic expression
Organic acidurias (excepted MSUD) Cystic fibrosis Erythropoietic protoporphyria Gaucher disease

Tab. 1. Classification of inherited liver disorders. Inherited liver disorders represent a heterogeneous class of diseases which can be classified, according to the liver involvement in the pathogenesis, into monogenic disorders with: 1) primary hepatic expression with parenchymal damage, 2) primary hepatic expression without parenchymal damage, 3) both hepatic and extrahepatic expression. Examples of the different categories are listed. Adapted from (Fagiuoli et al., 2013).

1.3 Current therapies for inherited liver disorders

1.3.1 Therapies to control the disease phenotype

For most inherited liver diseases, available treatments rely on the manipulation of the metabolic pathway by diet, drugs, vitamin cofactors, enzyme induction, end-product replacement and alternative pathway activation (Brunetti-Pierri & Lee, 2005). All these treatments aim to ameliorate the disease manifestations in order to avoid an acute crisis, limiting the quality of life of treated patients.

Enzyme replacement therapy (ERT) could be a potential therapeutic option when the pathogenesis results from a deficient or dysfunctional enzyme. One ERT product has been

successfully used to treat Gaucher's disease. Then, several ERT drugs have been developed to control the disease phenotype of different lysosomal storage disorders (LSDs), but their effectiveness, varying among them, is still lower than in type I Gaucher, highlighting many limitations of the therapeutic approach. The most important one is represented by the blood brain barrier (BBB) which limits the access of the enzyme to brain tissues (Kobayashi, Carbonaro et al., 2005), greatly reducing the therapeutic impact of the strategy. Furthermore, ERT is extremely expensive, it requires the administration of the therapeutic enzyme all life-long and its cost-effectiveness should be discussed (Lachmann, 2011).

1.3.2 The orthotopic liver transplantation

Since the involvement of the liver differs among liver-based disorders, with significant differences in morbidity and mortality, the therapeutic value of orthotopic liver transplantation (OLT) varies among them. OLT represents the only permanent available cure for diseases in which the damage triggers hepatic complications which, thereby, cause morbidity (i.e., genetic cholestatic disorders, Wilson's disease, hereditary hemochromatosis, tyrosinemia, α1 antitrypsin deficiency), and also for those disorders in which the liver is near-normal but triggers extra-hepatic complications which are responsible of the consequent morbidity and lethality (i.e., urea cycle disorders, Crigler-Najjar syndrome, familial amyloid polyneuropathy, primary hyperoxaluria type 1, atypical haemolytic uremic syndrome-1) (Fagiuoli et al., 2013).

OLT represents a therapeutic option by substituting an injured liver or by supplying a tissue that can replace a mutant protein (Fagiuoli et al., 2013).

Even if OLT in recent years has ameliorated the outcome of many of inherited liver disorders, it still suffers from several limitations. It is a very invasive procedure with substantial risks (5-10% patient mortality within 5 years after liver transplant) (Adam, Karam et al., 2012), shortcomings, such as re-transplantation in 20 % of the cases (Adam et al., 2012), and adverse effects due to prolonged exposure to immunosuppressive drugs used to avoid graft rejection (de-novo malignancies, cardiovascular complications and infections) (Benten, Staufer et al., 2009, Haagsma, Hagens et al., 2001, Herrero, 2009, Vajdic & van Leeuwen, 2009). Furthermore, availability of an immune-compatible organ is very low and patients have to wait for transplantation for a time that is determined by the indication list for LT (Adam et al., 2012). All these considerations about available therapeutic treatments for liver inherited disorders highlight the nowadays emerging clinical need to find alternative and resolutive cures for many monogenic diseases.

1.4 Liver-directed gene therapy

Gene therapy approaches are mainly based on gene addition strategies to cure inherited disorders characterized by the deficiency or absence of one gene product. Most of them adopt an AAV vector to transfer the functional gene and its regulatory elements. Recombinant adeno-associated virus (rAAV) vectors have some features that make them a gene delivery system of choice. Indeed, they are non-pathogenic and thereby safe (Berns & Linden, 1995, Erles, Sebokova et al., 1999), they can infect both dividing and non-dividing cells, they exist in different serotypes with cellular specific tropism (Wu, Asokan et al., 2006), they are mainly episomal as they integrate randomly at very low rate (Nakai, Wu et al., 2005). The non-integrative form of AAV vectors can be an advantage and a disadvantage at the same time because of the episomal DNA loss in a context of a growing organ (Bortolussi, Zentillin et al., 2014b, Cunningham, Spinoulas et al., 2009, Wang, Wang et al., 2012).

AAV-mediated gene therapy to the liver has shown both efficacy and safety in adult patients (George, Sullivan et al., 2017, Nathwani, Reiss et al., 2014, Nathwani, Rosales et al., 2011a, Rangarajan, Walsh et al., 2017), leading to nowadays several clinical trials ongoing. However, it faces potential limitations in pediatric/neonatal settings. Indeed, in the context of a growing organ, such as the liver during childhood, efficacy decreases as a consequence of vector loss associated to hepatocyte duplication (Bortolussi et al., 2014b, Cunningham et al., 2009, Wang et al., 2012). Moreover, in these cases, re-administration of the therapeutic vector may be required, but this procedure is not possible due to the presence of neutralizing antibodies against the AAV-capsid antigens, generated after the first gene transfer (Calcedo & Wilson, 2016, Chirmule, Xiao et al., 2000, Nathwani, Gray et al., 2007, Nathwani, Tuddenham et al., 2011b).

Even if the delivery of the therapeutic transgenes by rAAV vectors was successful in many cases, resulting in ameliorated phenotypes, many concerns are still present, such as transient and unregulated expression (Nathwani et al., 2011a, Russell & Kay, 1999), potential random integration (Hendrie, Hirata et al., 2003) with increased mutagenic and oncogenic risks (Garrick, Fiering et al., 1998), and transgene silencing (Donsante, Miller et al., 2007).

1.5 Liver-directed genome editing

Gene editing is defined as the specific and permanent modification of the genome and it is a promising approach to cure monogenic inherited disorders. Indeed, it overcomes many of

the limitations of gene addition strategies by *in vivo* manipulating the disease-causing genes to restore gene function, maintaining the endogenous gene regulation. Several approaches have been applied to this aim: single-strand oligonucleotides (Andrieu-Soler, Halhal et al., 2007, Huen, Lu et al., 2007), triplex-forming oligonucleotides (Vasquez, Narayanan et al., 2000), RNA-DNA hybrids (Kren, Parashar et al., 1999), small DNA fragments and AAV vectors (Miller, Wang et al., 2006, Russell & Hirata, 1998, Vasileva & Jessberger, 2005).
AAV engineered vectors can be used for gene repair approaches, targeting the diseased locus or multiple several genomic loci site-specifically, resulting in stable therapeutic gene expression and in the correction of the mutated phenotype. As a consequence, they represent a powerful therapeutic tool applicable to many human disorders (Hendrie & Russell, 2005, Parekh-Olmedo, Ferrara et al., 2005). AAV-mediated homologous recombination has been used to repair several disease mutations (insertions, deletions, substitutions) both *in vitro* (Inoue, Dong et al., 2001, Inoue, Hirata et al., 1999) and *in vivo* (Barzel, Paulk et al., 2015, Paulk, Wursthorn et al., 2010, Porro, Bortolussi et al., 2017). Paulk *et al*. adopted this strategy to correct a mouse model of Hereditary tyrosinemia type I (HT1), a genetic metabolic disease characterized by fumarylacetoacetate (FAH) deficiency (Paulk et al., 2010). The FAH enzyme catalyzes the last reaction of the tyrosine catabolic pathway and its deficiency results in the accumulation of toxic metabolites, such as fumarylacetoacetate, into hepatocytes leading to severe liver damage (Paulk et al., 2010). Blocking upstream steps in the metabolic pathway with the inhibitor 2-(2-nitro-4-trifluoromethylbenzoyl)-1,3-cyclohexanedione (NTBC) limits toxic accumulation of metabolites (Al-Dhalimy, Overturf et al., 2002). The $Fah^{mut/mut}$ mouse has the same human point mutation (G→A) in exon 8 of the fumarylacetoacetate (FAH) gene, leading to exon 8 skipping and to sequent production of a truncated and unstable FAH protein (Aponte, Sega et al., 2001, Paulk et al., 2010). Paulk *et al*. administered an AAV vector containing the wild-type sequence of FAH in neonatal and adult $Fah^{mut/mut}$ mice (Paulk et al., 2010). Since corrected cells have a selective advantage over mutated hepatocytes, with the strong selection of edited hepatocytes using NTBC, cells that had undergone integration by homologous recombination could survive and repopulate the liver. Even if the efficiency of targeting was low, in the range of 1 corrected hepatocyte over 10000 cells, multiple rounds of NTBC administration rescued the diseased phenotype of both neonatal and adult $Fah^{mut/mut}$ mice (Paulk et al., 2010). However, the selective advantage of corrected hepatocytes, from which HTI can benefit, is not present in many liver inherited disorders and challenge researchers to find alternative strategies to increase the therapeutic efficacy of gene editing by enhancing gene-targeting rate.

1.6 The DNA DSBs repair mechanisms

DNA double strand breaks (DSBs) normally occur during the cell cycle and can be induced from both exogenous and endogenous sources (Lieber, 2010). Indeed, they could result from ionizing radiations, from the collapse of the replication fork or, moreover, they can be associated with development-associated programs, as meiosis and V(D)J recombination. Since DNA DSBs are lethal if unrepaired, or may lead to chromosomal aberrations potentially inducing tumors if miss-repaired, cells have developed several pathways to repair them. The two main mechanisms that cells adopt to repair DSBs are non-homologous end joining (NHEJ) and homologous recombination (HR) (Fig. 1; Tab. 2) (Shibata & Jeggo, 2014).

NHEJ is the main repair pathway and is active during all phases of the cell-cycle. The cells repair the genomic lesions without using a template sequence, resulting, thereby, in insertions and/or deletions (INDELs). When INDELs are located within ORF of genes, they could lead to the introduction of premature stop codons, with the subsequent mRNA degradation by non-sense mediated decay, or to the synthesis of non-functional truncated proteins.

There are two different NHEJ mechanisms:

1. Canonical NHEJ (c-NHEJ): it is active during all phases of the cell cycle and consists in the direct ligation of unprocessed cleaved ends;
2. Alternative NHEJ (a-NHEJ): it is active when c-NHEJ players are not present. It consists in the direct re-ligation of cleaved ends, by the annealing of short micro-homology sequences and subsequent end ligations. It results in large deletions responsible of genetic instability and chromosomal translocations.

Cells can repair DSBs by the HR pathway when a homologous sequence, acting as a template, is present, normally occurring after replication in late S/G2 phase. In this case, the genomic lesions are repaired with high fidelity.

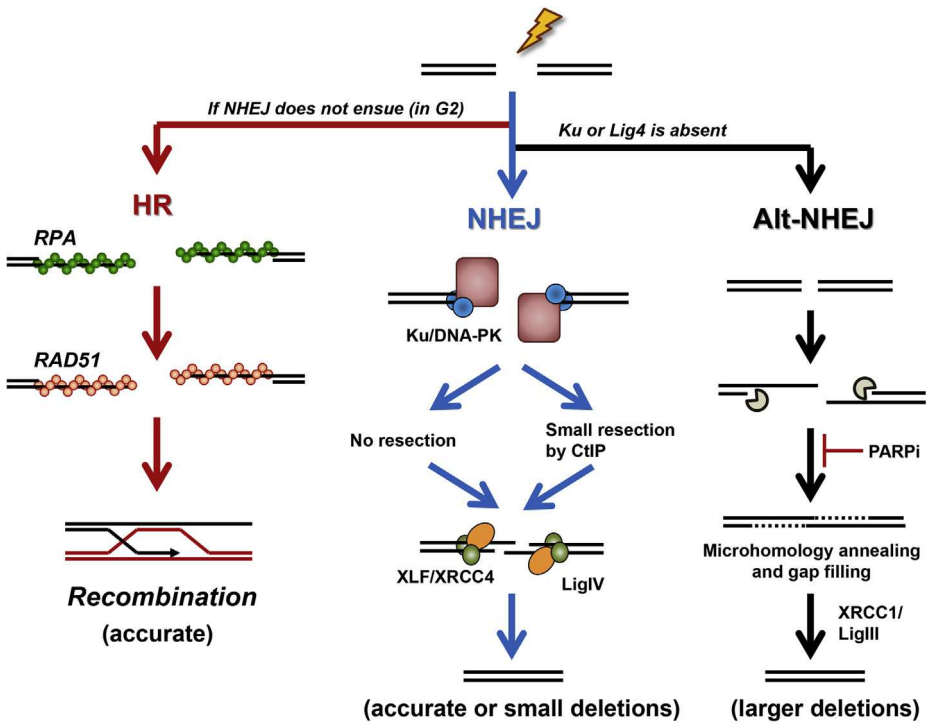

Fig. 1. Pathways of DNA DSBs repair mechanisms. The two main mechanisms that cells adopt to repair DNA DSBs are non-homologous end joining (NHEJ) and homologous recombination (HR). NHEJ can occur as canonical or alternative mechanism (Alt-NHEJ) (Shibata & Jeggo, 2014).

The repair machinery used by cells to repair DNA double-strand breaks (DSBs) has been useful to develop genome editing strategies aimed at generating site-specific changes in the genomic sequence (Gasiunas & Siksnys, 2013). Both repair pathways, NHEJ and HR, indeed, can be adopted to introduce site-specific genome modifications (Tab. 2). NHEJ, which is an error-prone mechanism, can be useful to introduce insertions/deletions (INDELs) leading to gene disruption in most of cases, whereas HR can be adopted for introduce specific desired genome modifications by using a donor template sharing homology with the target sequence, leading to gene insertions or corrections.

NHEJ	HDR
Without a donor template and during all phases of the cell cycle	With a donor template and occurring in late S/G2 phase
INDELs: - Mutations in ORFs resulting in mRNA degradation by non-sense mediated decay - Production of non-functional truncated proteins	The HDR machinery uses a donor template, resulting in the accurate repair of the DSB.
Results in: - Directly re-joining the two DSB ends - INDELs	Results in: - Gene corrections - Gene insertions
Applications: - Disruption of a WT gene - Correction of a mutated gene by changing the reading frame	Applications: - Correction of a mutated gene using a donor DNA with the correct sequence - Generation of specific gene mutations using a donor DNA with a mutated sequence - Targeting an ORF into a "safe harbor locus"

Tab. 2. Comparison between NHEJ and HDR pathways.

1.6.1 Strategies to interfere with DNA DSBs repair mechanisms

Several compounds have been reported to interfere with DNA DSBs repair mechanisms *in vitro* (Chu, Weber et al., 2015, Jayathilaka, Sheridan et al., 2008, Vartak & Raghavan, 2015) and *in vivo* (Maruyama, Dougan et al., 2015, Paulk, Loza et al., 2012, Srivastava, Nambiar et al., 2012). These strategies can be adopted to enhance the HR rate by promoting HR directly or by inhibiting NHEJ (Fig. 2). Srivastava and colleagues, by using a cell-free assay, identified a small-molecule named Scr7 that inhibits the joining of DSBs in a concentration-dependent manner by blocking Ligase IV binding to DNA (Srivastava et al., 2012). As a consequence, DSBs accumulate within the cells and activate the intrinsic apoptotic pathway (Srivastava et al., 2012). Srivastava *et al.* by using Scr7 were able to impede tumor progression in mouse models and, furthermore, enhance the sensitivity of cancer cells to radio- and chemotherapeutic agents (Srivastava et al., 2012). Chu *et al.* taking advantage of Scr7 were able to increase the efficiency of HDR up to 5-fold by suppressing the NHEJ in both human and mouse cell lines (Chu et al., 2015). Scr7 has been used also by Maruyama *et al.* to increase up to 19-fold of HDR-mediated genome editing in mammalian cell lines and in mice (Maruyama et al., 2015). Paulk *et al*. showed that the natural product vanillin can reduce NHEJ rate by inhibiting the DNA-dependent protein kinase (DNA-PK), shifting, thereby, the balance of the DNA repair mechanism towards the HR repair pathway (Paulk et al., 2012). By using a rAAV-based homology vector in combination with vanillin, they

were able to increase gene correction frequencies up to 10-fold over rAAV alone, in a mouse model of hereditary tyrosinemia type I (Paulk et al., 2012).

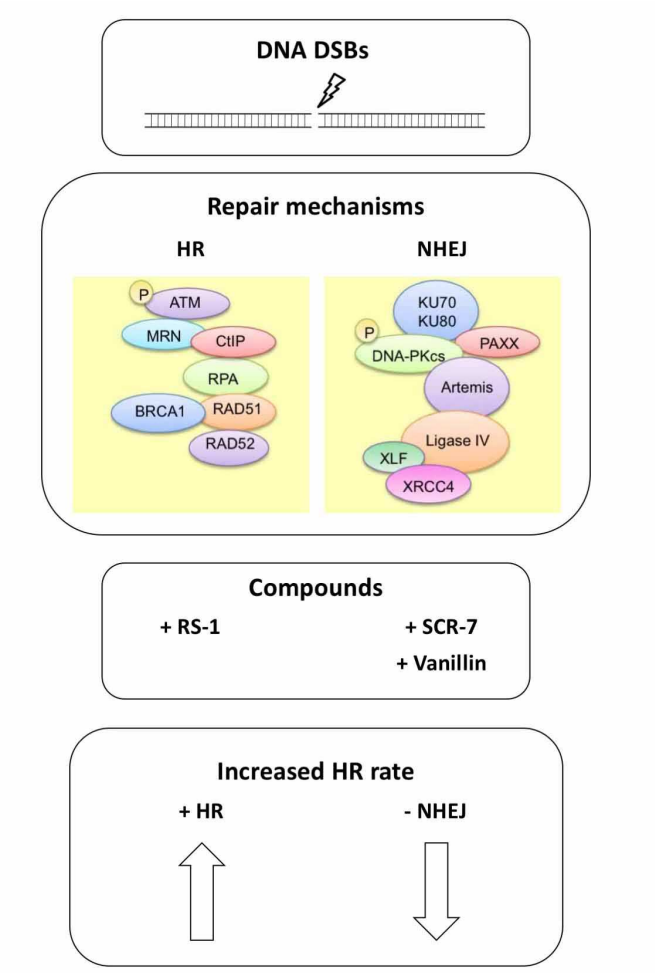

Fig. 2. Compounds can interfere with DSBs repair mechanisms. It is possible to interfere with DSBs repair mechanisms in order to promote HR by using specific compounds, such as RS-1, Scr7 and Vanillin. Adapted from (Vartak & Raghavan, 2015).

1.7 The engineered endonucleases

The discovery that site-specific DNA DSBs can stimulate the endogenous repair mechanisms is at the basis of genome editing strategies (Jasin, 1996, Rouet, Smih et al., 1994). In fact, the efficiency of spontaneous HR, which occurs only in late S/G2, is low and could not guarantee a targeting rate high enough to reach a therapeutic effect. By inducing site-specific DNA DSBs, it is possible to enhance the rate of HR of several orders of magnitude (Jasin, 1996, Rouet et al., 1994). Genome editing tools should: a) be efficient at inducing modifications in target cells with a high rate; b) be specific and have no or very low off-target activity; c) be simple to design/program and assemble, to target any sequence within the genome, with a relatively low cost (Gasiunas & Siksnys, 2013). Genome

engineers adopted engineered endonucleases to specifically “cut and sew” DNA in order to introduce site-specifically desired nucleotide sequences (Fig. 3; Tab. 3). Endonucleases can target any locus of interest to induce DNA DSBs which can, thereby, stimulate DNA damage response mechanisms to obtain gene knockouts, gene conversions and gene correction (Rouet et al., 1994).

Meganucleases were the first genome-editing tool that has been developed by re-engineering the DNA-binding specificity of naturally occurring homing endonucleases. They consist in a sequence-specific and programmable domain whose recognition motif, longer than 12 bp, targets the nuclease domain at desired sequence to induce DSBs (Paques & Duchateau, 2007). Even if several studies adopted meganucleases for genome editing purposes (Gurlevik, Schache et al., 2013, Riviere, Hauer et al., 2014), their used is limited since it is difficult to separate the DNA-binding and cleavage domains and to engineer proteins with novel specificities.

A second class of engineered endonucleases was generated with zinc finger DNA binding domains of transcription factors and the FokI restriction endonuclease. Since the DNA-binding and the recognition domains of the FokI restriction endonuclease function independently from each other (Li, Wu et al., 1992), by replacing the recognition domain with a zinc finger module, new chimeric nucleases called zinc finger nucleases (ZFNs) with novel binding specificities were generated (Kim & Chandrasegaran, 1994). A similar strategy was applied using transcription activator-like effectors (TALE). By combining the FokI restriction domain with TALE arrays, the TALE nucleases (TALENs) were developed (Christian, Cermak et al., 2010). The most important limits of these programmable endonucleases reside in the complicated and expensive methodologies needed to generate the enzymes, and the requirement of a different one for each specific DNA target sequence (Tab. 4).

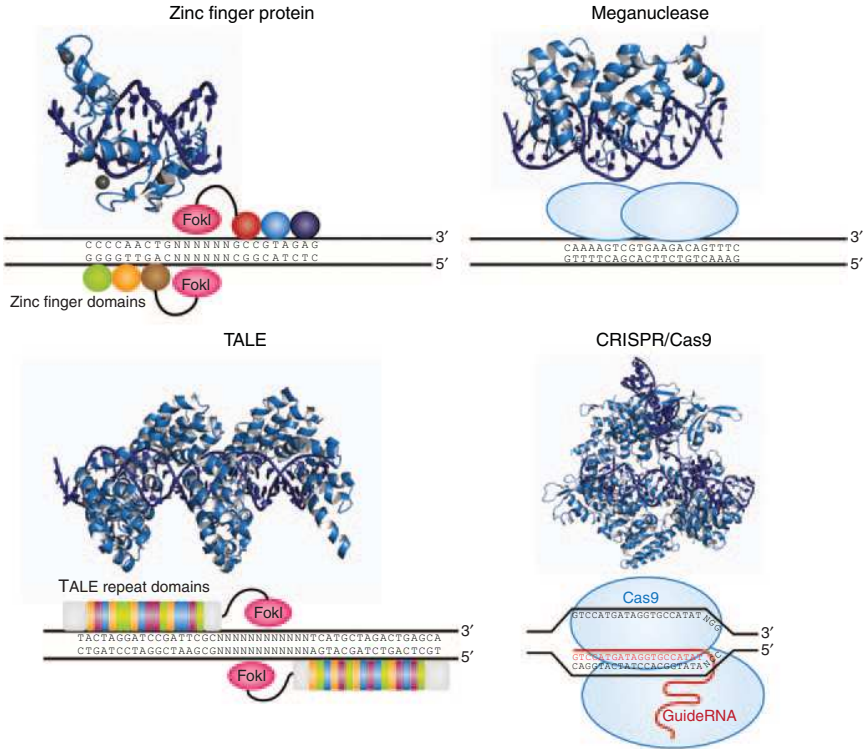

Fig. 3. Available engineered endonucleases. Meganucleases, Zinc Finger Nucleases (ZFNs), TALE Nucleases (TALENs) and CRISPR/Cas9 are genome editing tools able to target DNA DSBs in a site-specific manner (Maeder & Gersbach, 2016).

1.7.1 The CRISPR/Cas9 system

The CRISPR/Cas (Clustered Regularly Interspaced Short Palindromic Repeat (CRISPR)/CRISPR-associated) system was firstly discovered in the 1987 as an adaptive immune system of *E. Coli* and in the 2013 started to be used as a genome editing tool (Hsu, Scott et al., 2013). Nature developed the CRISPR/Cas machinery to protect bacteria and archaea from phage infection. It consists in an array of short repeat sequences interspaced by unique and size-regular DNA sequences, called spacers, and "cas" genes. By the incorporation of the invading DNA into the host genome as spacers, the infected microorganism can generate small RNA molecules (crRNA) that can guide the effector nuclease, encoded by "cas" genes, to cut the foreign DNA, with the protection in successive infection events (Fig. 4).

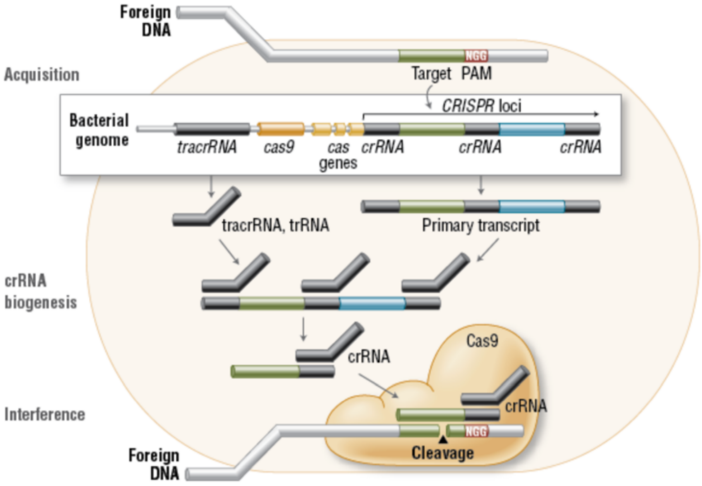

Fig. 4. The CRISPR/Cas system. The CRISPR/Cas machinery protects bacteria and archea from phages. The infected organism incorporates the invading DNA into the genome as spacers by which small RNA molecules are generated (crRNA) and target the Cas9 nuclease, encoded by "cas" genes, to digest the foreign DNA.

For the immunity process three stages are required (adaptation, expression and interference) and different CRISPR/Cas subtypes (I, II and III) have been discovered in terms of architecture structure, mainly represented by the effector complex (Fig. 5). In subtype I, the effector nuclease complex, called Cascade (CRISPR associated complex for antiviral defence), binds the target sequence which is cleaved by another associated cas protein, called Cas3 (Brouns, Jore et al., 2008, Sinkunas, Gasiunas et al., 2013). In subtype III, the effector complex is represented by the Cas RAMP module (Cmr) and the crRNA (Hale, Zhao et al., 2009, Zhang, Rouillon et al., 2012). In the CRISPR/Cas subtype II, the effector nuclease, the cas9, makes a complex with the CRISPR RNA (crRNA) and the trans-activating RNA (tracRNA).

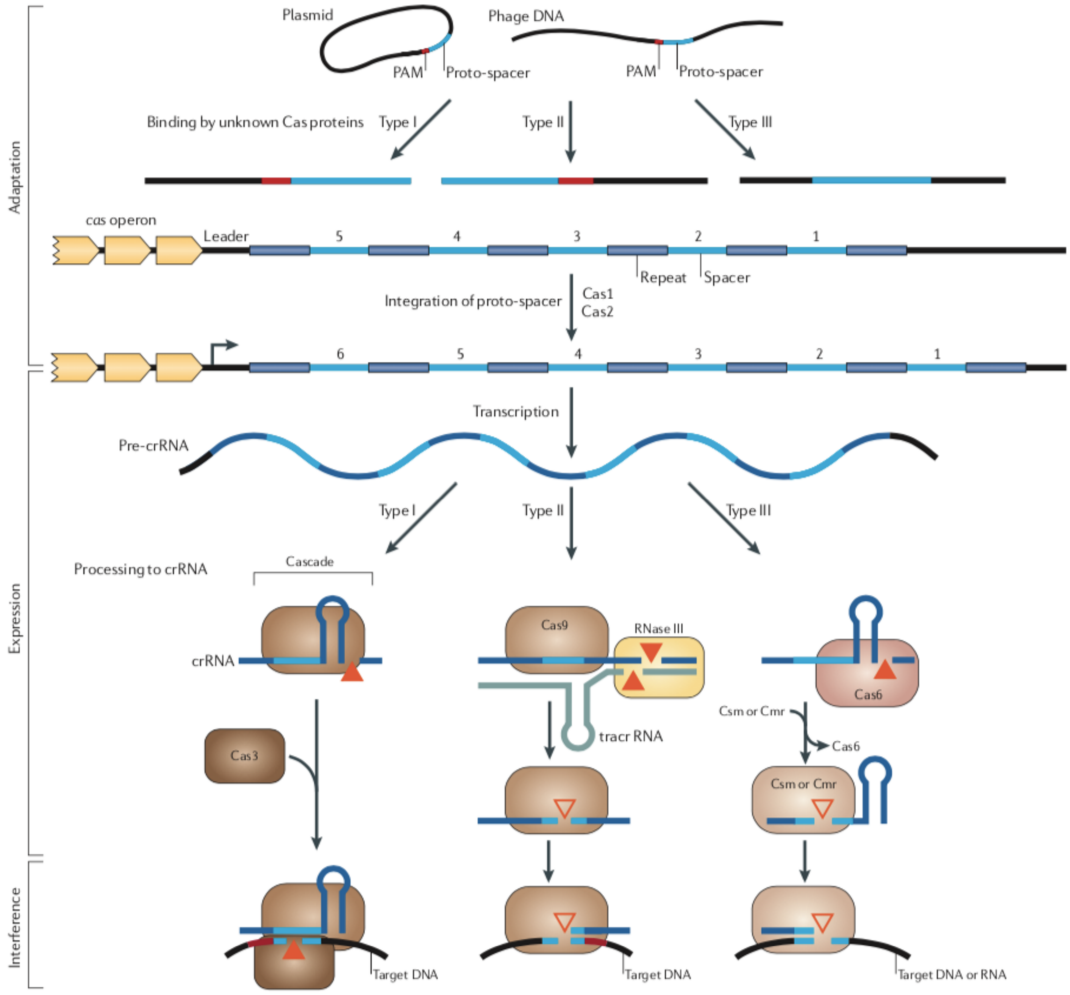

Fig. 5. The different CRISPR/Cas systems. The three stages of CRISPR/Cas adaptive immune system (adaptation, expression and interference) differs among subtype I, II and III. Modified by (Makarova, Haft et al., 2011).

In particular, the subtype II has been useful to develop an engineered machinery aimed at inducing site-specific DNA DSBs. Indeed, the crRNA and tracRNA can be engineered in a single molecule, the guide RNA (sgRNA), to target the cas9 at desired DNA sequence (Fig. 6). Complexing with sgRNA, cas9 can recognize the protospacer, which is a nucleotide stretch matching the crRNA, and a protospacer adjacent motif (PAM) in the target sequence. After the recognition event, Cas9 generates the R-loop, in which the displaced DNA strand is cut by the RuvC-like nuclease domain, whereas the DNA strand complexed with RNA by the HNH one.

Theoretically, sgRNAs can be designed to target any desired sequence, but, actually, several aspects make this a challenge. First, the PAM sequence, which differs among Cas9 variants, limits the targetable sites. The possibility could be also influenced by the chromatin structure, even if it has been shown that methylation does not interfere in *in vitro* and *in vivo* conditions (Hsu et al., 2013). Secondary RNA structures could also interfere with the

recognition of the desired site, since it is based on the complementarity and consequent hybridization between sgRNA and target sequences (Gasiunas & Siksnys, 2013).

As already mentioned before, targeting specificity of engineered endonucleases at the desired locus is as important, at least, as its efficiency. Several strategies can be adopted to reduce off target activity of Cas9 nucleases: 1) using longer PAM sequences or reducing the amount of used cas9 (depends on the cas9 type); 2) using two Cas9 nickase mutants to induce nicks in both DNA strands thus, doubling the recognition sequence; and 3) using inactive cas9 nuclease fused to the FokI nuclease domain, which work only as dimers. Even if these approaches can lead to an improved specificity, their use is limited by: 1) decreased on-target modification rate; 2) and 3) the need of two sgRNAs targeting very close sequences, with reduced targetable sequences (Gasiunas & Siksnys, 2013, Slaymaker, Gao et al., 2016). Instead of adopting these strategies, it is possible to engineer the Cas9 nuclease, attenuating for example its helicase activity by decreasing the positive charge of the groove between HNH, RuvC and PAM domains responsible of stabilization the non-target strand, to encourage more stringent base pairing between sgRNA and target DNA strand resulting in a reduction in off target activity (Slaymaker et al., 2016).

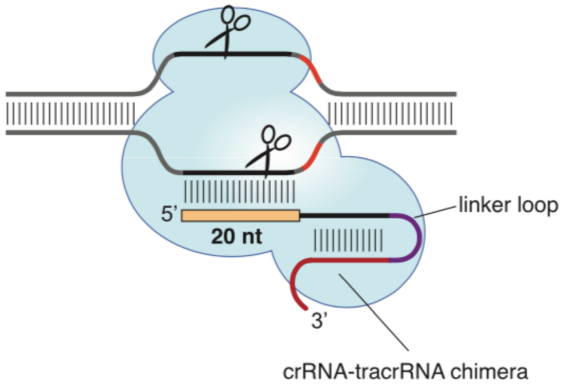

Fig. 6. The CRISPRII/Cas system. The crRNA and tracRNA can be engineered in a single guide RNA (sgRNA) to target the cas9 at desired DNA sequence (Jinek, Chylinski et al., 2012).

From the discovery of *Staphylococcus pyogenes* (*Sp*) Cas9 as a powerful genome editing tool, several nuclease variants, such as *Staphylococcus aureus* (*Sa*), have been identified and characterized by determining their sizes, required PAM sequences and cleavage efficiencies (Esvelt, Mali et al., 2013, Ran, Cong et al., 2015). *Staphylococcus pyogenes* Cas9 (*Sp*Cas9) is 1368 amino acid log and requires the NGG PAM at the 3' of the target site (Gasiunas & Siksnys, 2013, Mojica, Diez-Villasenor et al., 2009). *Sp*Cas9 can tolerate *in vitro* up to six mismatches, whose importance is modulated by the distance from the PAM sequence.

Mismatches at the distal end of the PAM sequence are more tolerated than those in its proximity, which are not allowed (Jinek et al., 2012). *In vivo*, *Sp*Cas9 can tolerate up to four mismatches, depending on the locus, base position, identity, and Cas9/sgRNA dosage (Fu, Foden et al., 2013, Hsu et al., 2013, Mali, Aach et al., 2013, Pattanayak, Lin et al., 2013). *Staphylococcus aureus* Cas9 (*Sa*Cas9) is 1053 amino acid long, being shorter than *Sp*Cas9, and requiring the NNGRRT PAM at the 3' of the target site (Ran et al., 2015). The advantage of the smaller size of *Sa*Cas9 is relevant when considering AAV vectors as delivery tools. Being encoded by 3159 nucleotides, the *Sa*Cas9 leaves 1.8 kb of free space in the vector, since the AAV packaging capacity is about 4.7 to 5.0 kb (Wu, Yang et al., 2010).

	MEGANUCLEASES	*ZFNs*	*TALENs*	*CRISPRII/CAS9*
Structure	Endonucleases with a large recognition site (>14 bp). The same domain has the target recognition and cleavage capacity.	Chimeric enzymes consisting in a DNA binding domain fused to the nuclease domain of FokI.	Chimeric enzymes consisting in a DNA binding domain fused to the nuclease domain of FokI.	Cas9 enzyme is guided to the target by a RNA-sequence.
Recognition site	14-40 bp	9-18 bp *2	14-20 bp *2	22 bp
Specificity	Small number of mismatches tolerated	Small number of mismatches tolerated	Small number of mismatches tolerated	Mismatches tolerated
Efficiency Targeting	Low efficiency in targeting novel sequences	Non G-rich sequences difficult to be targeted	5' base must be a T for each monomer	PAM is required
Engineering	Protein engineering	Protein engineering	Complex molecular cloning	By changing a small portion of gRNA is possible to introduce several DSBs in the same cell
Viral Delivery	Possible and easy with viral vectors	Possible with viral vectors	The large size and repetitive nature of each monomers make the delivery difficult	Possible with viral vectors

Tab. 3. Comparison between the available platforms of engineered endonucleases. Meganuclease, ZFNs, TALENs and CRISPR/Cas system are characterized.

	ADVANTAGES	*DISADVANTAGES*
MEGANUCLEASES	Smallest class of endonucleases, 3' overhangs more recombinogenic than 5'	The same domain has both recognition and cleavage capacities -> Difficult to target new sequences
ZFNs	Small size, Engineered from human proteins, Used in clinical trial	Off-targets Difficult to generate specific versions to the desired target site
TALENs	High specificity, Unlimited targeting range	Sensitive to DNA methylation, Time-consuming synthesis, Large size, Susceptible to rearrangement due to the repetitive nature of TALENs, Difficult to be packaged in a viral vector due to instable nature of tandem repeat,
CRISPRII/CAS9	High specificity and high efficiency, Easy to target novel sequences, Multiple sgRNAs to induce DSBs at several loci	Large size, Requirement of the PAM sequence, not all sequences are targetable Off targets

Tab. 4. Advantages and disadvantages of meganucleases, ZFNs, TALENs and CRISPRII/Cas9 system.

Furthermore, the smaller size of *Sa*Cas9 permits the "all-in-one" AAV strategy of genome editing approaches, using, for example, a single AAV vector containing multiple sgRNAs to target specific deletions and multiplexed knockouts (Friedland, Baral et al., 2015). Moreover, it is possible to eliminate non-essential sequences for Cas9 activity and to use shorter human tRNA promoters, instead of U6 one, without interfering with the efficiency and specificity of the system (Friedland et al., 2015). Furthermore, it has been demonstrated that *Sa*Cas9 has a comparable on target cleavage efficiency with the *Sp*Cas9 nuclease (Friedland et al., 2015).

1.8 Genome editing with CRISPR/Cas9

From its discovery as a genome editing tool, the CRISPRII/Cas9 platform has been applied for several genome modification purposes, for instance to correct disease-causing mutations in mouse zygotes and human cell lines for cataract (Wu, Liang et al., 2013) and cystic fibrosis (Schwank, Koo et al., 2013). Nowadays, important evidences of the utility of the

CRISPR/Cas9 technology to also cure animal models of human inherited disorders have been emerging and increasing very fast.

Yang *et al*. tested a CRISPR/Cas9-based therapeutic strategy in a mouse model of ornithine transcarbamylase (OTC) deficiency, the most common inherited disorder of the urea cycle (Yang, Wang et al., 2016). The male sparse fur ash (spf^{ash}) mouse carries a point mutation (G→A) at the donor splice site at the end of exon 4 of the OTC gene, located in X chromosome, which is responsible of the altered splicing and consequent reduced amount of OTC mRNA and protein (Hodges & Rosenberg, 1989). The diseased mice retain about 5-8% of OTC residual activity and can survive only with a low-protein diet to prevent hyperammonemia crisis, which, otherwise, can lead to brain damage and death. Since OTC deficiency results in metabolic crises during the neonatal period, AAV-mediated non-integrative gene therapy is not effective during this temporal window due to episomal vector loss in the highly proliferating hepatocytes (Cunningham et al., 2009). Therefore, the authors designed a genome editing approach to treat the mutant mice. They reasoned that HDR repair mechanism, induced by DNA DSBs generated by CRISPR/Cas9 platform and by the presence of a donor template, can be adopted to correct the specific disease point-mutation and lead, as a consequence, to the permanent correction of the phenotype. To correct the single nucleotide mutation they intravenously infused two rAAV vectors: one to deliver the *Sa*Cas9, and one the sgRNA and donor DNA. The approach resulted in the reversion of the mutation in 10% of hepatocytes and, thereby, succeeded in improving the phenotype of the OTC deficient mice when treated during the newborn period. When applied to adult OTC-deficient animals, the efficiency of HDR-mediated correction was lower and DNA DSBs were mainly corrected by NHEJ, resulting in high frequency of INDELs with the disruption of the residual OTC activity, leading to death of the treated animals.

Yin *et al*. corrected a *Fah* mutation in hepatocytes in a mouse model of the human disease hereditary tyrosinemia type I (HTI) demonstrating efficacy of CRISPR/Cas9 mediated genome editing in adults (Yin, Xue et al., 2014).

1.9 Hemophilia A and B

An important class of monogenic diseases with primary hepatic expression without parenchymal damage is represented by bleeding disorders (Tab. 5) (Fagiuoli et al., 2013). Between them, hemophilia A and B are the most common, affecting 1 in 5000 and 1 in 30.000 male live births, respectively (Mannucci & Tuddenham, 2001). Hemophilia A and B result from the deficiency or dysfunction of coagulation factor VIII and IX, respectively.

The genes encoding factor VIII and IX both are located on the X chromosome, due to which almost all patients are males. According to the fraction of retained activity of the factor, three major hemophilic phenotypes can be recognized: 1) severe, with less than 1% of normal activity; 2) moderate, with 2-5% of normal activity; and 3) mild, with 6-30% of normal activity. As a consequence, the frequency and the severity of bleeding episodes in hemophilic patients differ among them. The therapeutic goal for hemophilia A and B is modest, since 1-2% of clotting factor can improve quality of life, while 5-20% can ameliorate severe bleeding phenotypes.

Features of inherited deficiencies of coagulation factor associated with bleeding disorders

DEFICIENT COAGULATION FACTOR	INCIDENCE IN GENERAL POPULATION	CHROMOSOME INVOLVED	MODE OF INHERITANCE
Fibrinogen	1:1 million	4	Autosomal recessive
Prothrombin	1:2 million	11	Autosomal recessive
Factor V	1:1 million	1	Autosomal recessive
Factor VII	1:500,000	13	Autosomal recessive
Factor VIII	1:10,000	X	X-linked
Factor IX	1:60,000	X	X-linked
Factor X	1:1 million	13	Autosomal recessive
Factor XI	1:1 million	4	Autosomal recessive
Factor XIII	1:1 million	6 (subunit A) 1 (subunit B)	Autosomal recessive

Tab. 5. Features of inherited deficiencies of coagulation factor associated with bleeding disorders. Adapted from (Mannucci & Tuddenham, 2001).

1.9.1 Current therapies for Hemophilia

1.9.1.1 Plasma derived factors

The management of hemophilia began in 1970s using plasma concentrates of coagulation factors. From their first use, safer plasma concentrates of coagulation factors have been produced in order to avoid post-transfusion infection events as happened with hepatitis B and C and with human immunodeficiency (HIV) viruses. To assess the safety of the plasma-derived factors, the viral load of the sample and the level of inactivation of the viruses are evaluated.

1.9.1.2 Recombinant factors

The high efficacy of two different recombinant factor VIII for hemophilia A was demonstrated in the early 1990s, leading to their license (Bray, Gomperts et al., 1994, Lusher, Arkin et al., 1993, Schwartz, Abildgaard et al., 1990, White, Courter et al., 1997). Their administration to hemophilic patients who had previously received plasma derived factors infrequently triggered the production of new anti-factor antibodies, called inhibitors (Bray et al., 1994, Lusher et al., 1993, Schwartz et al., 1990, White et al., 1997). Whereas, in previously untreated hemophilic patients, repeated infusions of the recombinant coagulation factors resulted in the generation of inhibitors, who could potentially neutralize the infused factors or interfere with the coagulation function. However, in most cases, inhibitors quickly disappeared or remained at low titers and persisting anti-factor antibodies were found only in 10-15% (Lusher et al., 1993, McMillan, Shapiro et al., 1988). In order to assess their safety, the evaluation of inhibitors was performed and it was demonstrated that recombinant factors are not more immunogenic than plasma derived factors (Ehrenforth, Kreuz et al., 1992) (Addiego, Kasper et al., 1993). Moreover, safety of recombinant factor IX for hemophilia B is a key issue since no human or animal proteins are available for its preparation (White, Shapiro et al., 1998). Clinicians can use recombinant factors instead of plasma derived ones to manage hemophilia, after the evaluation of costs, safety and availability of each therapeutic approach. Three important facts should be taken into account during this analysis: plasma-derived factors are becoming safer, recombinant factors cost at least twice than plasma derived ones and, furthermore, the production capacity of recombinant factors is limited. Nowadays, current treatments are based on intravenous injections of recombinant factors every 2-3 days, efficiently preventing spontaneous bleeding episodes in very severe phenotypes. However, the therapeutic strategy remains non-curative, invasive and very expensive. The economic aspect of the therapeutic treatment should be highly considered, since hemophilia, although affecting only a small portion of the population, is associated with high aggregate costs, varying from patient to patient in terms of disease severity, complications and treatments. These related costs are both direct, such as anti-hemophilic medications, clinician visits, hospitalizations, medical and surgical procedures, laboratory tests; and 2) indirect, consequent to the limited productivity of diseased people. It has been estimated that the mean healthcare costs for hemophilic patients, in the absence of inhibitors, in the US reaches $140,000 per year (Guh, Grosse et al., 2012).

1.9.2 Promising gene replacement therapy

For their features, hemophilia can be considered an ideal disease to be treated with gene replacement therapies. Indeed, the mutated phenotypes is due to deficiency or dysfunction of a single gene product and a small amount of its wild-type activity, about 1-2%, is enough to substantially ameliorate a very severe bleeding phenotype. Moreover, the involved protein circulates in plasma and different type of cells are able to make coagulation factors, whose site of synthesis is not crucial to their activity (Mannucci & Tuddenham, 2001). Furthermore, several animal models are available to evaluate both pre-clinically efficacy and safety of potential curative strategies.

Nathwani *et al*. supported the long-term therapeutic value of gene replacement strategy in non-human primates by a single intravenous injection of a self-complementary AAV vector encoding a codon optimized hFIX gene (scAAV2/8-LP1-hFIXco) (Nathwani et al., 2011a). In fact, juvenile male macaques which were transduced with a dose of 2E+11 vg/kg of therapeutic AAV vector expressed more than 10% of normal hFIX levels 5 years after vector infusion (Nathwani et al., 2011a). Nathwani *et al*. adopted also adenovirus-associated virus vector-mediated gene transfer to improve bleeding phenotypes in six patients with severe hemophilia B (Nathwani et al., 2011b). They performed a peripheral-vein administration of a single dose (2.0E+11 vg/kg for the low-dose group, 6.0E+11 vg/kg for the intermediate-dose group, 2.0E+12 vg/kg for the high-dose group) of scAAV serotype 8 expressing a codon optimized hFIX gene (scAAV2/8-LP1-hFIXco) without immunosuppressive therapy and they followed treated patients for 6 to 16 months (Nathwani et al., 2011b). In all patients FIX expression from 2 to 11% was observed (Nathwani et al., 2011b). Two patients were also treated with a glucocorticoid therapy, as a consequence of increased levels of liver transaminases in blood, resulting from the presence of AAV8-capsid-specific T-cells. Glucocorticoids treatment blocked the inflammatory process, and therapeutic expression was still in the range of 3 to 11% of normal values (Nathwani et al., 2011b). Upon showing efficacy, 4 additional patients were enrolled in the high dose cohort (2.0E+12 vg/kg of scAAV2/8-LP1-hFIXco) and were followed for a longer period (Nathwani et al., 2014). The intravenous infusion of a serotype 8 self-complementary AAV vector expressing a codon-optimized factor IX transgene resulted in long-term expression of therapeutic factor IX and clinical improvement without toxicity with a follow up period up to 3 years (Nathwani et al., 2014). More recently, George *et al.* delivered a hyperactive version of factor IX transgene (Padua mutation) to 10 males with hemophilia B using a dose of 5E+11vg/kg of a single-stranded adeno-associated viral vector with an engineered capsid and a liver specific

promoter (SPK-9001), (George et al., 2017). Before the infusion, all the participants had FIX activity less than 2% of normal levels which, after the gene transfer, increased to 33.7±18.5%. The long-lasting efficiency of the therapeutic strategy leads to the elimination of bleeding episodes and termination of prophylaxis (George et al., 2017).

Considering all these recent advances in liver-directed gene therapy aimed to cure hemophilia B, therapeutic approaches based on gene transfer for hemophilia A are still limited. The larger size of FVIII coding region, indeed, limits its use for gene replacement strategies. However, Rangarajan *et al.* recently treated males suffering from hemophilia A with a single intravenous infusion of three different doses (6.0E+12 vg/kg for the low-dose cohort, 2.0E+13 vg/kg for the intermediate-dose cohort, 6.0E+13 vg/kg for the high-dose cohort) of a serotype 5 adeno-associated virus vector encoding a B-domain deleted human factor VIII (AAV5-hFVIII-SQ), (Rangarajan et al., 2017). Six out of seven participants who were infused with the highest dose got benefit from the therapeutic treatment, normalizing FVIII activity over 1 year (Rangarajan et al., 2017).

1.10 The Crigler-Najjar syndrome

The Crigler-Najjar syndrome (CNS) is a paradigmatic example of inborn errors of metabolism and is the model disease adopted in this study. It is a very rare autosomal recessive disorder (0.6 to 1 affected per 1.000.000 live births) characterized by a severe unconjugated hyperbilirubinemia. It was described for the first time in six patients in 1952 (Crigler & Najjar, 1952). Crigler-Najjar (CN) patients carry mutations in the UGT1A1 gene (Aono, Yamada et al., 1993, Bosma, Chowdhury et al., 1992b, Canu, Minucci et al., 2013, Ritter, Yeatman et al., 1992b), which encodes the only liver enzyme able to conjugate bilirubin (Bosma, Seppen et al., 1994), resulting in a missing, truncated and/or inactive protein (Iyanagi, Emi et al., 1998, Kadakol, Ghosh et al., 2000). Thereby, unconjugated bilirubin (UCB), a water insoluble compound, cannot be excreted and it accumulates in lipophilic tissues, especially in the brain, resulting in bilirubin-induced neurological damage (BIND) and, eventually, death by kernicterus (Crigler & Najjar, 1952, Dobbs & Cremer, 1975). The conversion from a very severe phenotype to a milder one is possible by providing just from 5 to 10% of UGT1A1 activity (Bortolussi et al., 2014b, Fox, Chowdhury et al., 1998, Sneitz, Bakker et al., 2010).

1.10.1 The bilirubin metabolism

Bilirubin is the end product of heme catabolism (Bissell, 1975) and results from the degradation of erythrocyte haemoglobin in the reticuloendothelial system (about 80%) and from myoglobin and other heme-containing proteins in the bone marrow (for the remaining 20%), (Fig. 7) (London, West et al., 1950). The heme-oxygenase catalyzes the first reaction that converts heme into biliverdin (Tenhunen, Marver et al., 1968, Tenhunen, Marver et al., 1970), which is then reduced to unconjugated bilirubin (UCB) by the enzyme biliverdin reductase (Fig. 7, 8) (Tenhunen, Ross et al., 1970). UCB, which is water-insoluble, is, then, transported in the blood bound to albumin to reach the liver, from which it dissociates before entering hepatocytes (Sorrentino & Berk, 1988, Tiribelli & Ostrow, 1993). It is still not clear if UCB uptake in the liver is mediated by carriers or by passive diffusion, even if recent studies demonstrate an involvement of membrane-associated organic anion transport proteins (OATPs) (Hagenbuch & Meier, 2004, Memon, Weinberger et al., 2016). Once inside the hepatocytes, the cytoplasmic transport protein ligandin binds bilirubin, which is, then, transported to the endoplasmic reticulum where the UDP-Glucuronosyltransferase 1A1 (UGT1A1) enzyme mediates its conjugation to glucuronic acid (Fig. 9) (Bosma, 2003). Conjugated bilirubin (CB) is then excreted into the bile via ATP-binding cassette (ABC) transporters, among them the multidrug resistance-associated protein ABCC2/MRP2 transporter plays an important role (Jemnitz, Heredi-Szabo et al., 2010, Schmid & McDonagh, 1975). Intestinal flora de-conjugates part of the CB by beta-glucuronidase and degrades it to urobilinoids. A small amount of de-conjugated bilirubin could be re-absorbed by enterocytes and/or also be secreted back into the plasma and re-transported to the liver in a process called “enterohepatic circulation” (Vitek & Carey, 2003).

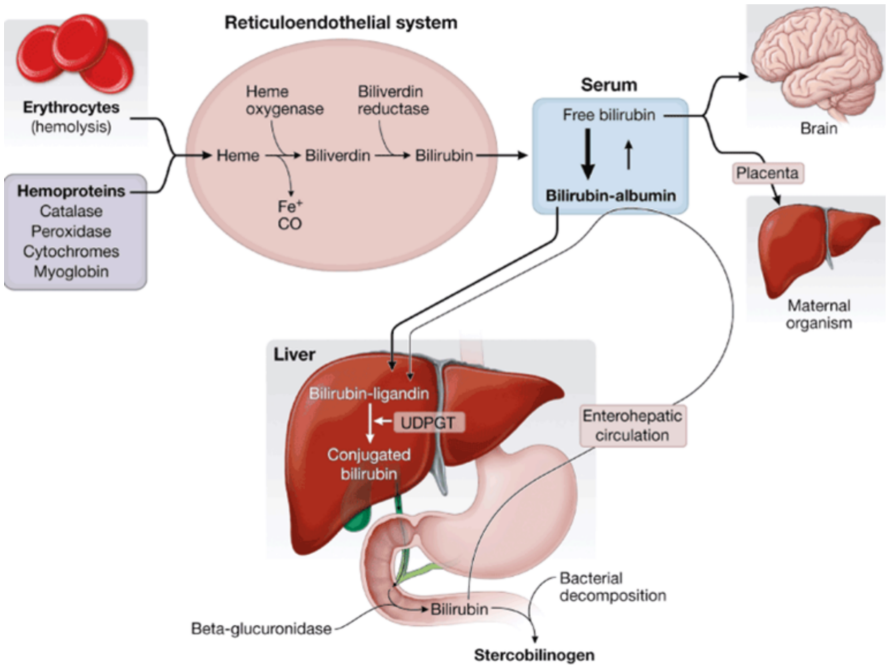

Fig. 7. Bilirubin metabolism. Adapted from (Stevenson, Maisels et al.).

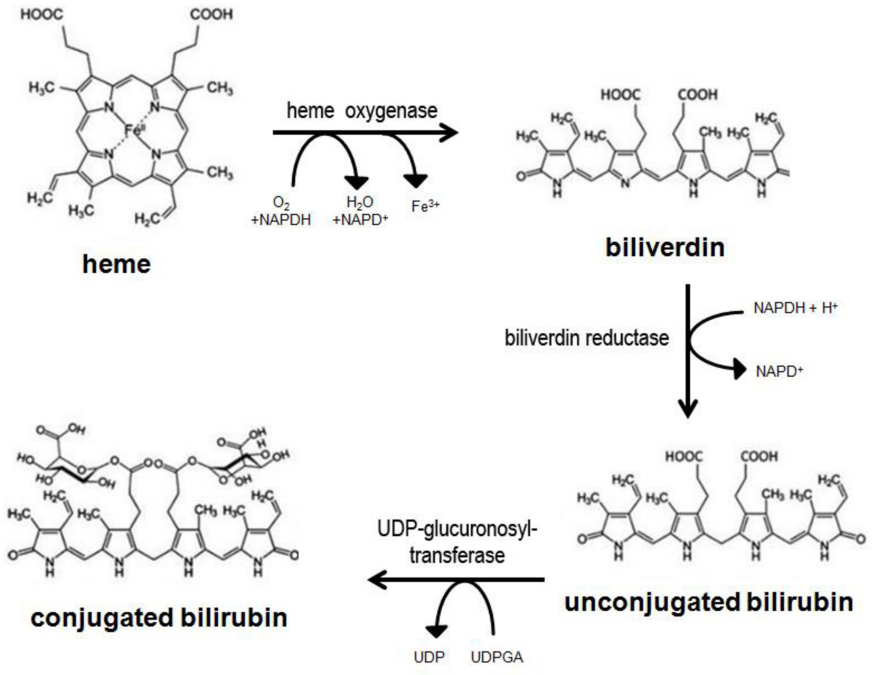

Fig. 8. Chemical reactions involved into bilirubin metabolism. Adapted from (Jangi, Otterbein et al., 2013).

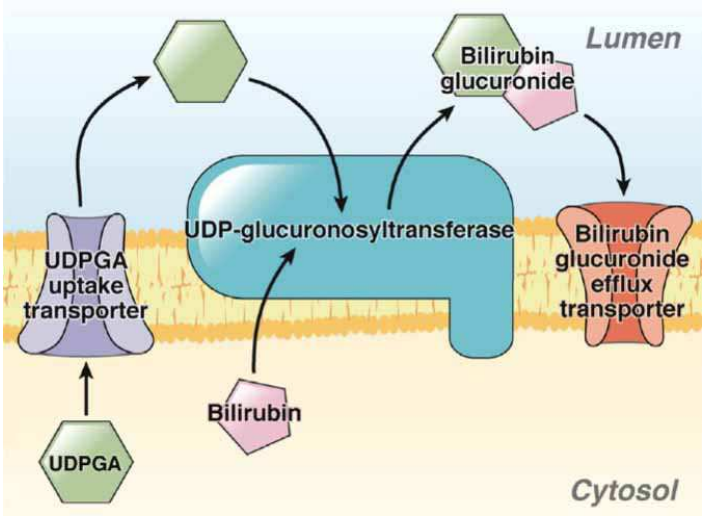

Fig. 9. Schematic representation of bilirubin conjugation into hepatocytes. Adapted from (Erlinger, Arias et al., 2014).

1.10.2 The hUGT1 locus

The hUGT1 locus has been mapped on chromosome 2q37. It is 200 kb-long (Ritter, Chen et al., 1992a) and has a particular structure consisting in 13 unique first exons (and promoters) and 4 common exons (Fig. 10) (Gong, Cho et al., 2001). It encodes 9 functional enzyme isoforms by the use of one of the alternative first exons (A8, A10, A9, A7, A6, A5, A4, A3, and A1) and the four common ones (2, 3, 4, 5). The use of the remaining 4 first exons (A12, A11, A13 and A2) do not lead the production of functional enzymes since they encode pseudogenes.

The UGT1 protein is an enzyme that localizes in the membrane of the endoplasmic reticulum. Its N-terminal domain is encoded by the first alternative exon and defines the substrate specificity, being variable among members of the UGT1 protein family (Meech & Mackenzie, 1997). The four common exons codify for the C-terminal domain, which consists in a sequence necessary for the binding of the co-substrate UDPGA and a sequence necessary to anchor the enzyme to the membrane of the endoplasmic reticulum (Kinosaki, Masuko et al., 1993, Mackenzie, Owens et al., 1997). The UGT1 family includes enzymes involved in the detoxification of compounds of different nature: bilirubin, amines, phenols, drugs, sexual hormones and chemotherapy drugs (You, 2004). The UGT1A1 isoform is the only one able to conjugate bilirubin (Bosma et al., 1994) and it localizes mainly to the liver.

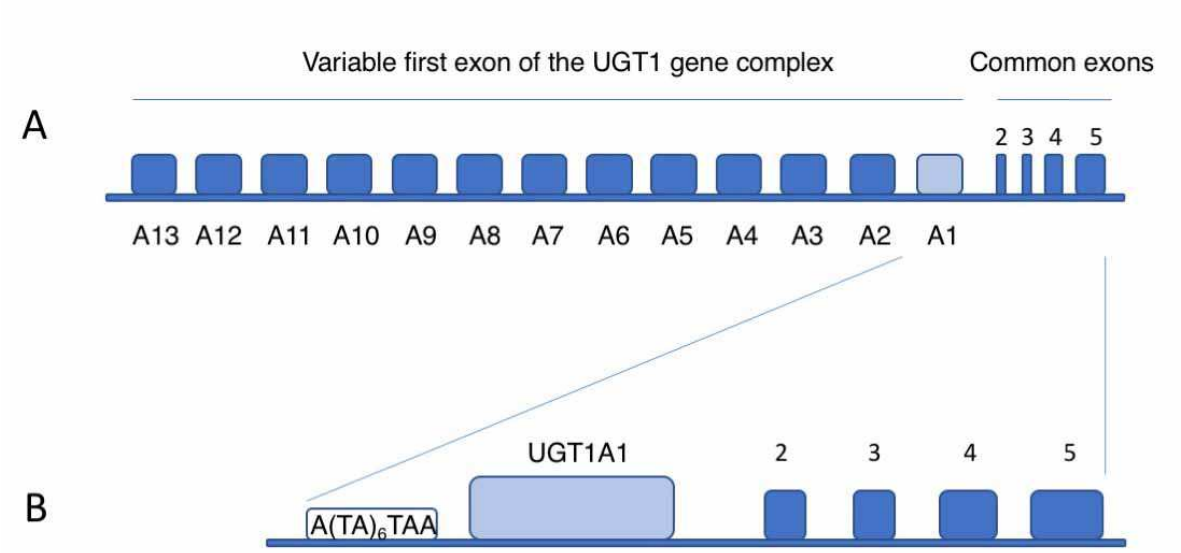

Fig. 10. The hUgt locus. (A) Organization of the hUGT1 locus. First alternative exons and four common ones are shown. **(B)** hUgt1a1gene. Adapted from (Clarke, Moghrabi et al., 1997).

1.10.3 The Crigler-Najjar type I and type II syndromes

According to the residual activity of the UGT1A1 enzyme (Seppen, Bosma et al., 1994), the Crigler-Najjar syndrome can be divided into: 1) type I (CNSI) with no bilirubin glucuronosylation activity (Sinaasappel & Jansen, 1991), 2) type II (CNSII) with residual bilirubin glucuronosylation activity (Arias, 1962). From the discovery of the first UGT1A gene mutations causing the disease (Bosma, Chowdhury et al., 1992a, Bosma et al., 1992b, Ritter et al., 1992a, Ritter et al., 1992b), different CN syndrome causing mutations have been reported (Aono et al., 1993, Labrune, Myara et al., 1994, Moghrabi, Clarke et al., 1993). CNSI is caused mainly by frameshift and non-sense mutations in the hUGT1a1 locus resulting in the complete absence of bilirubin glucuronosylation activity in the liver. UGT1 mutations in CNSI patients have been found in the first exon A1, responsible of the complete lack of the bilirubin UGT1 activity, and in the four common ones (2, 3, 4, and 5), being the most frequent and responsible for the lack of all UGT1 isoforms. CNSII patients have residual bilirubin glucuronosylation activity. UGT1A1 gene expression can be induced by treatment with phenobarbital, thereby, resulting in an increase in the overall glucuronosylation capacity (Arias, 1962, Clarke et al., 1997). This treatment is usually used to clinically differentiate CNSI from CNSII patients. CNSII causing mutations, mainly missense ones, have been found in the first exon A1 and in four common ones (2, 3, 4, and 5). The nature of the mutation influences the level of residual UGT1A1 activity and, thereby, the severity of the disease.

1.10.4 Therapeutic treatments to control Crigler-Najjar type I syndrome

1.10.4.1 Phototherapy

Phototherapy (PT) is the most common treatment used to control unconjugated hyperbilirubinemia (Maisels & McDonagh, 2008). Patients are exposed to light (emission range 400-525 nm, emission peak 450 nm), which is absorbed by skin capillaries and results in the conversion of water-insoluble unconjugated bilirubin into water-soluble photo-isomers that can be eliminated by the bile and, in a smaller amount, through the urine (Maisels & McDonagh, 2008). Phototherapy treatment requires from 10 to 12 hours of exposure per day and it is very efficient to manage non-genetic neonatal hyperbilirubinemia, since the liver conjugation machinery gets activated a few days after birth. It is also very useful to treat CN patients during the early period of life, but its efficacy decreases with their growth. Indeed, the increased thickness and pigmentation of the skin and the reduction in surface/body mass ratio negatively influence the efficiency of the treatment (Strauss, Robinson et al., 2006, Yohannan, Terry et al., 1983), requiring longer PT exposure time (Hansen & Horslen, 2008), with important limitations in the quality of patient life. Thereby, CNSI patients can benefit from PT temporarily and their UCB levels rise until liver transplantation, the only curative and definitive therapy, is performed (Fagiuoli et al., 2013).

1.10.4.2 Exchange transfusion

Exchange transfusion (ET) consists in the replacement of the hyperbilirubinemic blood of the patient with fresh and compatible one. ET is performed in acute cases of hyperbilirubinemia, when PT is not able to avoid the sudden increase in UCB levels and patients are at risk of brain damage. When performed in neonates, it is a procedure with high associated morbidity, mortality and risks (American Academy of Pediatrics Subcommittee on, 2004, Bhutani, Zipursky et al., 2013).

1.10.5 The curative treatment for Crigler-Najjar type I syndrome: the orthotopic liver transplantation

The orthotopic liver transplantation (OLT) represents the only permanent and definitive cure for Crigler-Najjar patients (Pett & Mowat, 1987). However, at the same time, it is a very invasive procedure with several risks that induce clinicians to postpone it as much as possible

(Fagiuoli et al., 2013). In fact, survival of patients 5 years after transplantation is 92-95%, while that of the graft is about 76-79% (Adam et al., 2012). Considering also that LT should be performed before neurological damage occurred, which is not predictable, the surgical procedure should be done in young patients (Hansen & Horslen, 2008). But, at the same time, CNSI children are usually both physically and mentally entirely healthy, until they suddenly develop permanent brain damage and eventually kernicterus. Therefore, the decision to transplant a child, who is jaundiced but otherwise healthy, is often postponed, sometimes until it is too late (Fagiuoli et al., 2013). These considerations highlighted the importance of the best timing of OLT which, nowadays, results a challenge for CNS (Fagiuoli et al., 2013).

1.10.6 The animal models of the Crigler-Najjar type I syndrome

The first animal model of unconjugated hyperbilirubinemia, the Gunn rat, was reported in 1938 as a spontaneously jaundiced mutated strain of the Wistar rat colony (Gunn, 1938). It was recognized as animal model for CNSI when it was understood the connection between its unconjugated hyperbilirubinemia and its inherited inability to conjugate bilirubin (Johnson, Sarmiento et al., 1959). Indeed, the Gunn rat carries a single base deletion in exon 4 of the Ugt1 gene which generates a premature stop codon leading to a truncated and inactive form of the enzyme (Emi, Ikushiro et al., 1995, Iyanagi, Watanabe et al., 1989). As a consequence, homozygous mutant rats, lacking of bilirubin glucuronosylation activity, have serum bilirubin levels between 3 and 10 mg/dL which, thereby, cause cerebellar hypoplasia already at post-natal day 9, granule and Purkinjie cells loss and reduction in the cerebellar layer thickness (Conlee & Shapiro, 1997). Even if the Gunn rat can be a model of bilirubin encephalopathy, neonatal jaundice and CNSI, it does not represent all features of human genetic hyperbilirubinemia, such as neonatal lethality, since mutant animals reach adulthood. Looking at the limits of the Gunn rat, researchers tried to generate animal models that mimic closely the human diseased phenotype. Tukey and colleagues generated the first mouse model of hyperbilirubinemia by introducing a neomycin cassette in the exon 4 of the Ugt1 gene (Nguyen, Bonzo et al., 2008). Ugt1$^{-/-}$ mice have no glucuronosylation activity and die within 15 days after birth. Two years later, by breeding a transgenic animal having the human transgene with a polymorphism in the UGT1A1 promoter, corresponding to the human UGT1A1*28 allele, with mutant Ugt1$^{-/-}$ mice, Tukey's group generated a mouse strain with a milder phenotype, partially rescuing lethality (Fujiwara, Nguyen et al., 2010). Three years later, in 2013, Chen *et al.* generated two conditional Ugt1$^{-/-}$ mice by Cre-

mediated recombination in the liver or in the intestine, in order to study the role played by different organs in the bilirubin metabolism (Chen, Yueh et al., 2013).

1.10.7 The mouse model of the Crigler-Najjar type I syndrome

A mouse model of the CNSI has been generated in the laboratory of "Mouse Molecular Genetics" (ICGEB, Trieste, Italy) by targeting a one-base deletion in the exon 4 of the Ugt1 gene, which results in a premature stop codon and a truncated UGT1A1 protein, lacking the transmembrane domain (Fig. 11A, B) (Bortolussi, Zentilin et al., 2012). Since the UGT1A1 enzyme is inactive and it cannot conjugate bilirubin, water-insoluble UCB accumulates in lipophilic tissues, preferentially in brain. Importantly, the mouse model reproduces the main features of the human disease: neonatal unconjugated hyperbilirubinemia and early lethality due to the neurological damage (Fig. 11C, D, E, F, G) (Bortolussi et al., 2012). The single point mutation was transferred to two different genetic backgrounds: C57BL/6 and FVB/NJ. The severity of the phenotype, as determined by 50% mortality and the extent of brain damage, depended on the genetic background of the animals: 50% survival of C57BL/6-hUgt1$^{-/-}$ mice was at P5, whereas it was at P11 in FVB/NJ-hUgt1$^{-/-}$ pups (Fig. 11D) (Bortolussi et al., 2014b). Furthermore, in order to study more in detail the differences among these strains, mice were exposed to PT for different periods. A PT window of 15 days resulted in the prevention of brain damage and in the derived rescue of all FVB/NJ mutant mice, whereas did not in C57BL/6-hUgt1$^{-/-}$ animals (Bortolussi et al., 2014b), confirming their more severe phenotype.

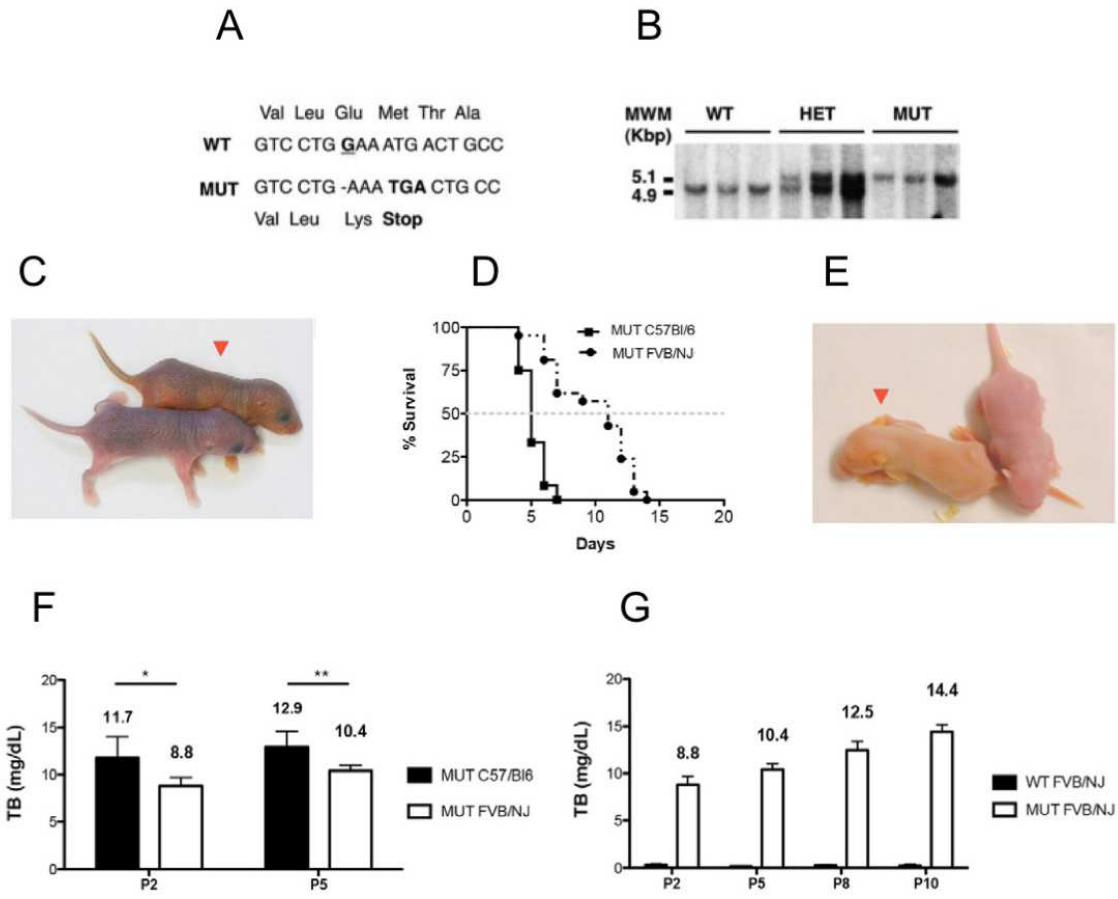

Fig. 11. The CNI mouse models. (A) Partial sequences of wild type (WT) and mutant (MUT) alleles of exon 4 of the hUgt1a1 gene showing the non-sense point mutation which generates a premature stop codon (Stop), **(B)** Southern blot analysis of genomic DNA of wild type (WT), heterozygous (HET) and mutant (MUT) mice, MWM: molecular weight marker, **(C)** Appearance of C57BL/6-hUgt1$^{-/-}$ pups, **(D)** Kaplan-Meier survival curves of mutant C57BL/6 and FVB/NJ mice **(E)** Appearance of FVB/NJ-hUgt1$^{-/-}$ pups, **(F)** Total Bilirubin (TB) levels in mutant C57BL/6 and FVB/NJ mice at post-natal day 2 and 5, **(G)** Total Bilirubin (TB) levels in mutant and wild type FVB/NJ mice at post-natal day 2, 5, 8 and 10. Adapted from (Bortolussi et al., 2012, Bortolussi et al., 2014b).

1.10.8 Gene therapy approaches in the Crigler-Najjar syndrome animal models

CN syndrome is an attractive disease to be cured with liver directed gene therapy for many reasons (Miranda & Bosma, 2009). It is well characterized both at biochemical and molecular level, 5-10 % of UGT1A1 WT activity converts a very severe phenotype to a life-compatible one (Bortolussi et al., 2014b, Fox et al., 1998, Sneitz et al., 2010), the therapeutic benefit of the treatment is evaluated by measuring plasma total bilirubin levels, it is a lethal monogenic disorder, it does not affect liver histology and animal models are available. Most developed gene therapy based approaches, including both non-viral and virus mediated methods have been applied in the Gunn rat. Non-viral approaches used receptor mediated

delivery of plasmids (Chowdhury, Hays et al., 1996, Danko, Jia et al., 2004, Jia & Danko, 2005) or chimeric oligonucleotides (Kren et al., 1999) for gene correction. Viral strategies are based on retro- (Aubert, Menoret et al., 2002, Branchereau, Ferry et al., 1993, Tada, Chowdhury et al., 1998), adeno- (Askari, Hitomi et al., 1996, Li, Murphree et al., 1998, Montenegro-Miranda, Pichard et al., 2014), adeno-associated- (Montenegro-Miranda, Paneda et al., 2013, Seppen, Bakker et al., 2006) or lenti- (Nguyen, Aubert et al., 2007, Nguyen, Bellodi-Privato et al., 2005, van der Wegen, Louwen et al., 2006) viral vectors. Even if these strategies succeeded to rescue the animal models, their therapeutic efficacy, in the context of a growing organ such as the liver during neonatal period, is limited because of the loss of episomal DNA (Cunningham et al., 2009, Wang et al., 2012). Indeed, investigating the persistence of the transgene DNA after a neonatal AAV-based gene therapy, it has been demonstrated that the highest number of viral genome copies is in 2 days after the gene transfer and declines within 1 week (Fig. 12) (Bortolussi et al., 2014b).

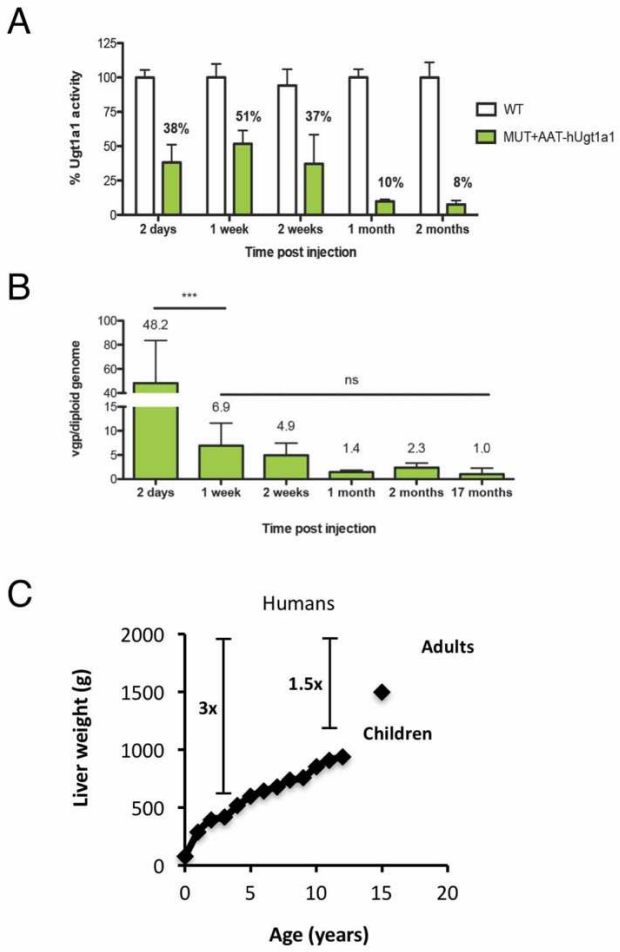

Fig. 12. The efficiency of AAV-based gene therapy decreases during time as a consequence of episomal DNA loss in a context of a growing organ. (A) (B) % of therapeutic efficiency decreases during time after AAV vector administration as a consequence of episomal DNA loss during hepatocytes proliferation (Bortolussi et al., 2014b). **(C)** Liver weight (g) increases during growth (Coppoletta & Wolbach, 1933, Garby, Lammert et al., 1993).

1.10.9 The GeneRide approach

A gene editing strategy without the use of endonucleases, called GeneRide, was developed by Barzel and colleagues in Mark Kay's Lab at Stanford, USA (Barzel et al., 2015) (Fig. 13). GeneRide is based on the spontaneous integration of a promoterless therapeutic cDNA into albumin locus without its disruption. A rAAV8-donor DNA vector carries a therapeutic cDNA, preceded by the 2A peptide and flanked by two albumin homologous regions, and mediates its insertion downstream the albumin coding sequence, just upstream the albumin stop codon. After the integration event mediated by spontaneous homologous recombination, a hybrid mRNA is produced from the strong albumin promoter and two functionally proteins are produced by P2A-mediated ribosomal skipping: albumin and therapeutic one (Fig. 13A). Barzel *et al.* applied GeneRide to a mouse model of hemophilia B (Barzel et al., 2015). By the injection of a serotype 8 AAV vector encoding the hFIX, all neonatal and adult treated mice ameliorated the diseased phenotype. The low on-target integration rate (of about 0.5%) resulted in stable hFIX plasma levels, ranging from 7 to 20% of the levels found in the normal population, normalizing coagulation times in all treated mice (Fig. 13B).

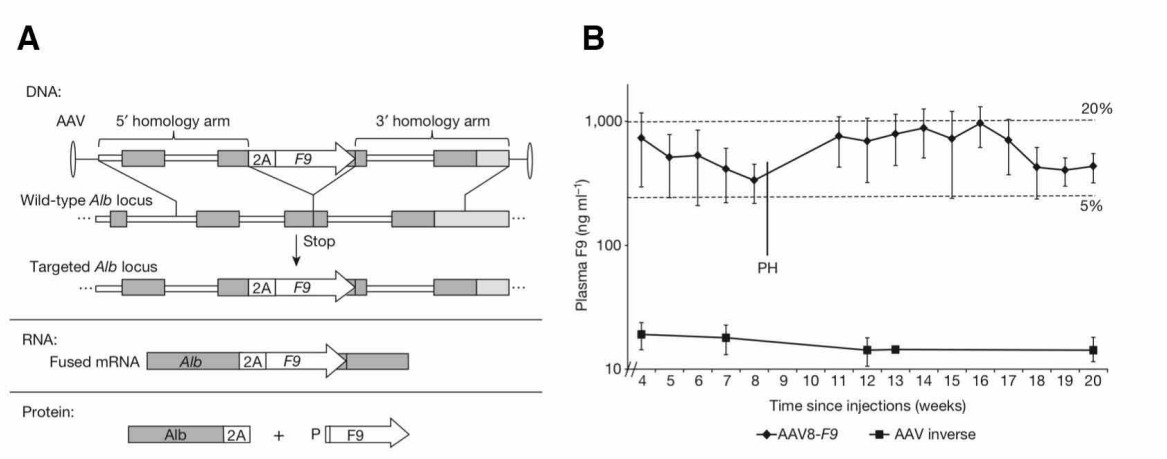

Fig. 13. GeneRide ameliorates hemophilia B in a mouse model. (A) The GeneRide construct, an rAAV8 vector, encodes a promoterless codon optimized human factor 9 (F9) whose coding cDNA is preceded by 2A-peptide coding sequence (2A) and flanked by albumin homologous regions (5' and 3' homology arms). After integration, mediated by spontaneous homologous recombination, into albumin locus (Wild-type and Targeted Alb locus), downstream albumin coding sequence and upstream albumin stop codon, a single fused mRNA is transcribed and two both functionally proteins are produced (Barzel et al., 2015). **(B)** Plasma hF9 values measured by ELISA in 2-days-old B6 injected mice with 2.5E+11 vg/mouse of either rAAV8-F9 (n=6) or inverse control (n=3). PH, partial hepatectomy. Dashed lines denote 5% and 20% of normal F9 levels (Barzel et al., 2015).

In the Mouse Molecular Genetics laboratory (ICGEB, Trieste, Italy), the GeneRide strategy has been already applied to a Crigler-Najjar type I syndrome (CNSI) mouse model, by just replacing the promoterless hF9 cDNA with the hUGT1A1 one (Porro et al., 2017) (Fig. 14). Ugt1$^{-/-}$ mice were intraperitoneally (IP) transduced at post-natal day 4 with the donor DNA vector encoding the therapeutic cDNA (1.0E+12 vgp/mouse of rAAV8 pAlb-UGT1A1) and maintained under phototherapy treatment (PT) up to post-natal day 8 and sacrificed at 30 days or 12 months of age, for a short and long term analysis, respectively (Fig. 14).

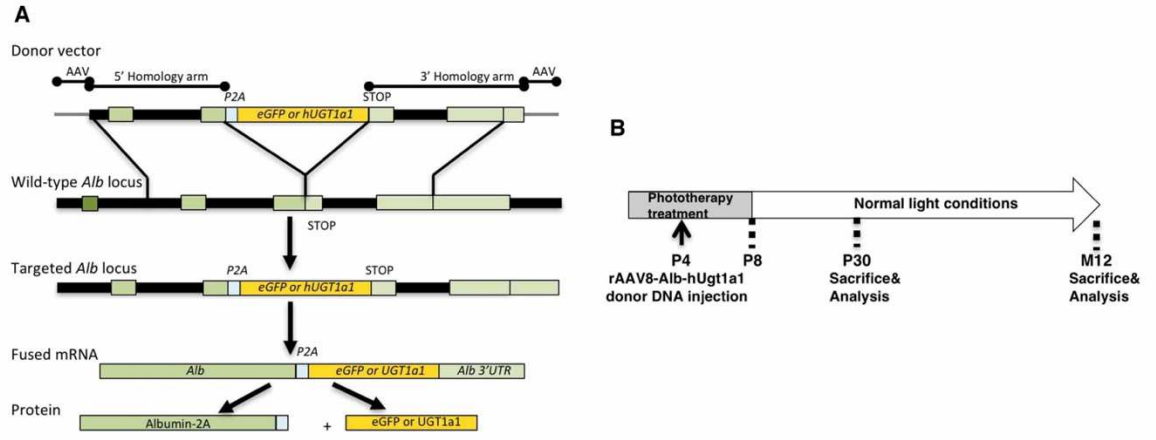

Fig. 14. GeneRide application in the Crigler-Najjar type I syndrome mouse model (A) The GeneRide construct, an rAAV8 vector, contains a promoterless eGFP or WT hUGT1A1 cDNAs preceded by 2A-peptide coding sequence (2A) and flanked by albumin homologous regions (5' and 3' homology arms). After integration, mediated by spontaneous homologous recombination into albumin locus (Wild-type and Targeted Alb locus), downstream albumin coding sequence and upstream albumin stop codon, a single fused mRNA is transcribed and two both functionally proteins are produced (Porro et al., 2017). **(B)** Experimental strategy. Ugt1$^{-/-}$ mutant mice were injected at post-natal day 4 (P4) with rAAV8 pAlb-UGT1A1 (1.0E+12 vgp/mouse) and maintained under phototherapy (PT) up to post-natal day 8 (P8). Mice were sacrificed at 30 days or 12 months of age (Porro et al., 2017).

GeneRide successfully rescued neonatal lethality. Indeed, all rAAV8-treated mice survived whereas untreated one died before postnatal day 19 (Fig. 15A). The treatment reduced toxic bilirubin levels to life-compatible ones up to 12 months after the vector administration (Fig. 15B), completely avoiding cerebellar and behavioral anomalies (Fig. 15C).

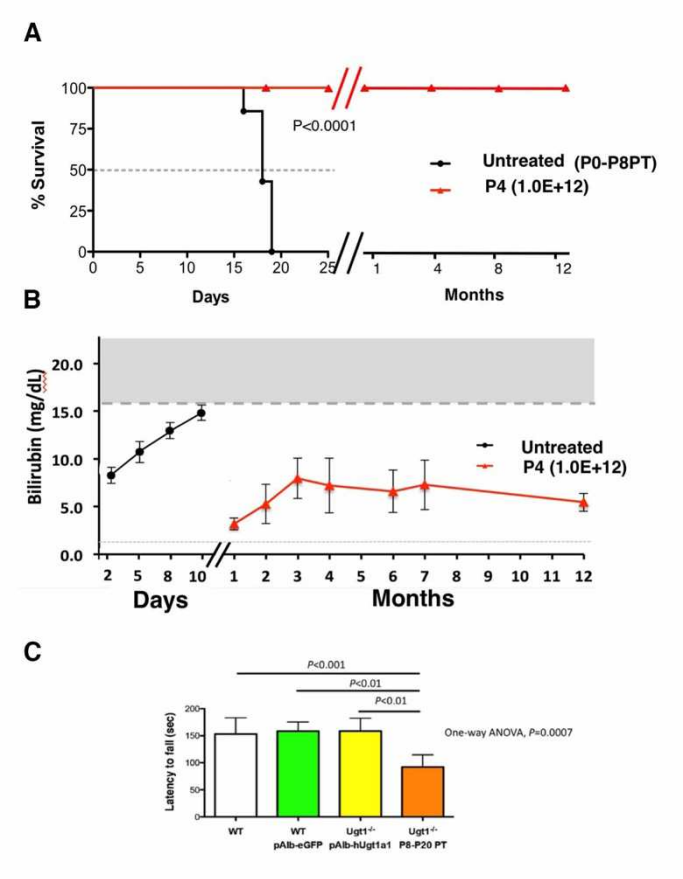

Fig. 15. GeneRide rescued neonatal lethality in a Crigler-Najjar type I syndrome mouse model. **(A)** Kaplan-Meier survival curve. All rAAV8 treated Ugt1$^{-/-}$ mice (n=5) survived, while all mutants treated only with PT up to P8 died in 19 days (n=6). **(B)** Plasma bilirubin levels. Untreated mice who received no PT died before 15 days (n=6). All rAAV8-treated Ugt1$^{-/-}$ mice had total bilirubin values that were life-compatibles up to 12 months after vector administration (n=5). The gray area in the graph indicates the range of total bilirubin levels resulting in brain damage and death. **(C)** Rotarod test of WT mice (n=13) and WT treated with rAAV8-Alb-eGFP donor vector (1.0E+12 vgp/mouse) and Ugt1$^{-/-}$ mice (n=5) treated with rAAV8-Alb-hUGT1a1 donor vector (1.0E+12 vgp/mouse). Ugt1$^{-/-}$ mice treated with PT from P8 to P20 (n=3) with cerebellar abnormalities were used as control (Bortolussi, Baj et al., 2014a).

AIM OF THE THESIS

The aim of this thesis is to develop therapeutic strategies, based on AAV-mediated gene targeting, to cure liver inherited disorders with pediatric onset by the use of a relevant animal model of human diseases.

We point to enhance the integration rate and the therapeutic efficiency of GeneRide, a strategy based on targeting the therapeutic cDNA into the albumin locus. To this purpose, we will evaluate different experimental strategies by determining:

- the ability of compounds to enhance HDR or to block NHEJ;
- the potential increase of HDR by promoting AAV transduction, silencing genes critical for AAV infection;
- the optimal AAV dose to generate DNA DSBs with engineered endonucleases;
- the most efficient AAV administration route;
- the best post-natal day for the delivery of AAV vectors.

The clinical potential of the selected approach will be tested in a very severe animal model of a liver-inherited disease, presenting neonatal lethality: the Crigler-Najjar type I syndrome. The safety of the approach will be assessed in WT and diseased animals, in short- and long-term experiments.

We aim to generate a proof-of-concept demonstrating the therapeutic efficacy and safety of the combination of GeneRide technology with the *Sa*Cas9 platform.

2. MATERIALS AND METHODS

2.1 Chemicals and standard solutions

2.1.1 Chemicals

1 kb Plus molecular weight marker (Invitrogen)

2-butanol (Sigma-Aldrich)

2-propanol

Acetic acid (Sigma-Aldrich)

Bilirubin Calibrator (Dyazyme Laboratories)

Blue bromo Phenol (Sigma-Aldrich)

Boric acid

Bovine Serum Albumin (Sigma-Aldrich)

Brefeldin A (Santa Cruz Biotechnology)

Bromo Cresol Green (Sigma-Aldrich)

Citric acid

Di-Thio-Treitol DTT (Invitrogen)

DMSO (Sigma-Aldrich)

dNTPs (Rovalab GmbH)

DOC (Sigma-Aldrich)

EDTA (Sigma-Aldrich)

Ethanol (Sigma-Aldrich)

EuroSafe nucleic acid stain (Euroclone)

Glycine (Sigma-Aldrich)

Heparin (Sigma-Aldrich)

HEPES

HPO_4 (Sigma-Aldrich)

H_2SO_4

KCl (Sigma-Aldrich)

KH_2PO_4 (Sigma-Aldrich)

L755505 (Santa Cruz Biotechnology)

Methanol (Sigma-Aldrich)

$MgCl_2$

Mouse serum albumin (Sigma-Aldrich)

NaCl (Sigma-Aldrich)

Na_2CO_3

Na_2EDTA

NaF (Sigma-Aldrich)

$NaHCO_3$

Na_2HPO_4 (Sigma-Aldrich)

NaN_3 (Sigma-Aldrich)

NaOH

NP-40 (Sigma-Aldrich)

OPD (Sigma-Aldrich)

PEG 4000

PFA (Sigma-Aldrich)

PhosphoSTOP (Roche)

Proteinase K (Roche)

Ponceau S staining (Sigma)

RS-1

SCR7 (Selleckchem)

SDS (Sigma-Aldrich)

Sharpmass VII Plus (Euroclone)

SIGMAFAST protease inhibitors (Sigma-Aldrich)

Sodium tetraborate (Sigma-Aldrich)

Succinic acid (Sigma-Aldrich)

TEMED (Sigma-Aldrich)

Tris (Invitrogen)

Triton-X 100 (Sigma-Aldrich)

Tween 20 (Sigma-Aldrich)

Xilene (Sigma-Aldrich)

2.1.2 Standard solutions

BCG solution: 26.2 mg of Bromo Cresol Green, 24.4 mg of NaN_3, 2.214 g of Succinic Acid, 1 mL of Triton X-100 dissolved in 250 mL of dH_2O, pH 4.2;

Blotting Solution 1: 200 mM Tris, 10 % v/v Met-OH;

Blotting Solution 2: 25 mM Tris, 10 % v/v Met-OH;

Blotting Solution 3: 25 mM Tris, 40 mM Glycine, 10 % v/v Met-OH;

Coating Buffer: 1.59 g Na_2CO_3, 2.93 g $NaHCO_3$ dissolved in 1 L of dH_2O, pH 9.6;

Electrophoresis sample buffer (ESB) 5x: 50 % w/v sucrose, 25 % w/v urea, 0.5 % v/v bromophenol blue, 5x TBE in dH_2O;

Genomic DNA (gDNA) extraction buffer: 100 mM Tris pH 8.0, 5 mM EDTA pH 8.0, 0.2 % SDS, 200 mM NaCl, 100 µg/mL proteinase K;

Luria-Bertani (LB) medium: 10 g/L Bacto-tryptone, 5 g/L yeast extract, 10 g/L NaCl pH 7.5 dissolved in dH_2O;

OPD Substrate: 5 mg OPD dissolved in 12 mL substrate buffer, 12 µl 30 % H_2O;

PBS 1x: 137 mM NaCl, 10 mM Na_2HPO_4, 2.7 mM KCl, 2 mM KH_2PO_4, pH 7.4;

Protein buffer: 150 mM NaCl, 1 % NP-40, 0.5 % DOC, 0.1 % SDS, 50 mM TrisHCl pH 8.0, 2x protease inhibitors, 1x phosphoSTOP;

Protein loading buffer 10x: 20 % SDS, 1 M DTT, 0.63 M Tris pH 7.0, 20 % BBP dissolved in 60 % sucrose, 10 mM EDTA;

Wash Buffer: 1.0 ml Tween-20 in 1 L of PBS;

Sample Diluent: 5.95 HEPES, 1.46 g NaCl, 0.93 g Na_2EDTA, 2.5 g BSA, 0.25 ml Tween-20, pH 7.2 in 250 mL of dH_2O;

SDS page running buffer 5x: 30 g Tris, 147 g Glycine, 5 g SDS dissolved in 1 L of dH_2O;

Stopping solution: 2.5 M HSO_4;

Substrate Buffer: 2.6 g citric acid, 6.9 g Na_2HPO_4, dissolved in 500 mL of dH_2O, pH 5.0;

TBE buffer 5x: 1.1 M Tris, 900 mM Borate, 25 mM EDTA, pH 8.3;

TE buffer: 10 mM Tris pH 8.0, 0.1 mM EDTA.

2.2 Construction of *Sa*Cas9-sgRNAs and donor DNA vectors

2.2.1 Construction of *Sa*Cas9-sgRNAs encoding vectors

Single guide RNAs (sgRNAs) were designed based on the *Sa*Cas9 PAM sequences (NNGRRT) identified in the genomic region flanking the albumin stop codon, located in exon 14. sgRNA coding oligonucleotides, specified in Tab. 6, were cloned into pX601 and pX602 plasmids, obtained from Addgene (http://www.addgene.org/). Both plasmids encode for the *Sa*Cas9 nuclease and for an incomplete sgRNA sequence. In the pX601 and pX602 plasmids the *Sa*Cas9 is under the transcriptional control of the Cytomegalovirus (CVM) or the thyroid-binding globulin (TBG) promoters, respectively. All identified sgRNAs were cloned into the pX601 plasmid for the *in vitro* assays, while sgRNA7 and sgRNA8 were further cloned into pX602 plasmid for the production of rAAV8 vectors for the *in vivo* experiments.

sgRNA	Oligonucleotides	5'-3' Sequence
sgRNA5	sgRNA5_up	CACCGCATCCATCATTTCTTTGTTTT
	sgRNA5_down	AAACAAAACAAAGAAATGATGGATGC
sgRNA6	sgRNA6_up	CACCGACCCTGAAAACAAAGAAATG
	sgRNA6_down	AAACCATTTCTTTGTTTTCAGGGTC
sgRNA7	sgRNA7_up	CACCGAAAAGTATTAGCAGGACTGT
	sgRNA7_down	AAACACAGTCCTGCTAATACTTTTC
sgRNA8	sgRNA8_up	CACCGATGACCATACGTGAAGACCT
	sgRNA8_down	AAACAGGTCTTCACGTATGGTCATC
sgRNA9	sgRNA9_up	CACCGAGATGTCAGAGAGCCTGCTTT
	sgRNA9_down	AAACAAAGCAGGCTCTCTGACATCTC

Tab. 6. Single guide RNAs coding oligonucleotides. Single guide RNAs (sgRNAs) coding oligonucleotides identified in the genomic region flanking the albumin stop codon, located in exon 14. All sgRNAs were cloned into pX601 plasmid, while sgRNA7 and sgRNA8 were further cloned into pX602 plasmid.

2.2.2 Construction of donor DNA encoding vectors

The eGFP-, hFIX- and hUGT1A1- donor vectors were prepared as previously described (Porro et al., 2017). The sgRNA8 PAM sequence of each donor vector was mutated to avoid the targeting of the donor vector by the *Sa*Cas9 nuclease, before and after homology directed repair (HDR). In specific, the NcoI-PflMI fragment of the original donor vector (Porro et al., 2017) was replaced with a synthetized fragment containing the modified PAM8 including the XhoI restriction site.

2.3 Animals

Animals were housed and handled according to institutional guidelines, and experimental procedures approved by International Centre for Genetic Engineering and Biotechnology (ICGEB, Trieste, Italy) review board, with full respect to the EU Directive 2010/63/EU for animal experimentation. The experimental procedures were approved by the Italian Ministry of Healt, authorization N. 996/2017-PR. Mice were maintained in the ICGEB animal house unit in a temperature-controlled environment with 12/12 hours of light/dark cycles and received a standard chow diet and water *ad libitum*. Wild type (WT) mice were used to test the efficiency of the compound vanillin and of the siRNAs RTBDN and WWC2 to enhance spontaneous homologous recombination. Furthermore, they were used to find the experimental conditions of the GeneRide and CRISPRII/*Sa*Cas9 coupling and as control. Ugt1$^{-/-}$ in FVB/NJ background was previously generated in Mouse Molecular Genetics group at ICGEB (Bortolussi et al., 2012). Ugt1$^{-/-}$ mice used in this study were at least 99.8%

FVB/NJ genetic background obtained after more than 10 backcrosses with FVB/NJ WT mice (Bortolussi et al., 2014a). Homozygous mutant animals ($Ugt1^{-/-}$) were obtained from heterozygous ($Ugt1^{+/-}$) mating and used to test the therapeutic efficiency of the GeneRide and CRISPRII/*Sa*Cas9 coupling. Males and females were used indistinctly for the experiments.

2.4 Genomic DNA extraction from mice tissues

Tail biopsies were approximately 0.5 cm long and stored at -20°C. Whole livers were extracted, reduced to powder in a mortar with liquid nitrogen and stored at -80°C.
Mice tails and liver powders (from 25 to 50 mg) were digested overnight at 55°C in 500 µl of genomic DNA (gDNA) extraction buffer. The day after, they were dissolved and centrifuged for 15 min at 13200 rpm (Eppendorf 5145D, max speed). The supernatants were transferred into a new tube and precipitated with an equal volume of 2-propanol. Tubes were centrifuged for 10 min at 13200 rpm, pellets were washed with 70 % Et-OH for 5 min at 13200 rpm and, then, re-suspended with an appropriate volume of TE buffer. The genomic DNA was stored at +4°C and warmed at +37°C before the use.

2.5 The T7E1 assay

The T7E1 assay was performed following the manufacturer's instructions (M0302, New England Biolabs, MA, United States). The PCR reactions were conducted, using the oligonucleotides (Eurofins Genomics) listed in Tab. 7, according to the protocol of the Taq polymerase used (Roche). The PCR program was optimized with the following cycles: 1 cycle of 2 minutes at 94°C; 30 cycles of 30 seconds at 94°C, 45 seconds at 60°C and 1 minute at 68°C; 1 cycle of 7 minutes at 68°C. The PCR amplicons were purified with Sephacryl™ S-400 beads (Sigma-Aldrich, St. Louis, Missouri, United States), following the manufacturer's instructions. Purified amplicons were denatured, self-annealed and treated with the T7E1 enzyme. After, digested and undigested mixes were visualized on a 2% agarose gel. Agarose powder was melted in 1x TBE buffer, used also as running buffer. Separated fragments were visualized using EuroSafe nucleic acid stain (EuroClone) at UV transilluminator. The fragment sizes were estimated running in parallel 1 kb Plus molecular weight marker (Invitrogen). The estimated gene modifications were calculated using the formula specified in the T7E1 protocol and described by Guschin et al (Guschin, Waite et al., 2010).

Gene	Oligonucleotides	5'-3' Sequence	bp
Albumin	FwStopmALB	GCCACACTGCTGCCTATTAAATACC	787
	RevStopmALB	CTTACATGAACCACTATGTGGAGTCC	

Tab. 7. Oligonucleotides for the PCR of T7E1 assay. Oligonucleotides used for the PCR of the T7E1 assay.

2.6 Ugt1 genotyping

Polymerase chain reaction (PCR) was conducted in a volume of 20 µl:

- 4 µl of polymerase reaction buffer 5x,
- 3 µl of $MgCl_2$ 25mM,
- 0.2 µl of dNTPs 100 nM (25 mM stock),
- 0.1 µl of GoTaq® Flexi DNA Polymerase (Promega, 0.25 units),
- 1 µl of primer forward (0.1 µg/µl),
- 1 µl of primer reverse (0.1µg/µl),
- dH_20 to a volume of 20 µl.

Oligonucleotides (Eurofins Genomics) used for Ugt1 genotyping are listed in Tab. 8.

The PCR thermo-cycler protocol used is the follow: 1 cycle of 3 minutes at 94°C; 30 cycles of 30 seconds at 94°C, 30 seconds at 63°C and 30 seconds at 72°C; 1 cycle of 2 minutes at 72°C.

After the amplification reactions, the obtained products were visualized in an electrophoretic apparatus using a 2% agarose gel. Agarose powder was melted in 1x TBE buffer, used also as running buffer. Separated fragments were visualized using EuroSafe nucleic acid stain (EuroClone) at UV transilluminator. The fragment sizes were estimated running in parallel 1 kb Plus molecular weight marker (Invitrogen).

Gene	Oligonucletides	5'-3' Sequence	Product	
			WT	Ugt1$^{-/-}$
mUgt1	EX4 SCREEN FOR	TCACCAGAGTAGGCATCTCATC	303	473
	UGT 9934 REV	GCTGTAAGACAATCTTCTCC		

Tab. 8. Oligonucleotides used for Ugt1$^{-/-}$ genotyping. Oligonucleotides used for the Ugt1$^{-/-}$ genotyping with the size of PCR products for WT and mutant mice.

2.7 Animals treatments

2.7.1 Phototherapy treatment

Phototherapy (PT) treatment was performed as previously described (Bortolussi et al., 2014a). Ugt1$^{-/-}$ and WT littermates newborns were exposed to blue fluorescent light (450 nm wavelength, 20 μW/cm^2/nm, Philips TL 20W/52 lamps; Philips, Amsterdam, The Netherlands) for 12 hours/day (synchronized with the light period of the light/dark cycle) from birth (P0) up to post-natal day 8 (P8) and then maintained under normal light conditions. This sole treatment results in increased survival of mice, with the death of all untreated mutant pups before P19 (Bortolussi et al., 2014a, Porro et al., 2017). The intensity of the emitted light was monitored monthly with an Olympic Mark II Bili-Meter (Olympic Medical, Port Angeles, WA, USA) (Bortolussi et al., 2012).

2.7.2 rAAV8 treatments

The rAAV vectors used in this study are based on AAV type 2 backbone, and infectious vectors were prepared by the AAV Vector Unit at ICGEB (Trieste, Italy, https://www.icgeb.org/AVU-facilities.html) in HEK293 cells by a cross-packing approach whereby the vector was packaged into AAV capsid 8, as described (Bortolussi et al., 2014b).

2.7.2.1 rAAV8 treatments in wild type mice

The efficiency of the natural compound vanillin and the siRNA RTBDN to enhance spontaneous homologous recombination *in vivo* was evaluated by injecting intraperitoneally WT mice at post-natal day 4 with the GeneRide vector encoding the hFIX [(rAAV8-r-hFIX, 5.0E+11 vg/mouse, (Barzel et al., 2015)] alone or in combination with the 6 days-long vanillin treatment (200mg/kg/day, from P4 to P9) or with the administration of the siRNA RTBDN (2.6 μg, at P3).

For the quality control of the siRNAs RTBDN and WWC2, WT mice were IP injected at post-natal day 4 with the episomal vector encoding the eGFP [rAAV8-pGG2-AAT-eGFP, 1.0E+11 vg/mouse, (Bortolussi et al., 2014b)] alone or in combination with one siRNA (2.6 μg).

For the *in vivo* efficiency evaluation of single guide RNA7 and 8 (sgRNA7, sgRNA8), WT mice were intraperitoneally (IP) injected at post-natal day 4 (P4). The rAAV8-*Sa*Cas9-

sgRNA7 was administered with a dose of 1.0E+12 vg/mouse. The rAAV8-*Sa*Cas9-sgRNA8 was administered with the following doses: 2.5E+11, 5.0E+11, 7.5E+11, 1.0E+12 vg/mouse.
For the comparison between intraperitoneal (IP) and intravenous (IV) administration routes, WT mice were IP- or IV- injected at post-natal day 4 (P4) with a dose of 1.0E+11 vg/mouse of the episomal rAAV8-pGG2-AAT-eGFP vector (Bortolussi et al., 2014b).
For the eGFP cDNA targeting mediated by the CRISPRII/*Sa*Cas9 platform, WT mice were IV-injected at post-natal day 4 (P4). The rAAV8-donor-eGFP was administered with a dose of 8.0E11 vg/mouse alone or in combination with two different doses, 2.0E11 or 6.0E11 vg/mouse, of the rAAV8-*Sa*Cas9-sgRNA8.
For the evaluation of the spontaneous recombination efficiency at post-natal day 2 (P2) and at post-natal day 4 (P4), WT mice were IV-injected at P2 or P4 with a dose of 8.0E11 vg/mouse of the rAAV8-donor-eGFP.
For the hFIX cDNA targeting mediated by the CRISPRII/*Sa*Cas9 platform, WT mice were IV-injected at post-natal day 2. The rAAV8-donor-hFIX was administered with a dose of 2.0E11 vg/mouse alone or in combination with two different doses, 6.0E10 or 2.0E11 vg/mouse, of the rAAV8-*Sa*Cas9-sgRNA8.

2.7.2.2 rAAV8 treatments in Ugt1$^{-/-}$ mice

For the rAAV8 treatment, Ugt1$^{-/-}$ mice were maintained under phototherapy (PT) from birth (P0) up to post-natal day 8 (P8). The rAAV8 vectors were administrated intravenously (IV) at post-natal day 2 (P2). The rAAV8-hUGT1A-donor was administered with a dose of 2.0E11 vg/mouse alone or in combination with two different doses, 6.0E10 or 2.0E11 vg/mouse, of the rAAV8-*Sa*Cas9-sgRNA8.

2.8 Biochemical analyses of plasma samples

Blood was obtained from anesthetized mice by retro-orbital or facial vein bleeding or by decapitation and collected in tubes containing 2 µl of 500 mM EDTA pH 8.0. Tubes were centrifuged at 2000 rpm (Eppendorf 5145D) for 15 min at room temperature (RT), plasma was transferred into new tubes and stored at -80°C.

2.8.1 Plasma hFIX measurement

Plasma hFIX concentration was determined by a sandwich-ELISA using the matched-paired antibody set (FIX-EIA, Enzyme Research Laboratories, USA), following the instructions of

the supplier (http://enzymeresearch.com/wp-content/uploads/2017/12/FIX-EIA1.pdf). For the construction of a reference curve, serial dilutions of human plasmas were used. A multi-plate reader (Perkin Elmer Envision Plate Reader, Walthman, MA) was used to read absorbance at 560 nm. Briefly, 100 µl/well of diluted capture antibody in coating buffer were plated in 96 wells plate (NUNC™) and incubated for 2 hours at RT. After 3x plate washings with wash buffer, reference and sample plasmas were serially diluted in sample diluent and 100 µl/well were transferred into the plate and incubated for 90 minutes at RT. After 3x plate washings, 100 µl/well of detecting antibody diluted in sample diluent were plated and incubated for 90 minutes at RT. After 3x plate washings, 100 µl/well of OPD substrate were applied. The colour reaction was stopped by applying 50 µl/well of 2.5 M H_2SO_4 and the plate read at wavelength of 490 nm. The hFIX concentrations were calculated by interpolating the samples absorbance with the reference curve, considering normal human levels around 5000 ng/mL.

2.8.2 Plasma total bilirubin measurement

Total bilirubin (TB) determination in plasma was performed using Direct and Total Bilirubin Reagent kit (BQ Kits, San Diego, CA), following the instructions of the supplier, as previously described (Bortolussi et al., 2014a). As quality control, three commercial bilirubin standards were used in each assay: Control Serum I, Control Serum II and Bilirubin Calibrator whose absorbance corresponds to 5 mg/dL (Dyazyme Laboratories, Poway, CA). A multi-plate reader (Perkin Elmer Envision Plate Reader, Walthman, MA) was used to read absorbance at 560 nm. Briefly, samples were transferred into a 96 wells plate (NUNC™) in duplicates. Then, 140 µl of Buffer Reagent were added to each sample duplicate. 2.5 µl of nitrate reagent were added only in one well of each sample duplicates, while the other one was used for background evaluation. Then, 150 µl of methanol were added to start the reaction. The bilirubin levels were calculated using the follow equation:

$C\ (mg/dL) = (A_{sample}-A_{blank})/(A_{calibrator}-A_{blank})*5$

2.8.3 Plasma albumin measurement

Plasma albumin levels were determined by modified Bromo Cresol Green (BCG) colorimetric method (Rodkey, 1965), as previously described (Vodret, Bortolussi et al., 2015). For the construction of a reference curve, mouse serum albumin (10 mg/mL, Sigma-Aldrich) was used. Briefly, 2 µl of plasma samples were diluted in a volume of 300 µl of dH_2O. Then, 200 µl of BCG solution were added to each sample. 10 min after, absorbance

values at 630 nm were evaluated by a multi-plate reader (Perkin Elmer Envision Plate Reader, Walthman, MA). Interpolating the samples absorbance with the MSA standard curve, plasma albumin levels were determined.

2.9 Preparation of total RNA from mouse liver

Whole livers were extracted, reduced to powder in a mortar with liquid nitrogen and stored at -80°C. Total RNA from mouse liver powder was prepared using TRI reagent solution (Invitrogen, Carlsbad, CA, United States), according to the manufacturer's instructions. The integrity of the extracted RNAs was controlled by running the samples on 1 % agarose gel.

2.9.1 Quantification and quality control of extracted RNA

RNA concentrations were measured by NanoDrop™ 1000 spectrophotometer (Thermo Scientific) at 260 nm. Absorbance ratios 260/280 and 260/230 nm indicated the quality of extracted RNA.

2.9.2 Reverse transcription (RT)

About 1 µg of total RNA was reverse-transcribed using M-MLV reverse transcriptase (Invitrogen, Carlsbad, CA, United States) following the manufacturer's instructions. The RT-reactions were conducted in a volume of 12 µl:

- 1 µg of total RNA,
- 1 µl of 10 mM dNTPs mix (10 mM of each dNTP),
- 5 µl of oligo dT (0.1 µg/µl)
- dH_2O to a volume of 12 µl.

Mixes were heated at 65°C for 5 min and then chilled on ice. Thereafter, 6 µl volume of a mix of 4 µl of 5x First-Strand buffer and 2 µl of 0.1 M DTT were added. After an incubation of 2 min at 37°C, 1 µl of M-MLV RT (200 units) was added and a second 1 hour long-incubation at 37 °C was did. The enzyme was heat-inactivated for 15 min at 70 °C. cDNA was kept at -20°C.

2.10 Quantitative real time RT-PCR (qRT-PCR)

Quantitative real time RT-PCR (qRT-PCR) was performed on a 96-well real time PCR plate using the iQ SYBER Green Supermix (Bio-Rad) and a C1000 Thermal Cycler CFX96 Real Time System (Bio-Rad) in a volume of 15 µl:

- 7.5 µl iQ SYBER Green Supermix
- 0.5 µl of primer forward (0.1 µg/µl)
- 0.5 µl of primer reverse (0.1 µg/µl)
- 5.5 µl of dH_2O
- 1.0 µl of cDNA diluited 1:10

Specific primers used to amplify the hybrid *Alb-eGFP*, the endogenous mouse *Albumin*, the inflammatory markers *TNFα*, *CD8*, *CD4* and *INFγ* cDNAs, the *SaCas9* or the *Gapdh* housekeeping gene are listed in Tab. 9. Expression of the gene of interest was normalized to albumin to estimate the relative expression of the Alb-eGFP and *Sa*Cas9 cDNA, while normalization to *GAPDH* was performed for inflammatory markers and albumin expression. The qRT-PCR protocol used consists in an amplification reaction and in a generation of a melting curve. Amplification reactions were conducted as follow: 1 cycle of 30 seconds at 98°C; 40 cycles of 5 seconds at 95°C, 25 seconds at 62°C. Melting curves were generated as follow: 10 seconds at 95°C and increasing the temperature from 65°C to 95°C at 0.5°C increment per second. The PCR products were verified running them on a 2.5 % agarose gel. Data were analyzed using the ΔΔCt method.

Gene	Primer	5'-3' Sequence
Alb-Egfp	GFP For	TGCCCGACAACCACTACCTG
	Alb11R	TGAGTCCTGAGTCTTCATGTCTT
Albumin	Alb10F	CTGACAAGGACACCTGCTTC
	Alb11R	TGAGTCCTGAGTCTTCATGTCTT
TNFα	mTNFa_DIR	TTCGAGTGACAAGCCTGTAG
	mTNFa_REV	AGACAAGGTACAACCCATCG
CD8	mCD8aDIR	TCAGTTCTGTCGTGCCAGTC
	mCD8_ex2_rev	GCACTGGCTTGGTAGTAGTA
CD4	mCD4DIR	GCAGCATGGCAAAGGTGTAT
	mCD4REV	AAACGATCAAACTGCGAAGG
IFNγ	mIFNg For	CACGGCACAGTCATTGAAAG
	mIFNg Rev	TTGCTGATGGCCTGATTGTC
Albumin	mALB For	GCATGAAGTTGCCAGAAGAC
	mALB Rev	TCTGCATACTGGAGCACTTC
Gapdh	RT-mGAPDH dir	ATGGTGAAGGTCGGTGTGAA
	RT-mGAPDH rev	GTTGATGGCAACAATCTCCA
Cas9	2F-CAS9 (1164 dir)	CACAACGTGAACGAGGTGGAA
	Cas9_1234 rev	TTTCTCTTCCAGGGCCTTGC

Tab. 9. Oligonucleotides used for qRT-PCR

2.11 Quantitative real time PCR (qPCR)

Quantitative real time PCR (qPCR) was performed on a 96-well real time PCR plate using the iQ SYBER Green Supermix (Bio-Rad) and a C1000 Thermal Cycler CFX96 Real Time System (Bio-Rad) in a volume of 15 µl:

- 7.5 µl iQ SYBER Green Supermix
- 0.5 µl of primer forward (0.1 µg/µl)
- 0.5 µl of primer reverse (0.1 µg/µl)
- 5.5 µl of dH_2O
- 1.0 µl of gDNA

Specific primers used to determine the number of viral genome particles per cells of the rAAV8-*Sa*Cas9-sgRNA8 are listed in Tab. 10. For the construction of a reference curve, serial dilutions of pX602-*Sa*Cas9-sgRNA8 were used.

The qPCR protocol used consists in an amplification reaction and in a generation of a melting curve. Amplification reactions were conducted as follow: 1 cycle of 30 seconds at 98°C; 40 cycles of 5 seconds at 95°C, 25 seconds at 62°C. Melting curves were generated as follow:

10 seconds at 95°C and increasing the temperature from 65°C to 95°C at 0.5°C increment per second.

Oligonucleotides	5'-3' Sequence	bp
pX602TBGdir	aaggatcacccagcctctgc	151
pX602TBGrev	tggcaagagtgtcttcagcagg	

Tab. 10. Oligonucleotides used for the determination of viral genome particles of rAAV8-*Sa*Cas9-sgRNA8.

2.12 Preparation of total protein extracts from liver

Whole livers were extracted, reduced to powder in a mortar with liquid nitrogen and stored at -80°C. Liver total protein extracts were obtained as previously described (Bortolussi et al., 2012). Briefly, liver powder was homogenized, using a mechanical homogenizer (IKA ULTRA-TURRAX T25), in protein buffer, centrifuged twice at maximum speed (Eppendorf 5145D) for 10 min at 4°C. Supernatants were transferred into a fresh tube and stored at -80°C. Bradford (Bio-Rad) method was used to determine total protein concentration. Samples were analysed by Western blot (WB).

2.13 SDS-PAGE and Western blot

SDS-PAGE was used for proteins separation. Polyacrylamide gels were cast with Protogel (30 % w/v acrylamide/methylene biacrylamide solution, National diagnostics). Depending on the size, running gels from 8% to 12% were used, as specified in Tab. 11. Vertical electrophoresis chambers were used. Proteins samples were added with an appropriate volume of 10x protein loading buffer and dH_2O, denatured for 5 min at 95°C and loaded onto gels. Protein marker Sharpmass VII Plus (Euroclone) was run in parallel with protein samples to estimate protein size. Gels were run in 1x running buffer at 25 mA. Then, proteins were transferred onto a nitrocellulose membrane using Lightning Blot™ System (Perkin Elmer). In specific, three 3mm papers were soaked in Blotting Solution 1, the nitrocellulose membrane after its activation in Blotting Solution 2 was added and other three 3mm paper soaked in Blotting Solution 3 were used to cover the membrane. Blotting was run for 15 min at 27 V. Ponceau S staining (Sigma) was used to control the correct run and transfer. Membranes were then blocked and incubated with the primary antibodies (specific conditions are summarized in Tab. 12). After washings, secondary antibodies were added

and after washings, blots were developed using the enhanced chemiluminescence procedure (Thermo Fisher Scientific, Waltham, MA, United States).

	Stacking (mL)	**Running (mL)**		
		8%	**10%**	**12%**
Protogel	1.6	2.6	3.3	4.0
1.5 M Tris pH 8.0	0	2.5	2.5	2.5
0.5 M Tris pH 6.8	1.5	0	0	0
dH2O	6.0	4.9	4.1	3.4
10 % SDS	0.1	0.1	0.1	0.1
10 % APS	0.1	0.1	0.1	0.1
TEMED	10	20	20	20

Tab. 11. Running gels from 8% to 12%used for SDS-PAGE.

Specific experimental conditions were used for each WB anaylsis.

For the eGFP Western blot analysis, 20 µg of total protein extracts from WT untreated and treated mice were analyzed. Membranes were saturated by incubation with 5 % w/v non-fat dry milk in PBS-0.1 % w/v Tween-20 at RT for 2 hours. Then, blots were incubated with the anti-eGFP rabbit polyclonal antibody (1:1000; sc-8334, Santa Cruz Biotechnology) or anti-actin rabbit polyclonal antibody (1:2000, A-2066, Sigma-Aldrich) at 4°C overnight, washed and incubated with the secondary antibody for 1 hour.

For the Ugt Western blot analysis 40 µg of total protein extracts from mutant treated, untreated and WT mice were analyzed. For Ugt1 detection, membranes were stripped with 500 mM Tris-HCl pH 6.8, 10 ml 10 % SDS and 350 µl ß-Mercaptoethanol at 65°C for 1 hour. Membranes were then saturated by incubation with Chemiluminescent Blocker (Millipore, Burlington, MA, United States) at RT for 2 hours. Then, blots were incubated with the anti-human UGT1 rabbit polyclonal antibody (1:600; H-300, Santa Cruz Biotechnology) or anti-actin rabbit polyclonal antibody (1:200, A-2066, Sigma Aldrich) at 4°C overnight, washed and incubated with the secondary antibody for 1 hour.

For the *Sa*Cas9 Western blot analysis, 40 µg of total protein extracts from untreated and treated WT mice were analyzed. Membranes were saturated by incubation with Chemiluminescent Blocker (Millipore, Burlington, MA, United States) at RT for 2 hours. Then, blots were incubated with the anti-*Sa*Cas9 (1:5000) at 4°C overnight or anti-hsp (1:8000) at RT for 1 hour. Anti-*Sa*Cas9 blot was then incubated with anti-rabbit (1:3000), while anti-hsp blot with anti-rat (1:3000) at RT for 1 hour.

Protein name	Supplier	#code	Source	Application	Dilution
eGFP	Santa Cruz	sc-8334	rabbit polyclonal	WB	1:1000
Actin	Sigma-Aldrich	A-2066	rabbit polyclonal	WB	1:2000
Ugt1a	Santa Cruz	H-300	rabbit polyclonal	WB	1:600
*Sa*Cas9	abcam	EPR19795	rabbit monoclonal	WB	1:5000
Hsp70	Sigma-Aldrich	H-5147	rat polyclonal	WB	1:8000

Tab. 12. Antibodies used for WB analysis.

2.14 Histological analysis

After sacrifice, livers and brains were extracted and fixed with 4% PFA in PBS overnight at 4°C and kept in 20% sucrose in PBS and 0.02% sodium azide at 4°C.
Paraffin-embedded liver sections (5 µm) were stained with hematoxylin-eosin (H&E) and Masson's trichrome as previously described (Bortolussi et al., 2014a, Bortolussi et al., 2012). For eGFP experiments liver specimens were frozen in optimal cutting temperature compound (BioOptica, Milano, Italy), 14 µm slices were obtained in a cryostat, washed twice with PBS and mounted with Vectashield (Vector Laboratories, CA, United States).

2.14.1 Immunofluorescence analysis

For immunofluorescence (IF) analysis, specimens were frozen in optimal cutting temperature compound (BioOptica, Milano, Italy) and 14 µm slices were obtained in a cryostat.
For hUgt1a1 immunofluorescence (IF), liver specimens were incubated with sodium citrate pH 9.0 prior to blocking step. Next, they were blocked with 10% NGS (Dako) and then incubated with the anti-hUgt1a1 antibody (Sigma, St. Louis, MO) for 2 hours at RT in 2% NGS blocking solution (Tab. 13). After 3 x 5 min washes with PBS, specimens were incubated with the secondary antibody (Alexa Fluor 488, Invitrogen Carlbad, CA) for 2h at RT. Nuclei were visualized by addition of Hoechst (10 µg /ml, Invitrogen) for 5 min.
For calbindin immunofluorescence (IF), brain specimens were incubated with sodium citrate prior to blocking step. Next, specimens were blocked with 10% NGS (Dako) and then incubated with the anti-Calbindin antibody for 2h at RT in 2% NGS blocking solution (Synaptic Systems, Göttingen, Germany) (Tab. 13). After 3 x 5 min washes with PBS,

specimens were incubated with the secondary antibody (Alexa Fluor 568, Invitrogen Carlbad, CA) for 2h at RT. Nuclei were visualized by addition of Hoechst (10 µg /ml, Invitrogen) for 5 min.

Protein name	Supplier	#code	Source	Application	Dilution
hUgt1a1	Sigma-Aldrich	SAB2701158	rabbit polyclonal	IF	1:200
Calbindin	Synaptic Systems	214002	rabbit polyclonal	IF	1:400

Tab. 13. Antibodies used for IF analysis

2.14.2 Quantification analysis

Quantification of eGFP-positive cells was performed as follows. Each animal was imaged (20X) in two liver sections. Five imaged for section were analyzed per animal. The ratio between the number of the total eGFP positive cells and the nuclei per mice was calculated. Quantification of hUgt1a1 positive cells was performed as follows. Each animal was imaged in (10X) four liver sections. The ratio of the total number of hUgt1a1 positive cells/total number of nuclei counted in all acquired images per animal was calculated. Measurements were averaged for each animal and the results were expressed as mean ± SD for each treatment.

Cerebellar layer thickness was performed on Hoechst-stained sections by measuring the layer depth (µm) as previously described (Bortolussi et al., 2012). PC density analyses were performed as previously described (Bortolussi et al., 2014a, Bortolussi et al., 2012).

Images were acquired on a fluorescence microscopy. Digital images were collected using Leica software and analyzed using ImageJ (U.S. National Institutes of Health, Bethesda, MD, USA).

2.15 Illumina sequencing on- and off-targets

Off-target loci were predicted using the CasOffinder software (http://www.rgenome.net/cas-offinder/) (Bae, Park et al., 2014). Genomic DNA from the predicted off-target regions and that of the albumin on-target site were PCR amplified and sent to BMR Genomics (Padova, Italy) for Illumina sequencing. The primers used for the PCR amplifications are listed in Tab. 14 and contained the complementary regions and a tail on the 5' and 3' end, which was necessary for the sequencing reaction.

Sequenced libraries were first split into locus-specific bins based on the best match to a corresponding source locus using the BBSplit tool [BBtools, https://jgi.doe.gov/data-and-tools/bbtools/] and reads in each bin were counted to verify that they were sufficient to provide deep coverage. Sequencing runs for the Gm29874 locus were subsequently repeated as they were not originally represented in quantities comparable to the other two off-target and an on-target locus. Each read bin was then separately mapped to its corresponding locus target with bwa (Li & Durbin, 2009). All unmapped reads and reads without both pairs mapping to the target sequence were filtered out with samtools (Li, Haurigot et al., 2011). Indels were left-aligned using the GATK LeftAlignIndels function (McKenna, Hanna et al., 2010). All reads below the mapping quality of Q30 ad positions below the base calling quality of Q20 were removed from subsequent analysis. Base and INDELs frequencies were called at each target position from the aligned and post-processed BAM files by using the custom R script based on the Bioconductor's Rsamtools package [Rsamtools, http://bioconductor.org/packages/release/bioc/html/Rsamtools.html]. Samples and targets without the *Sa*Cas9 treatment were used as a control and alternative base and INDELs frequencies (thereinafter jointly termed as alternative variants) were used to model the experimental error with the beta-binomial distribution with the R ebbr package. Parameters for the beta-binomial function were estimated from all depth/alternative variant count ratios in non-treated samples. The 99.9^{th} percentile of the distribution was taken as the error likelihood threshold and then each sample was statistically evaluated at each position to estimate whether the depth/alternative variant at a specific site within the sample was above or below the likelihood threshold for error. The estimates were done separately for SNPs and INDELs. Subsequently, each sample's IINDEL and SNP frequency profiles were separated into 'signal' and 'noise' parts, based on whether they exceed the error likelihood. From these profiles, the overall statistics was compiled on the magnitude and overall event count (event = alternative variant in the significant signal range).

Gene	Oligonucleotides	5'-3' Sequence	bp
Gm29874	Gm29874_for2_tail	*TCGTCGGCAGCGTCAGATGTGTATAAGAGACAG*ATCTTATGGACTGAGCCACC	491
	Gm29874_rev2_tail	*GTCTCGTGGGCTCGGAGATGTGTATAAGAGACAG*TAGAGGTGGACTTCAGCATG	
Kif21a	Kif21a_FOR1_tail	*TCGTCGGCAGCGTCAGATGTGTATAAGAGACAG*CAAGGACCTTTAGCCTCTGA	478
	Kif21a_REV2_tail	*GTCTCGTGGGCTCGGAGATGTGTATAAGAGACAG*TGTCAGGCTACCAAGGATAC	
Tubgcp2	Tubgcp2_FOR2_tail	*TCGTCGGCAGCGTCAGATGTGTATAAGAGACAG*AAGGCAGAGACCTTCAGTTG	522
	Tubgcp2_REV2_tail	*GTCTCGTGGGCTCGGAGATGTGTATAAGAGACAG*TGGAGAAACACTTGAGGCAG	
Alb	pAB1403dir_tail	*TCGTCGGCAGCGTCAGATGTGTATAAGAGACAG*GCCTATGGCTATGAAGTGCAAATCCTA	517
	Revstop_malb_tail	*GTCTCGTGGGCTCGGAGATGTGTATAAGAGACAG*GGACTCCACATAGTGGTTCATGTAAG	

Tab. 14. Oligonucleotides used for Illumina sequencing.

2.16 Statistics

The Prism package (GraphPad Software, La Jolla, CA) was used to analyzed the data. Results are expressed as means ± SD. Values of $P < 0.05$ were considered statistically significant. Depending on the experimental design, Student's *t*-test or one-way or two-way ANOVA, with Bonferroni's *post hoc* comparison tests, was used, as indicated in the legends to the figures and text.

3. RESULTS

3.1 The GeneRide approach

AVV-mediated gene therapy to the liver successfully corrected hyperbilirubinemia in a lethal mouse model of the Crigler-Najjar Syndrome (CNS) (Bortolussi et al., 2014b), but its therapeutic efficacy decreased as a consequence of the reduction of transgene expression due to episomal DNA loss during hepatocyte proliferation. Since re-administration of the therapeutic gene in the clinical setting is not possible because of the presence of neutralizing antibodies generated against the AAV-capsid antigens after the first vector infusion, we investigated alternative strategies.

Gene editing is a promising approach that overcomes AAV-mediated gene therapy limitations in neonatal/pediatric settings by the permanent modification of the genome. Barzel and colleagues, in Mark Kay's Lab at Stanford, developed a gene editing strategy without nucleases, called GeneRide, showing ameliorated coagulation parameters in a hemophilia B mouse model (Barzel et al., 2015). The GeneRide approach takes advantage of a rAAV donor vector carrying a promoterless therapeutic cDNA flanked by albumin homology regions that can mediate its site-specific integration by homologous recombination into the albumin locus. The therapeutic cDNA is inserted after the albumin coding sequence, just upstream its stop codon, resulting in the transcription of a chimeric mRNA that is then translated into two both functionally proteins, albumin and the therapeutic one. GeneRide was already applied to the CNS mouse model in the Mouse Molecular Genetics Lab (ICGEB, Trieste, Italy) rescuing neonatal lethality by inserting a promoterless human uridine glucuronosyl transferase A1 (*UGT1A1*) cDNA into the albumin locus (Porro et al., 2017). Even if the approach was able to convert a very severe phenotype to a mild one with life-long therapeutic efficiency, the targeting rate represented by the spontaneous homologous recombination was too low for a potential clinical application.

3.2 The potential of the vanillin compound to promote spontaneous homologous recombination

Aiming to a potential application of the approach into the clinic, we looked for experimental strategies able to increase the low integration rate obtained with the GeneRide in the absence of nucleases (Porro et al., 2017) and we reasoned that promoting HDR or blocking NHEJ could boost transgene precise integration. Since Paulk *et al*. showed that the natural product vanillin can reduce NHEJ rate by inhibiting the DNA-dependent protein kinase (DNA-PK) (Paulk et al., 2012), we decided to test vanillin in combination with the GeneRide construct encoding the promoterless hFIX cDNA *in vivo*.

3.2.1 Experimental plan

In order to test the potential of the natural compound vanillin to enhance HDR, 4-days-old WT mice were intraperitoneally (IP) injected with a dose of 5.0E11 vg/mouse of the GeneRide construct encoding the hFIX [rAAV8-donor-hFIX; (Barzel et al., 2015)] alone or in combination with a 6-days-long treatment with vanillin (200 mg/kg/day). Retro-orbital bleeding was performed in 1-month-old mice and the plasma hFIX concentration was evaluated performing an ELISA-test based on the use of an antibody able to detect only the human FIX protein (Fig. 16).

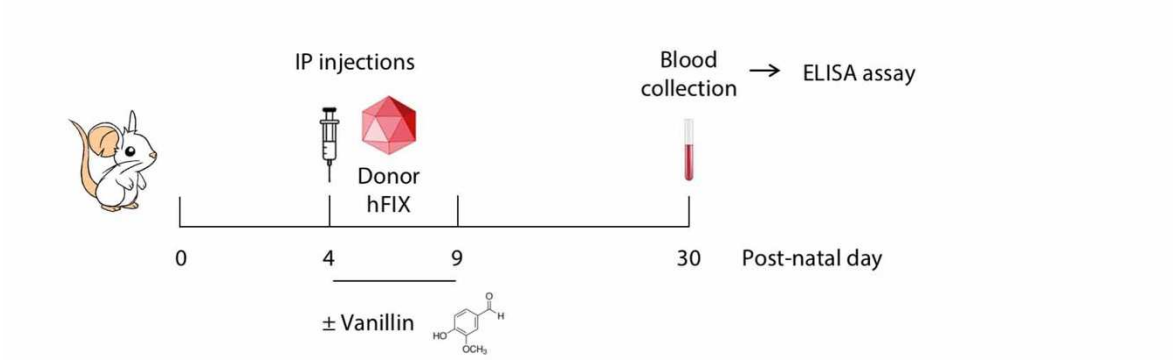

Fig. 16. The evaluation of the potential of vanillin *in vivo*. WT newborn mice (3 mice per experimental group) were intraperitoneally (IP) injected at post-natal day 4 (P4) with the rAAV8-donor-hFIX [5.0E11 vg/mouse, (Barzel et al., 2015)] alone (without vanillin) or in combination with 6-days-long vanillin treatment (200 mg/kg/day, + vanillin). Blood samples were collected by retro-orbital bleeding at 1 month of age. A very specific ELISA assay was performed and plasma hFIX concentrations were evaluated.

3.2.2 Vanillin does not increase the spontaneous homologous recombination rate

The analysis of plasma hFIX values, obtained in the ELISA assay, did not show any significant difference between AAV and vanillin coupled treatments over the AAV administration alone (Fig. 17). Additionally, no effects had been previously obtained *in vivo* with Scr7 (data not shown). Since I had already tested vanillin (Paulk et al., 2012) and other compounds *in vitro*, such as RS-1 (Jayathilaka et al., 2008), Scr7 (Chu et al., 2015, Srivastava et al., 2012, Vartak & Raghavan, 2015), Brefeldin-A, L755507, and no one was able to increase homologous recombination (data not shown), we decided to interrupt the investigation of the potential use the compounds to increase HDR and we looked for other strategies.

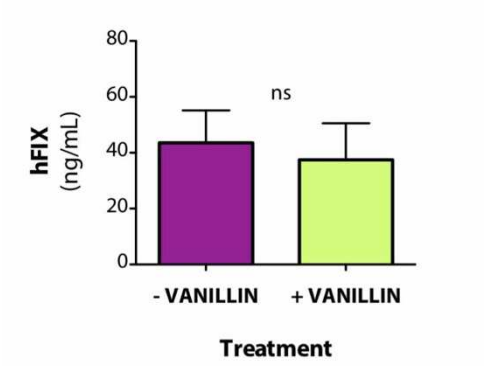

Fig. 17. Vanillin does not enhance spontaneous homologous recombination *in vivo*. Plasma hFIX concentrations (ng/mL) of mice treated with the donor-hFIX AAV8 vector (rAAV8-donor-hFIX, 5.0E11 vg/mouse) alone (- vanillin) or in combination with the natural compound vanillin (200 mg/kg/day, + vanillin). The 6-days-long vanillin treatment did not enhance spontaneous homologous recombination of the donor-hFIX AAV8 vector in WT newborn mice. Student *t*-test, unpaired t test, ns, P = 0.5785. N = 3 per experimental group.

3.3 The potential of siRNAs to promote spontaneous homologous recombination by enhancing AAV transduction

Since recombination rate is also related to the levels of DNA present in the nucleus, enhancing AAV transduction could increase the amounts of donor template used by the cells for repairing DNA DSBs, improving the overall efficiency. Mano *et al*. identified, by a high-throughput whole genome siRNA screening, 1483 genes interfering viral infection, which significantly affected AAV transduction *in vivo* (Mano, Ippodrino et al., 2015). We selected RTBDN among the genes having the higher effect in increasing AAV transduction after their siRNA-mediated knock-down. Thus, we *in vivo* tested the siRNA against the RTBDN mRNA in combination with the GeneRide donor construct encoding the promoterless hFIX cDNA *in vivo*.

3.3.1 Experimental plan

I tested the siRNA RTBDN by intraperitoneally injecting 4-days-old WT mice with the rAAV8-donor-hFIX (5.0E11 vg/mouse) alone or in combination with the siRNA RTBDN (2.6 μg/mouse). Plasma hFIX concentration (ng/mL) in 1-month-old mice was evaluated with a human-specific ELISA assay (Fig. 18).

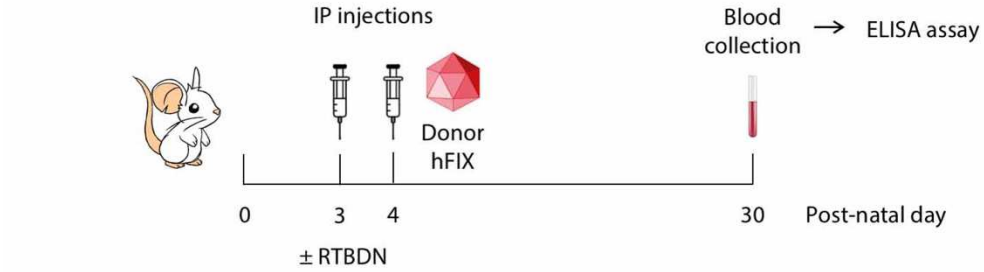

Fig. 18. The evaluation of the potential of siRNA RTBDN *in vivo*. WT newborn mice (3 mice per experimental group) were intraperitoneally (IP) injected at post-natal day 4 (P4) with the rAAV8-donor-hFIX [5.0E11 vg/mouse, (Barzel et al., 2015)] alone (- RTBDN) or in combination with a post-natal day 3 (P3) treatment with the siRNA RTBDN (2.6 µg/mouse, + RTBDN). Blood samples were collected by retro-orbital bleeding at 1 month of age. A human-specific ELISA assay was performed and plasma hFIX concentrations were evaluated.

3.3.2 The RTBDN treatment does not result in the increase of spontaneous homologous recombination rate

The results of the ELISA assay did not show any significant difference in plasma hFIX concentration levels between mice treated with the coupled AAV-siRNA treatments over those with the AAV one alone (Fig. 19).

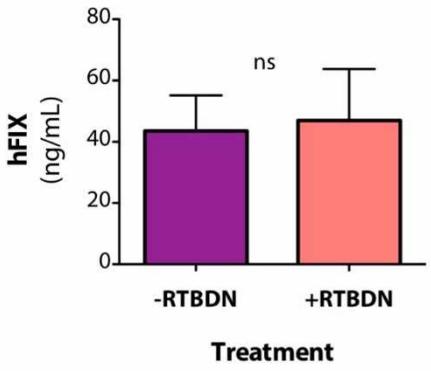

Fig. 19. The siRNA RTBDN does not enhance spontaneous homologous recombination *in vivo*. Plasma hFIX concentrations (ng/mL) of mice treated with the donor-hFIX AAV8 vector (rAAV8-donor-hFIX, 5.0E11 vg/mouse) alone (- RTBDN) or in combination with the siRNA RTBDN (2.6 µg/mouse, + RTBDN). The post-natal day 3 treatment with the siRNA RTBDN did not enhance spontaneous homologous recombination of the donor-hFIX AAV8 vector in WT newborn mice. Student *t*-test, unpaired t test, ns, P = 0.7895. N = 3 per experimental group.

3.4 The ability of siRNAs to induce AAV transduction

3.4.1 Experimental plan

Since in our first experimental approach we did not observe any effect in HDR rate, we specifically looked at viral transduction trying to reproduce the results obtained by Mano *et al.* (Mano et al., 2015). We evaluated the efficiency of two siRNAs with the highest activity and lowest toxicity, RTBDN and WWC2, to enhance viral transduction of an episomal rAAV8 vector encoding the eGFP cDNA under the transcriptional control of the α1-antitrypsin (AAT) promoter. I injected 4-days-old WT mice with the episomal rAAV8-pAAT-eGFP (1.0E+11vgp/mouse) alone or in combination with one of the two siRNAs, RTBDN or WWC2. I sacrificed the animals and collected the liver two weeks after the injections and evaluated the number of eGFP-positive cells in liver sections (Fig. 20).

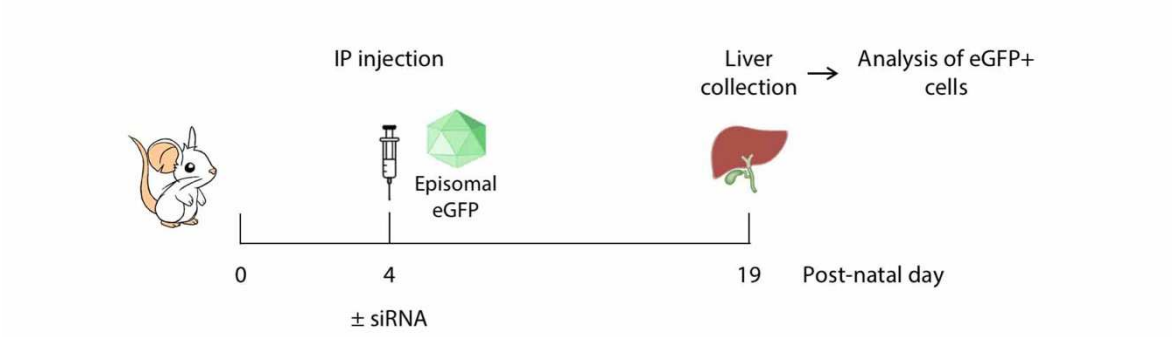

Fig. 20. The evaluation of the quality of the siRNAs RTBDN and WWC2 *in vivo*. WT newborn mice were intraperitoneally (IP) injected at post-natal day 4 (P4) with the rAAV8-pGG2-AAT-eGFP episomal vector (1.0E11 vg/mouse) alone (- siRNA) or in combination with the siRNA (2.6 μg/mouse, + siRNA). Liver was collected at P19 and the number of eGFP-positive cells was determined.

3.4.2 The siRNAs treatment does not increase viral transduction

To evaluate the efficiency of the siRNA treatment in AAV transduction, I determined the number of eGFP-positive hepatocytes in liver sections of 2-weeks-old treated mice. I observed no significant differences in the number of eGFP-positive cells with any of the two treatments (Fig. 21), suggesting that these siRNAs had no effect in increasing AAV transduction in the experimental conditions tested. Since many differences were present between the experimental strategy and conditions we used and those by Mano and colleagues, such as the age and strain of the injected mice and the administration routes, that could explain the discrepancies between ours and theirs results, we decided to not investigate

further the siRNA effect in enhancing viral transduction and we looked for a more promising strategy.

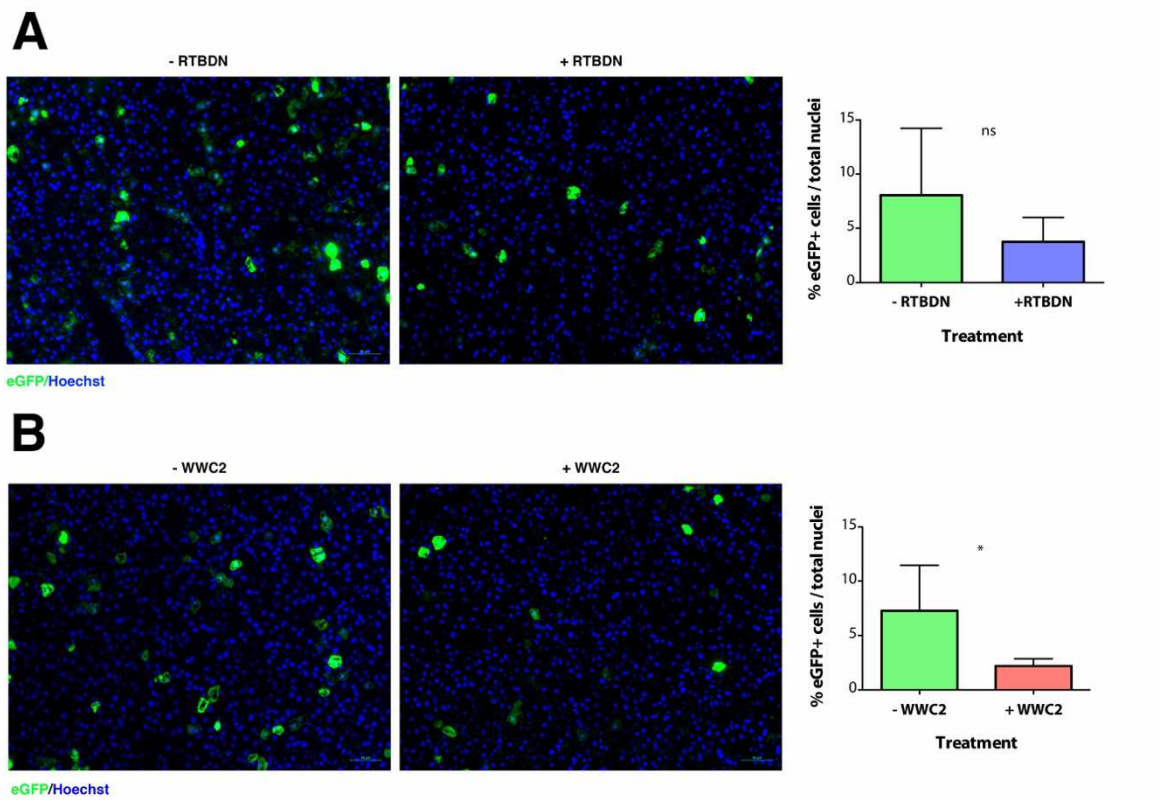

Fig. 21. The siRNAs RTBDN and WWC2 do not enhance AAV viral transduction *in vivo*. (A) The treatment with the siRNA RTBDN did not enhance transduction of the rAAV8-pGG2-AAT-eGFP vector in WT newborn mice. Left panel: Histological analysis of liver sections of mice treated with the rAAV8-pGG2-AAT-eGFP vector alone (-RTBDN) or in combination with the siRNA (+ RTBDN). Right panel: The % of eGFP-positive cells per total nuclei. Student *t*-test, unpaired t test, ns, P = 0.2391. N = 4 per experimental group. **(B)** The siRNA WWC2 did not enhance transduction of the rAAV8-pGG2-AAT-eGFP vector in WT newborn mice. Left panel: Histological analysis of liver sections of mice treated with the rAAV8-pGG2-AAT-eGFP vector alone (-WWC2) or in combination with the siRNA (+ WWC2). Right panel: The % of eGFP-positive cells per total nuclei. Student *t*-test, unpaired t test, *, P = 0.0285. N = 5 per experimental group.

3.5 Coupling GeneRide to CRISPR/*Sa*Cas9 platform

3.5.1 The rationale

It is well known that the presence of double strand breaks (DSBs) enhances homology directed repair rate (Rouet et al., 1994) and it is also possible to generate them site-specifically with engineered endonucleases (Carroll & Beumer, 2014). Therefore, in order to increase recombination rate and efficiency of the GeneRide approach, I combined it with the CRISPR/*Sa*Cas9 system (Ran et al., 2015) (Fig. 22). We expect that the *Sa*Cas9 nuclease will induce a DNA double strand break (DSB) into albumin sequence that flanks its stop

codon. In the presence of a donor template carrying a therapeutic cDNA, the DSB will be repaired by the homology directed repair (HDR) mechanism, leading to the site-specific insertion of the therapeutic sequence into the albumin locus. As a consequence of the integration event, a hybrid mRNA should be produced and translated into two functionally proteins, the albumin and the therapeutic one.

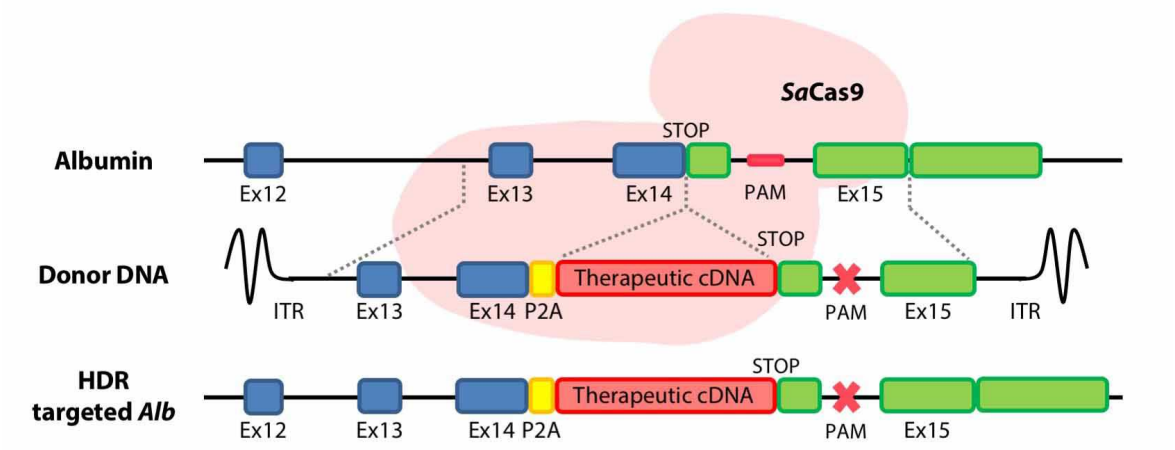

Fig. 22. Coupling GeneRide to CRISPR/*Sa*Cas9 platform. Recombination of the donor vector (Donor DNA; containing the therapeutic cDNA preceded by the 2A-peptide (P2A), and flanked by the albumin homologous regions, with modified PAM8 sequence), enhanced by DNA DSBs generated by the *Sa*Cas9 nuclease, results in the HDR-targeted albumin allele, in the chimeric mRNA and in the translation of two both separate and functionally proteins. Rectangles represent exons; thin black lines, introns; AAV inverted terminal repeats (ITR), wavy lines. Albumin exons 12 to 15 are indicated; STOP, Albumin stop codon; PAM, protospacer adjacent motif.

3.5.2 Experimental strategy

In order to target specifically and efficiently the liver, I selected serotype 8 AAV capsid for its preferential liver transduction (Asokan, Schaffer et al., 2012). The strategy that I developed in this study is based on the use of two rAAV8 vectors: one encodes the donor DNA template containing the promoterless therapeutic cDNA flanked by the albumin homology regions, and the other one encodes both the *Sa*Cas9 and the sgRNA targeting the albumin locus (Fig. 23). Neonatal mice are intravenously injected with both rAAV8 vectors, resulting in the integration of the therapeutic cDNA into the albumin locus and production of the therapeutic protein, leading to the permanent restoration of the defective liver function. The strategy can be applied to cure different disease-causing mutations using the same rAAV8 vectors, and several liver metabolic diseases by just replacing the therapeutic cDNA in the donor rAAV.

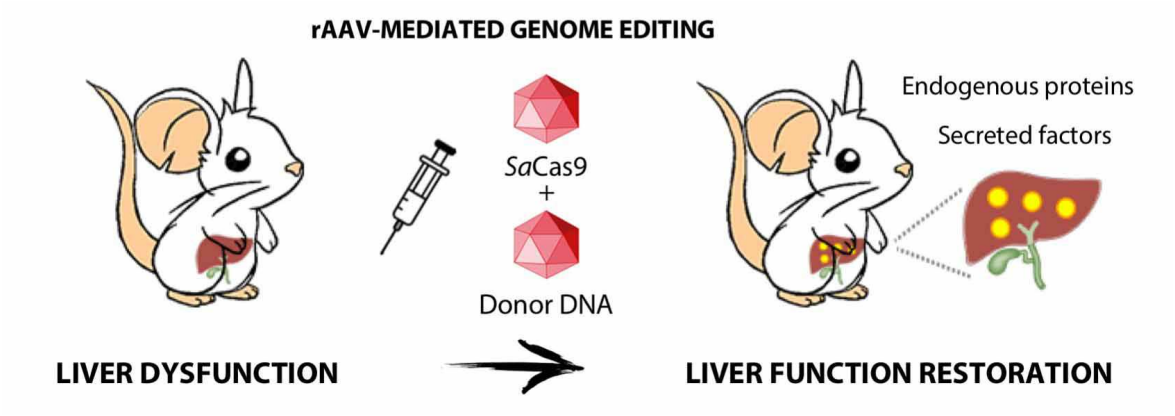

Fig. 23. GeneRide-CRISPR/*Sa*Cas9 coupled strategies can correct different liver metabolic diseases. Neonatal mice with a liver dysfunction are intravenously injected with two rAAV8 vectors: one encoding the *Sa*Cas9 and the sgRNA and one the donor DNA template. The therapeutic cDNA, once integrated, produces the defective or missing protein, such as secreted factors or endogenous enzymes, with the permanent restoration of the liver function. The therapeutic strategy can be applied to cure different disease-causing mutations and liver metabolic disorders, by just replacing the therapeutic cDNA.

3.6 The efficiency of the CRISPR/*Sa*Cas9 platform

3.6.1 Design of the single guide RNAs and their *in vitro* testing

In order to efficiently induce DNA DSBs in the albumin locus, I first looked for *Sa*Cas9 PAM sequences (NNGRRT) (Ran et al., 2015) in the genomic region flanking the exon 14 of the albumin gene, where the stop codon is located (Fig. 24). I identified 5 PAM sequences (PAM9, PAM7, PAM6, PAM5 and PAM8) and designed the corresponding sgRNAs (sgRNA9, sgRNA7, sgRNA6 and sgRNA8, respectively). My colleagues cloned all selected sgRNAs into the pX601 plasmid, which expresses the *Sa*Cas9 and the sgRNA under the transcriptional control of the CMV and U6 promoters, respectively (Fig. 25), and tested them *in vitro* in tissue culture cells (F. Porro and R. Sola, data not shown). The sgRNA7 and sgRNA8, whose target sequences were located in introns 13 and 14, respectively, resulted the most active ones to target the albumin endogenous locus and, thereby, were selected for *in vivo* experiments.

Fig. 24. Design of sgRNAs targeting the albumin locus. The 500 bp-long albumin sequence is shown. Albumin exon 14 (capital letters), albumin stop codon (STOP), flanking introns (small caps), the identified PAMs and correspondent designed sgRNAs are shown.

Fig. 25. *In vitro* testing of sgRNAs. The pX601-*Sa*Cas9 vector was used for the *in vitro* testing of all designed sgRNAs. ITR, inverted terminal repeat; CMV, Cytomegalovirus promoter; *Sa*Cas9, *Staphylococcus aureus* CAS9; bGHpA, bovine growth hormone polyadenylation signal; sgRNA, single guide RNA; Guide, incomplete sgRNA-coding sequence; U6, RNA pol III promoter.

3.6.2 *In vivo* testing of the single guide RNAs 7 and 8

In order to test the efficacy of the CRISPR/*Sa*Cas9 platform *in vivo*, my colleagues cloned the most active sgRNAs, the sgRNA7 and sgRNA8, into the pX602 plasmid, which differs from the previous one used for *in vitro* testing (pX601 plasmid) for expressing the *Sa*Cas9 nuclease under the control of the liver-specific thyroid-binding globulin (TBG) (Fig. 26).

Fig. 26. The pX602-*Sa*Cas9 plasmid. The pX602-*Sa*Cas9 vector was used for the *in vivo* testing of sgRNA7 and sgRNA8. ITR, inverted terminal repeat; TBG, thyroid-binding globulin promoter; *Sa*Cas9, *Staphylococcus aureus* CAS9; bGHpA, bovine growth hormone polyadenylation signal; sgRNA, single guide RNA; Guide, incomplete sgRNA-coding sequence; U6, RNA pol III promoter.

After the cloning of the guides, single rAAV8 vectors for each sgRNA were produced by the AAV Vector Unit at ICGEB (Trieste, Italy).

3.6.2.1 Experimental plan

To evaluate the *in vivo* efficacy of both sgRNAs to target the endogenous albumin locus, I intraperitoneally (IP) injected 4-days-old WT mice with a dose of 1.0E12 vg/mouse of the single rAAV8 vectors encoding the sgRNA7 (rAAV8-*Sa*Cas9-sgRNA7) or the sgRNA8 (rAAV8-*Sa*Cas9-sgRNA8). Two weeks after vector administration, I collected the livers, extracted genomic DNA and performed the T7 endonuclease 1 (T7E1) assay (Fig. 27).

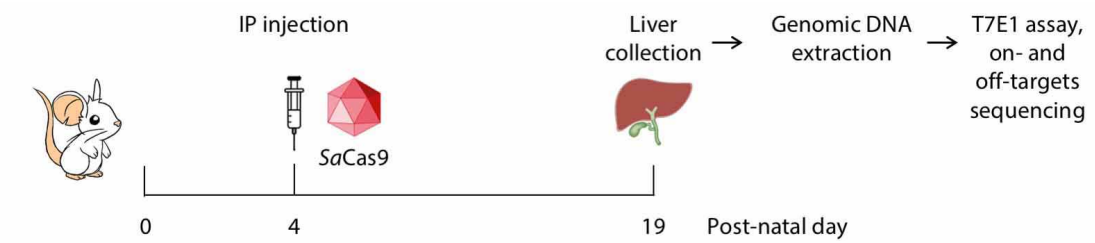

Fig. 27. *Sa*Cas9-sgRNA7 and -sgRNA8 *in vivo* testing. WT newborn mice were intraperitoneally (IP) injected at post-natal day 4 (P4) with rAAV8-*Sa*Cas9-sgRNA7 or rAAV8-*Sa*Cas9-sgRNA8 (1.0E12 vg/mouse) and the liver was collected at P19. Genomic DNA was extracted, the target region PCR amplified and the T7E1 assay was performed.

3.6.2.2 The T7E1 assay

Since genome editing can target preferentially some loci than others, it is relevant to evaluate the specific targeting rate for each locus. The T7E1 assay is an enzyme mismatch cleavage method useful for this purpose and is adopted to estimate the mutation hit-rate at a given locus (Vouillot, Thelie et al., 2015). It is based on the amplification, mediated by PCR, of target genomic regions of samples treated with the nuclease, on the denaturation and self-annealing of derived amplicons and on their treatment with the T7E1 enzyme. This endonuclease can recognize and cut mismatches in hetero-duplexes generated by INDELs introduced by NHEJ mechanism used by cells to repair induced DNA DSBs. Cleavage products are detected by standard agarose gel electrophoresis and the estimated gene modification is calculated using a formula described by Gushin *et al*. (Guschin et al., 2010). The determination of targeting efficacy by the T7E1 cleavage assay confirmed the *in vitro* results. Both sgRNAs were able to induce DNA DSBs in the target region next to the albumin stop codon and, furthermore, the sgRNA8 was the most active one, with an overall efficiency of 24 % (Fig. 28). Considering its higher activity and the fact that the target site is located more than 100 bp downstream the 5' of intron 14, far from the splice site and, thereby, with low probabilities to affect albumin pre-mRNA splicing of targeted alleles because of error-prone NHEJ mechanism, I selected the sgRNA8 for the next *in vivo* experiments.

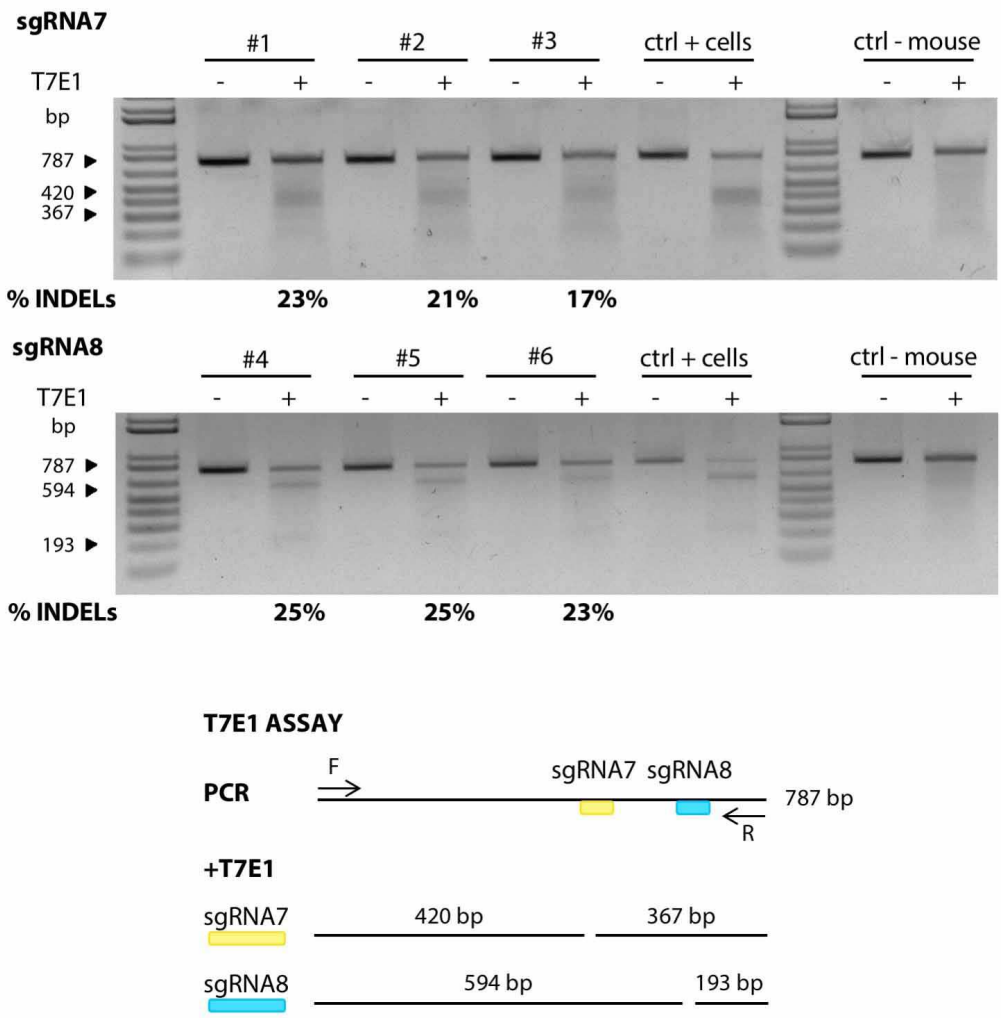

Fig. 28. *Sa*Cas9-sgRNA7 and -sgRNA8 *in vivo* efficiency. The T7E1 assay results and the derived percentage of INDELs (% INDELs) for the sgRNA7 and sgRNA8 are shown. Three mice for each sgRNA were treated and analyzed; ctrl + cells, cells treated with the corresponding pX602-*Sa*Cas9 vector, ctrl - mouse, untransduced mice. In the lower panel the expected bands of T7E1 assay for both sgRNA7 and sgRNA8 treated samples; F and R, forward and reverse PCR primers.

3.6.3 The *Sa*Cas9-sgRNA8 dose-finding experiment

3.6.3.1 Experimental plan

Since for the *in vivo* testing (Fig. 28) I transduced mice with a single high amount of rAAV8-*Sa*Cas9-sgRNA8 (1.0E12 vg/mouse), a dose-finding experiment was planned to determine the lowest one having the maximum possible effect. Then, 4-days-old WT mice were IP injected with different doses of rAAV8-*Sa*Cas9-sgRNA8: 2.5E+11, 5.0E+11 and 7.5E+11 vg/mouse (Fig. 29). Two weeks after the rAAV8 administration, I collected liver, extracted the genomic DNA and performed the T7E1 assay.

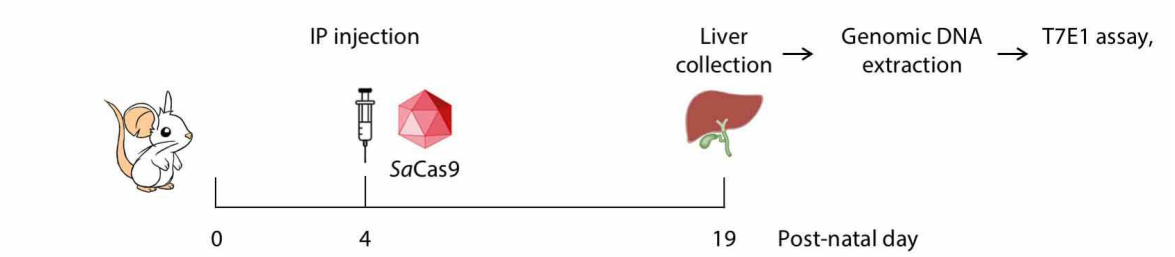

Fig. 29. *Sa*Cas9-sgRNA8 dose-finding experiment. WT newborn mice were intraperitoneally (IP) injected at post-natal day 4 (P4) with rAAV8-*Sa*Cas9-sgRNA8 (2.5E+11, 5.0E+11 and 7.5E+11 vg/mouse) and the liver was collected at P19. Genomic DNA was extracted, the target region PCR amplified and the T7E1 assay was performed.

3.6.3.2 The T7E1 assay

Estimation of INDELs percentage (% INDELs) for each dose obtained with the T7E1 assay (Fig. 30) resulted in low activity for the 2.5E11 and 5.0E11 vg/mouse (~5-6%), with an important increase for the 7.5E11 and 1.0E12 vg/mouse doses (25.5 and 31.6%, respectively). Since the increase in activity between the two higher doses was minor, I selected 7.5E11 vg/mouse of rAAV8-*Sa*Cas9-sgRNA8 as the lowest dose having the maximum effect, and it was, thereby, employed for next set of experiments.

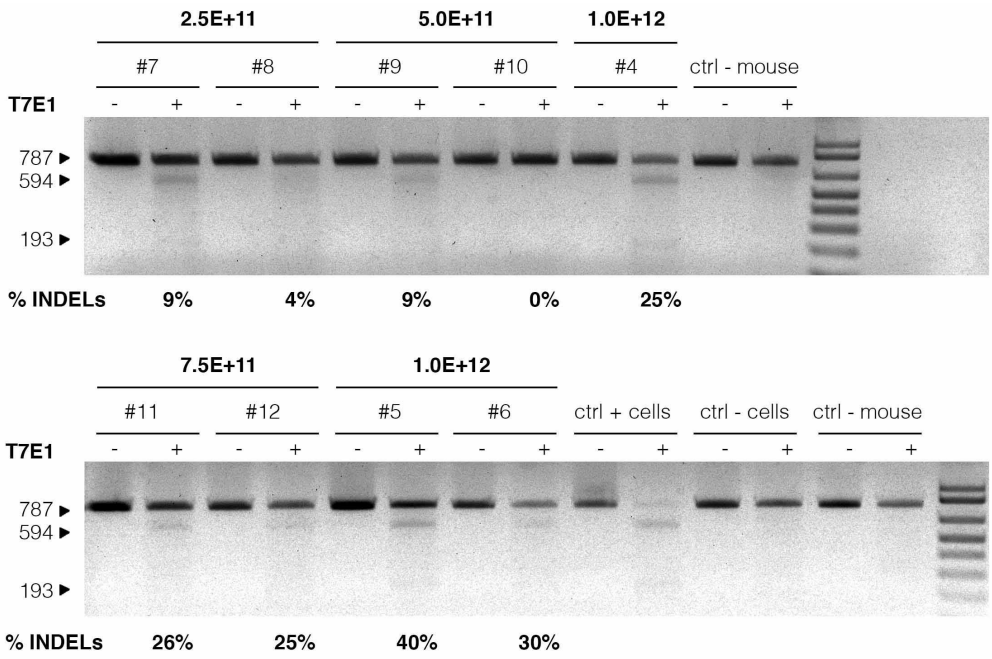

Fig. 30. Determination of the lowest and most effective dose of rAAV8-*Sa*Cas9-sgRNA8. 4-days-old WT mice were intraperitoneally transduced with different doses of rAAV8-*Sa*Cas9-sgRNA8: 2.5E+11 (#7, #8), 5.0E+11 (#9, #10), 7.5E+11 (#11, #12) and 1.0E+12 (#4, #5, #6) vg/mouse. The T7E1 assay results and the derived percentage of INDELs (% INDELs) for each rAAV8 dose are indicated. ctrl + cells, cells treated with the corresponding pX601-*Sa*Cas9 vector, ctrl - cells, untreated cells, ctrl - mouse, untransduced mice.

3.7 Comparison between intraperitoneal and intravenous administration routes

3.7.1 Experimental plan

Since one important concern of gene therapy is the potential genotoxicity of the rAAV vector, with the aim of reducing this important risk, I investigated the use of a more efficient administration route (Daly, Ohlemiller et al., 2001, Gombash Lampe, Kaspar et al., 2014, Kienstra, Freysdottir et al., 2007). Thereby, I compared intraperitoneal (IP) and intravenous (IV) injections using an episomal rAAV8 vector encoding the eGFP reporter gene under the transcriptional control of the liver-specific alpha1 anti-trypsin promoter (Fig. 31). I intraperitoneally or intravenously transduced WT newborn mice at post-natal day 4 with the same dose of 1.0E+11 vg/mouse of the rAAV8-pGG2-AAT-eGFP vector. I sacrificed and collected the liver two weeks after vector administration and evaluated the number of eGFP-positive cells in liver sections.

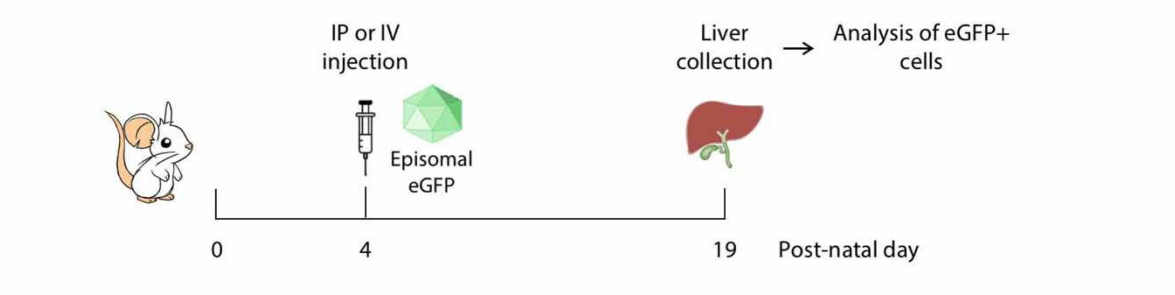

Fig. 31. IP versus IV administration routes comparison. WT newborn mice were intraperitoneally (IP) or intravenously (IV) transduced at post-natal day 4 with the same dose (1.0E+11 vg/mouse) of the rAAV8-pGG2-AAT-eGFP episomal vector. The liver was collected at post-natal day 19 and the number of eGFP positive cells in liver sections was evaluated.

3.7.2 Intravenous delivery results in higher efficiency of transduction

Quantification analysis of liver sections indicated that intravenous delivery was ~9 fold more efficient than intraperitoneal one (6.2 vs 0.7 %, respectively; Fig. 32) and, therefore, it was selected for the next experiments.

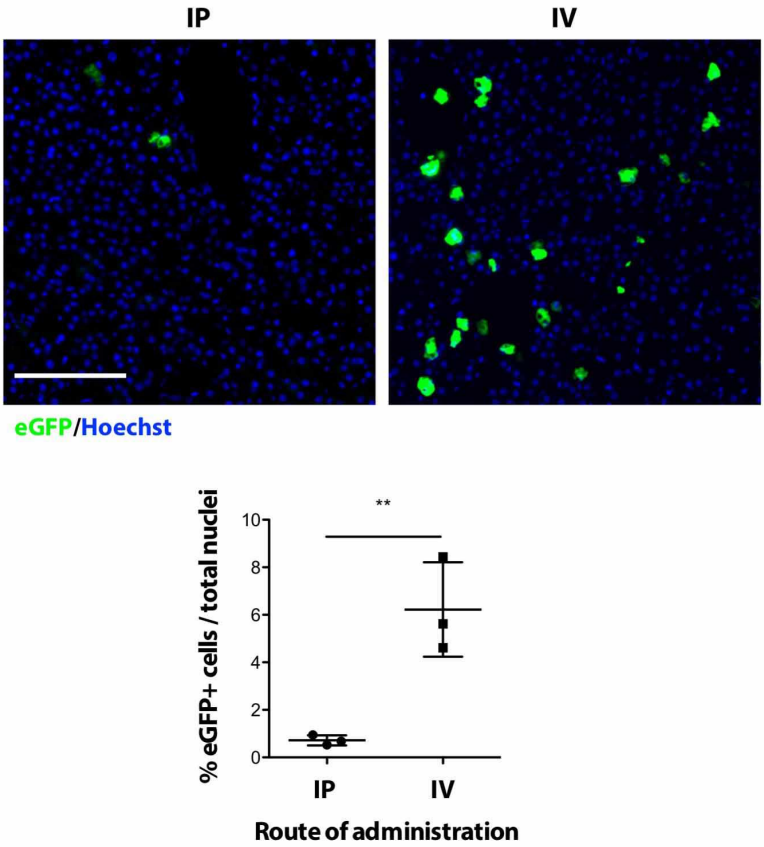

Fig. 32. The intravenous route of administration is more efficient than the intraperitoneal one. Histological analysis of liver sections of IP- or IV-transduced mice. Nuclei were counterstained with Hoechst. Representative images are shown. Scale bar 500 μm. Lower panel, quantification of the number of eGFP-positive hepatocytes. Student's *t*-test, **, P = 0.0088, n = 3 per experimental group, 10 images per animal were analyzed.

3.8 Coupling GeneRide and CRISPR/*Sa*Cas9 strategies to increase eGFP targeting rate

3.8.1 Experimental scheme

In order to find the best experimental conditions of the strategy to apply to the Crigler-Najjar type I syndrome mouse model, after the selection of the most efficient sgRNA, AAV dose and administration route, I coupled GeneRide with the CRISPR/*Sa*Cas9 platform using the eGFP reporter cDNA, which encodes for a cytoplasmic protein, to target the albumin locus (Fig. 33). To avoid potential cleavage of the donor DNA by the *Sa*Cas9 nuclease, before and after the homology directed repair mechanism, I modified its sgRNA8 PAM sequence. I

transduced WT mice at post-natal day 4 with the donor DNA encoding the eGFP (rAAV8-donor-eGFP, 8.0E11 vg/mouse) alone, or in combination with the *Sa*Cas9-sgRNA8 encoding vector using two different doses (rAAV8-*Sa*Cas9-sgRNA8, 2.0E11 or 6.0E11 vg/mouse for the low (HDR L) and high (HDR H) *Sa*Cas9 dose, respectively). Two weeks after the administration, I collected the liver and evaluated the number of eGFP positive cells in liver sections of rAAV8-treated mice.

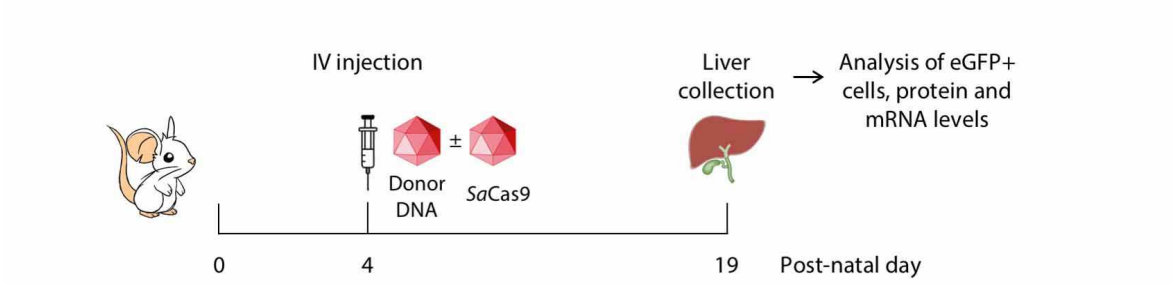

Fig. 33. Targeting of the eGFP cDNA by coupling GeneRide with CRISPR/*Sa*Cas9 platform. WT newborn mice were IV transduced with the donor-eGFP vector alone (rAAV8-donor-eGFP, 8.0E11 vg/mouse) or in combination with the *Sa*Cas9-sgRNA8 encoding vector (rAAV8-*Sa*Cas9-sgRNA8), using two different doses (2.0E11 or 6.0E11 vg/mouse). Livers were collected at P19 and analyzed.

3.8.2 Coupling GeneRide to *Sa*Cas9 results in increased number of recombinant hepatocytes

Quantification analysis of the liver sections showed that the percentage of recombinant hepatocytes were ~6% and ~13% in the low (HDR L) and high (HDR H) *Sa*Cas9 dose, respectively, reaching up to 24% in some mice in the higher dose group, with an overall increase of ~26-fold respect to spontaneous HR (Fig. 34).

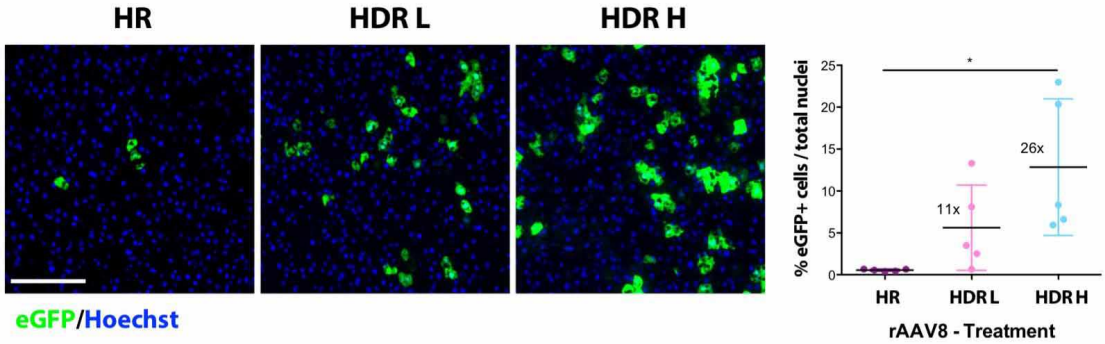

Fig. 34. Efficient targeting of the eGFP cDNA by coupling GeneRide with CRISPR/*Sa*Cas9 platform in WT newborn mice. Histological analysis of liver sections of mice treated with the rAAV8-donor-eGFP alone (HR) or in combination with rAAV8-*Sa*Cas9-sgRNA8, with two different *Sa*Cas9 doses (low, HDR L; or high, HDR H). Nuclei were counterstained with Hoechst. n=5 per group. Scale bar 500 µm. One-way ANOVA: *, P = 0.0141; Bonferroni's Comparison Test: HR versus HDR L, t = 1.447, ns; HR versus HDR H, t = 3.506, P < 0.005; HDR L versus HDR H, t = 2.059, ns.

I also evaluated the levels of eGFP protein in transduced mice by Western blot analysis. Mice treated with both rAAV8 vectors (rAAV8-donor-eGFP and rAAV8-*Sa*Cas9-sgRNA8, at low and high *Sa*Cas9 dose, HDRL and HDR H, respectively) produced an amount of the reporter protein that was up to ~30 fold higher than in mice treated with the eGFP donor vector alone (HR) (Fig. 35).

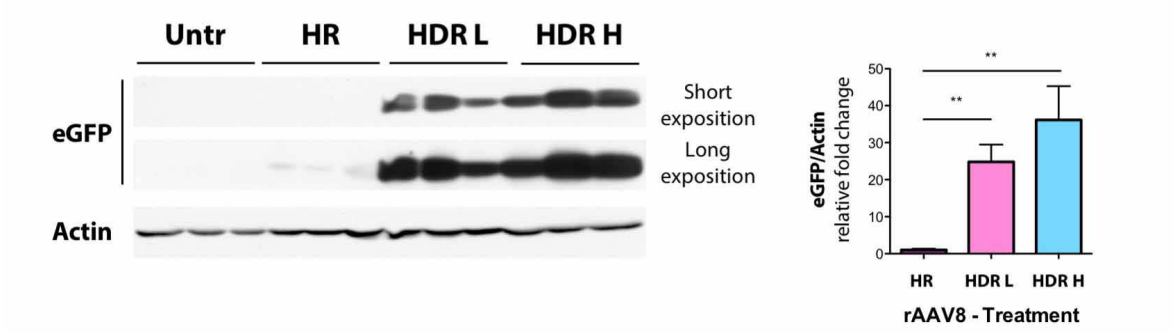

Fig. 35. eGFP protein levels in rAAV8-transduced mice. WB analysis of liver protein extracts. Short and long expositions are shown. One-way ANOVA: ***, P = 0.0010; Bonferroni's Multiple Test: HR versus HDR L, t = 4.914, P < 0.01; HR versus HDR H, t = 7.256, P < 0.01; HDR L versus HDR H, t= 2.342, ns; n = 3 per treatment.

Additionally, I determined the eGFP mRNA levels by quantitative RT-PCR and observed a significant correlation with protein expression levels (Fig. 36).

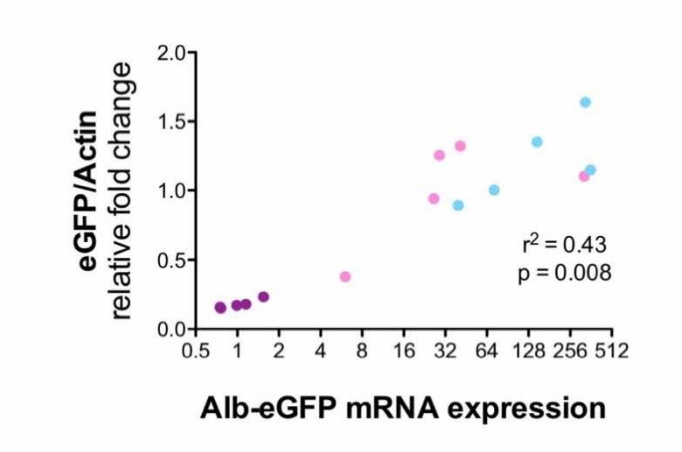

Fig. 36. Correlation between eGFP and hybrid Alb-eGFP mRNA levels. Correlation, **, P = 0.0084, r^2 = 0.4257; n = 5 per treatment; 10 images per animal were analyzed.

3.9 Comparison of recombination efficacy between post-natal day 2 and 4 vector administration

3.9.1 Experimental plan

Since the overall strategy developed in this study is based on homologous recombination, which is more efficient in highly proliferative cells (Cunningham, Dane et al., 2008), I speculated that an earlier rAAV8 administration could result in a higher integration rate. Therefore, I compared the spontaneous recombination efficiency at post-natal day 2 and at post-natal day 4 by intravenously injecting WT mice with the donor-eGFP vector (rAAV8-donor-eGFP, 8.0E11 vg/mouse). I collected the liver two weeks after the administration and evaluated the number of eGFP-positive cells in liver sections (Fig. 37).

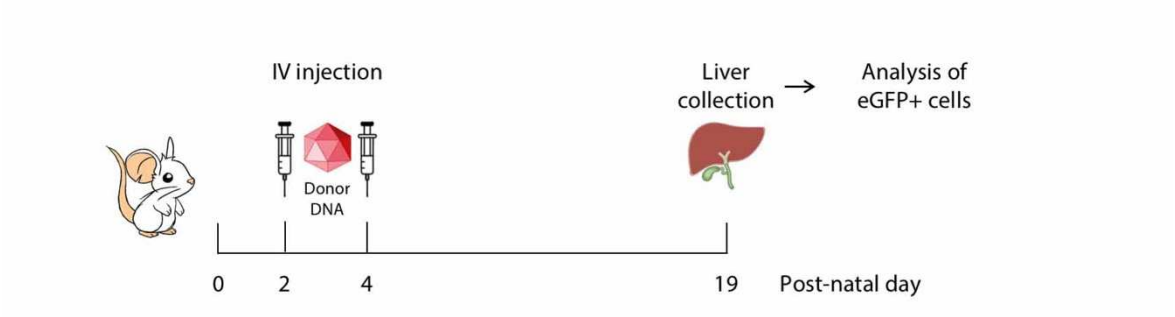

Fig. 37. Post-natal day 2 versus post-natal day 4 administration. WT newborn mice were IV transduced with rAAV8-donor-eGFP (8.0E11 vg/mouse) at post-natal day 2 or post-natal day 4. Liver was collected at P19 and the number of eGFP-positive cells was determined.

3.9.2 P2 viral transduction resulted in increased homologous recombination rate

Quantification analysis of liver sections from P2 and P4 treated mice showed that P2 transduction resulted in up to 4-fold higher number of recombinant hepatocytes than in P4-treated mice, reaching ~2% of spontaneous recombination. Thereafter, I selected post-natal day 2 administration for the next experiments (Fig. 38).

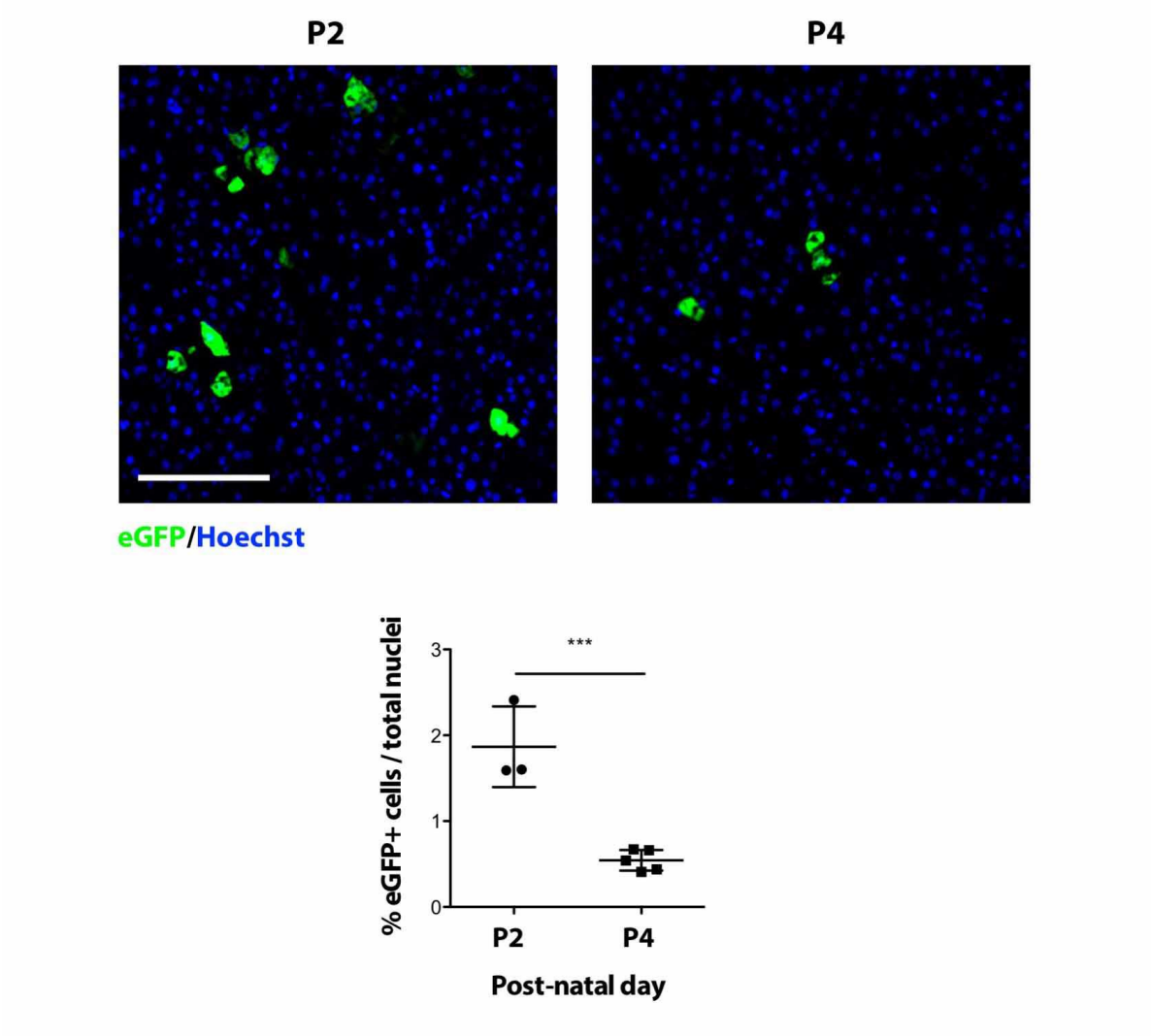

Fig. 38. Spontaneous homologous recombination is more efficient at P2 administration than at P4 one. Histological analysis of liver sections. Nuclei were counterstained with Hoechst. Scale bar 500 μm. Lower panel, quantification of the number of eGFP positive hepatocytes. Student's *t*-test, ***, P = 0.0008. n=3 and 5 for the animals transduced at P2 and P4, respectively; 10 images per animal were analyzed.

3.10 Efficient targeting and long-lasting gene expression of the hFIX reporter cDNA by coupling GeneRide with CRISPR/*Sa*Cas9 platform

3.10.1 Experimental plan

In order to evaluate the life-long efficiency by coupling GeneRide and CRISPR/*Sa*Cas9 strategies, I took advantage of the hFIX reporter cDNA, which encodes for a secreted protein. I transduced 2-days-old WT newborns with the donor DNA containing the hFIX cDNA (rAAV8-donor-hFIX, 2.0E11 vg/mouse) alone, or in combination with the *Sa*Cas9-sgRNA8 encoding vector using two different doses [rAAV8-*Sa*Cas9-sgRNA8, 6.0E10 or 2.0E11 vg/mouse, for the low (HDR L) and high (HDR H) *Sa*Cas9 dose, respectively]. I collected blood from rAAV8-treated and untreated mice by retro-orbital bleeding at 1, 2, 3,

6 and 10 months, which was the last analyzed time-point, when I performed the sacrifice of the animals (Fig. 39).

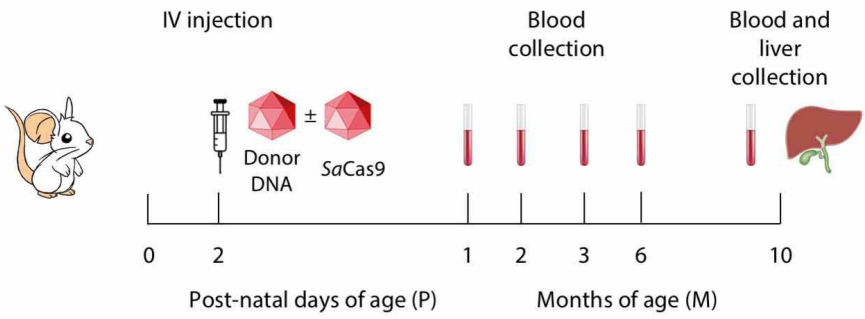

Fig. 39. Targeting of the hFIX cDNA by coupling GeneRide with CRISPR/*Sa*Cas9 platform. 2-days-old WT newborn mice were intravenously (IV) transduced with rAAV8-donor-hFIX alone (2.0E11 vg/mouse, HR) or in combination with rAAV8-*Sa*Cas9-sgRNA8, using two different *Sa*Cas9 doses (6.0E10 vg/mouse, HDR L; or 2.0E11 vg/mouse, HDR H). Blood was collected at 1, 2, 3 6 and 10 months of age and mice were sacrificed at 10 months. Liver was extracted.

3.10.2 Increased hFIX targeting rate by coupling GeneRide with CRISPR/*Sa*Cas9 platform

To evaluate the hFIX concentration in plasma of all rAAV8-transduced animals, I used a very specific ELISA-test that is based on the use of an antibody able to discriminate the human protein version from the mouse one. ELISA analysis showed that all mice treated with both donor-hFIX and *Sa*Cas9-sgRNA8 rAAV8 vectors (HDR L and HDR H) had significantly higher levels of plasma hFIX concentration than those obtained in mice transduced with the donor- hFIX alone (HR). The overall increase was roughly up to 100-fold and the corresponding hFIX values ranged from 100 to 200 % of those found in the normal human population. Importantly, these increased levels of hFIX were stable even 10 months after the administration (Fig. 40).

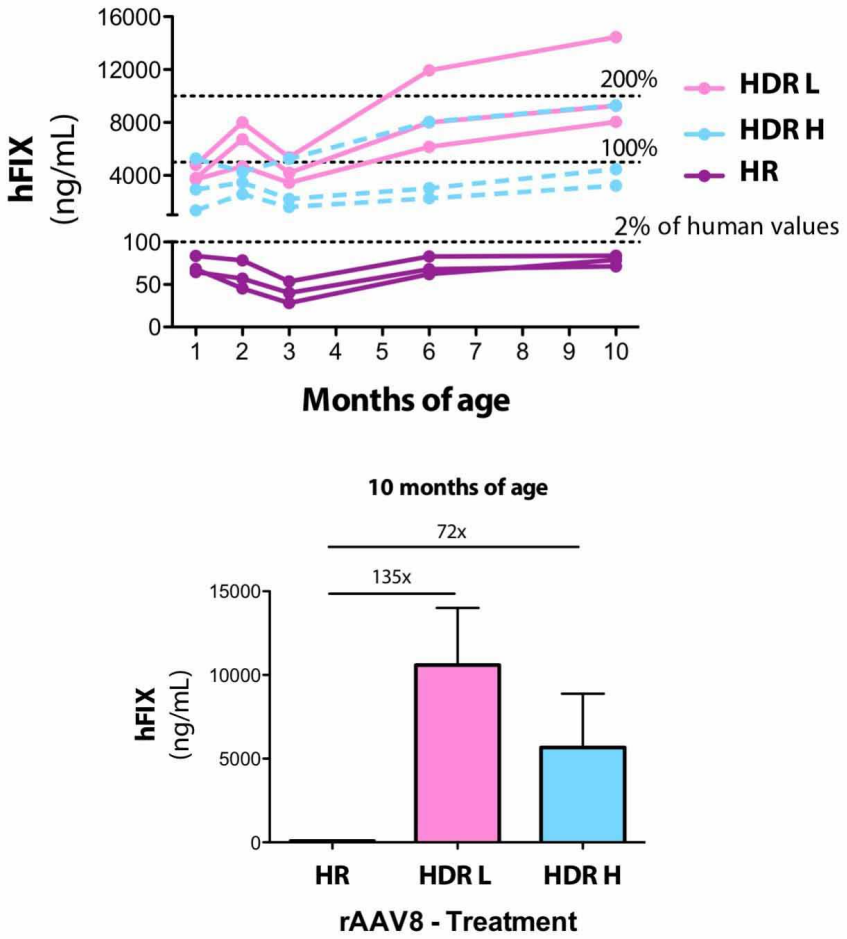

Fig. 40. Efficient targeting of the hFIX cDNA by coupling GeneRide with CRISPR/ *Sa*Cas9 in WT newborn mice. hFIX concentration (ng/mL) in plasma of rAAV8-treated WT mice. 100 ng/mL corresponds to 2% of normal values in human population. hFIX plasma concentration increased more than100-fold in mice treated with both donor and *Sa*Cas9 encoding vectors (HDR L and HDR H) respect to once treated with the donor alone (HR) and those levels were stable even 10 months after vectors administration. n = 3 for each experimental group.

3.11 Efficient, long-lasting and safe coupling of GeneRide to CRISPR/*Sa*Cas9 in CNSI mice

3.11.1 Experimental plan

In order to determine the therapeutic potential, I tested the approach in a very severe mouse model of the Crigler-Najjar syndrome type I (Bortolussi et al., 2012), a paradigmatic liver disease caused by mutations in the Ugt1 gene, selecting the best experimental conditions determined in the previous sections. I transduced Crigler-Najjar type I syndrome (CNSI) mice at post-natal day 2 by intravenously injection with the donor DNA vector encoding the hUGT1A1 alone (rAAV8-donor-hUGT1A1, 2.0E11 vg/mouse) or in combination with the *Sa*Cas9-sgRNA8 encoding vector using two different doses [rAAV8-*Sa*Cas9-sgRNA8,

6.0E10 or 2.0E11 vg/mouse for the low (HDR L) and high (HDR H) *Sa*Cas9 dose, respectively] (Fig. 41). I maintained rAAV8-treated and -untreated mice under phototherapy (PT) treatment from birth (P0) up to post-natal day 8 (P8) to allow the expression of the therapeutic protein and to avoid the risk of bilirubin-induced brain damage. This short PT treatment is not sufficient to rescue lethality of the mouse model and results in death of all mice at a later time-point [at P19 instead of P11 in untreated mice, {Bortolussi, 2014 #13)]. To monitor the therapeutic efficacy of the strategy during time, I collected blood at 1, 4, 5 and 10 months of age. I sacrificed all mice for analysis at 10 months of age.

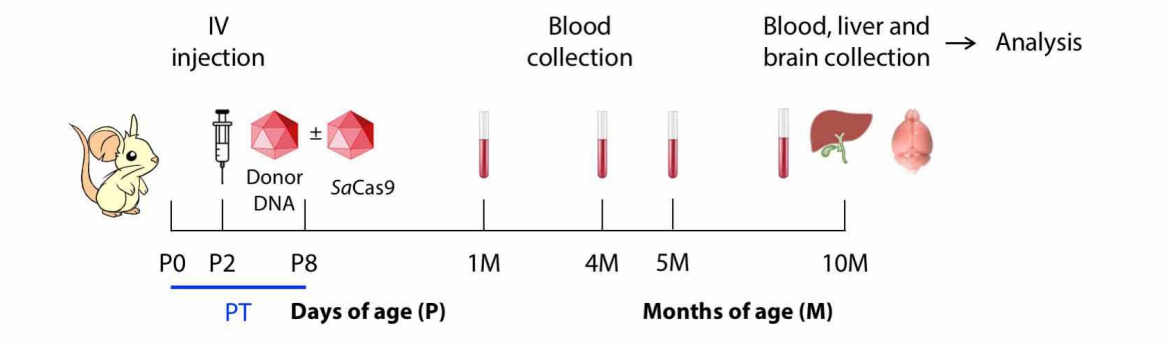

Fig. 41. Coupling GeneRide to CRISPR/*Sa*Cas9 platform in Crigler-Najjar mice. Ugt1$^{-/-}$ newborns were intravenously (IV) transduced with rAAV8-donor-hUGT1a1 alone (2.0E11 vg/mouse, HR) or in combination with rAAV8-*Sa*Cas9-sgRNA8 using two different *Sa*Cas9 doses (6.0E10 vg/mouse for the low (HDR L) or 2.0E11 vg/mouse for the high one (HDR H)). Mice were maintained under phototherapy (PT) from birth to post-natal day 8 (P0-P8 PT). Blood was collected at 1, 4, 5 and 10 months and mice were sacrificed at 10 months. Liver and brain were extracted.

3.11.2 GeneRide and CRISPR/*Sa*Cas9 coupling results in complete rescue from neonatal lethality with life-long normal plasma bilirubin levels

All the rAAV8 treatments, consisting in the donor vector alone (HR) or in two different combinations of donor and nuclease-encoding vectors (HDR L and HDR H), resulted in the rescue from neonatal lethality. Indeed, newborns who received only phototherapy from birth to post-natal day 8 died before day 19 because of the very severe brain damage induced by unconjugated hyperbilirubinemia (Fig. 42), as previously observed {Bortolussi, 2014 #13}.

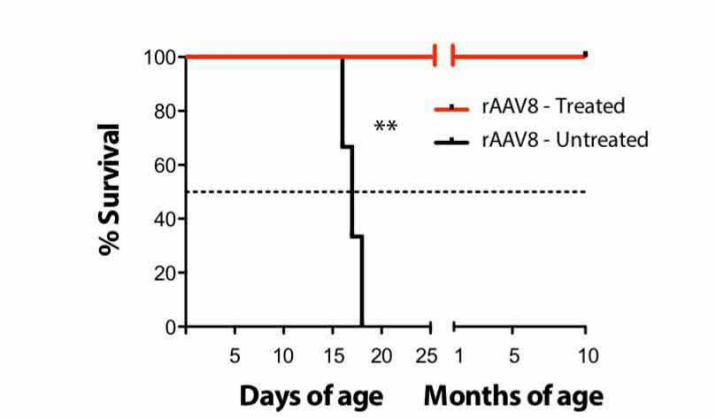

Fig. 42. The rescue of neonatal lethality of CNSI mice. Kaplan-Meier survival curve. All rAAV8-treated mice survived, while all mutant mice treated only with PT up to P8 died before P19. Long-rank (Mantel-Cox) Test, **, P = 0.0020. n =3 per rAAV8-untreated, n = 8 per rAAV8 treated.

I determined the overall efficacy of the treatment by measuring the levels of total bilirubin (TB) in the plasma of the animals. All mice treated with both donor-hUGT1A1 and *Sa*Cas9-sgRNA8 rAAV8 vectors (HDR L and HDR H) had plasma bilirubin levels significantly lower than those of mice treated with only donor-hUGT1A1 (HR). Furthermore, these values were similar to those of WT littermates for all the duration of the experiment, up to 10 months after the rAAV8 administration (Fig. 43), suggesting the life-long therapeutic efficacy of the developed strategy.

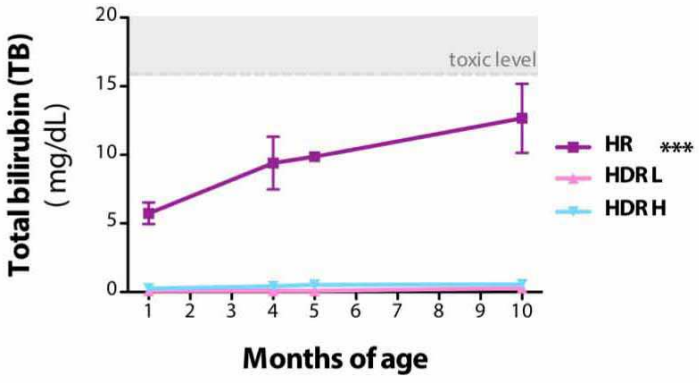

Fig. 43. GeneRide coupled to CRISPR/*Sa*Cas9 platform converted a lethal phenotype with a normal one with life-long efficacy. Total bilirubin (TB) levels were determined in plasma at 1, 4, 5 and 10 months. TB levels of all rAAV8-treated mice were similar to WT littermates up to 10 months after the administration. Two-way ANOVA, Treatment, ***, Time, **, Interaction, ***, HR versus HDR L/H, ***, n =3 per HR, HDR H; n = 2 per HDR L.

3.11.3 The therapeutic protein is produced at supra-physiological levels by 3-4% of hepatocytes

I determined hUGT1A1 protein levels by Western blot using an antibody that can recognize both mouse and human versions (Fig. 44). WB analysis showed that mice transduced with both rAAV8 vectors (HDR L and HDR H) produced supra-physiological amounts of the therapeutic protein reaching levels that were up to 6-fold higher than those detected in the same amount of WT liver protein extracts. I was not able to detect any signal in the mice treated with the donor-hUGT1A1 alone (HR), suggesting that the protein levels could be below the WB detection limit reached with the utilized antibody.

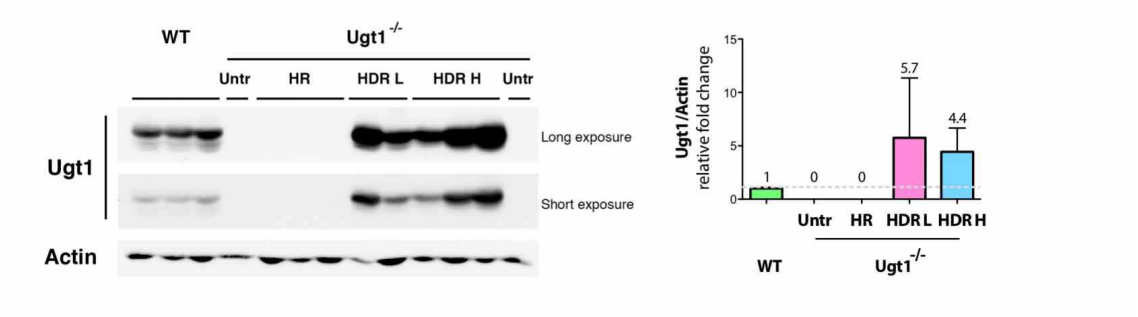

Fig. 44. GeneRide- and *Sa*Cas9- treated mice produced a supra-physiological amount of UGT1. WB analysis of liver protein extracts using an anti-Ugt1 antibody with human and mouse specificity. Treated animals with both donor-hUGT1A1and *Sa*Cas9-sgRNA8 encoding vectors (HDR L and HDR H) had UGT1A1 protein levels that were 4/6-fold higher than those present in the same amount of WT liver protein extracts. Short and long expositions are shown. Right panel: Quantification of the WB. One-way ANOVA, P = 0.0088, **; Bonferroni's multiple comparison test, UNTR/HR versus HDR H, *; n = 3 per WT, HR, HDR H; n = 2 per Untr, n = 2 per HDR L.

In order to estimate the percentage of recombinant hepatocytes, I performed the immunofluorescence analysis of liver sections with a human-specific anti-UGT1A1 antibody. Quantification analysis showed that 3.0 to 3.6 % of hUGT1A1-positive hepatocytes were present in HDR L and HDR H experimental groups, which produced a supra-physiological amount of the therapeutic enzyme. The number of recombinant cells increased up to 90 times in mice treated with both donor-hUGT1A1 and *Sa*Cas9-sgRNA8 vectors respect to those present in mice treated with the donor vector alone. Furthermore, edited cells were organized in clusters, suggesting the presence of early recombination events and clonal proliferation (Fig. 45).

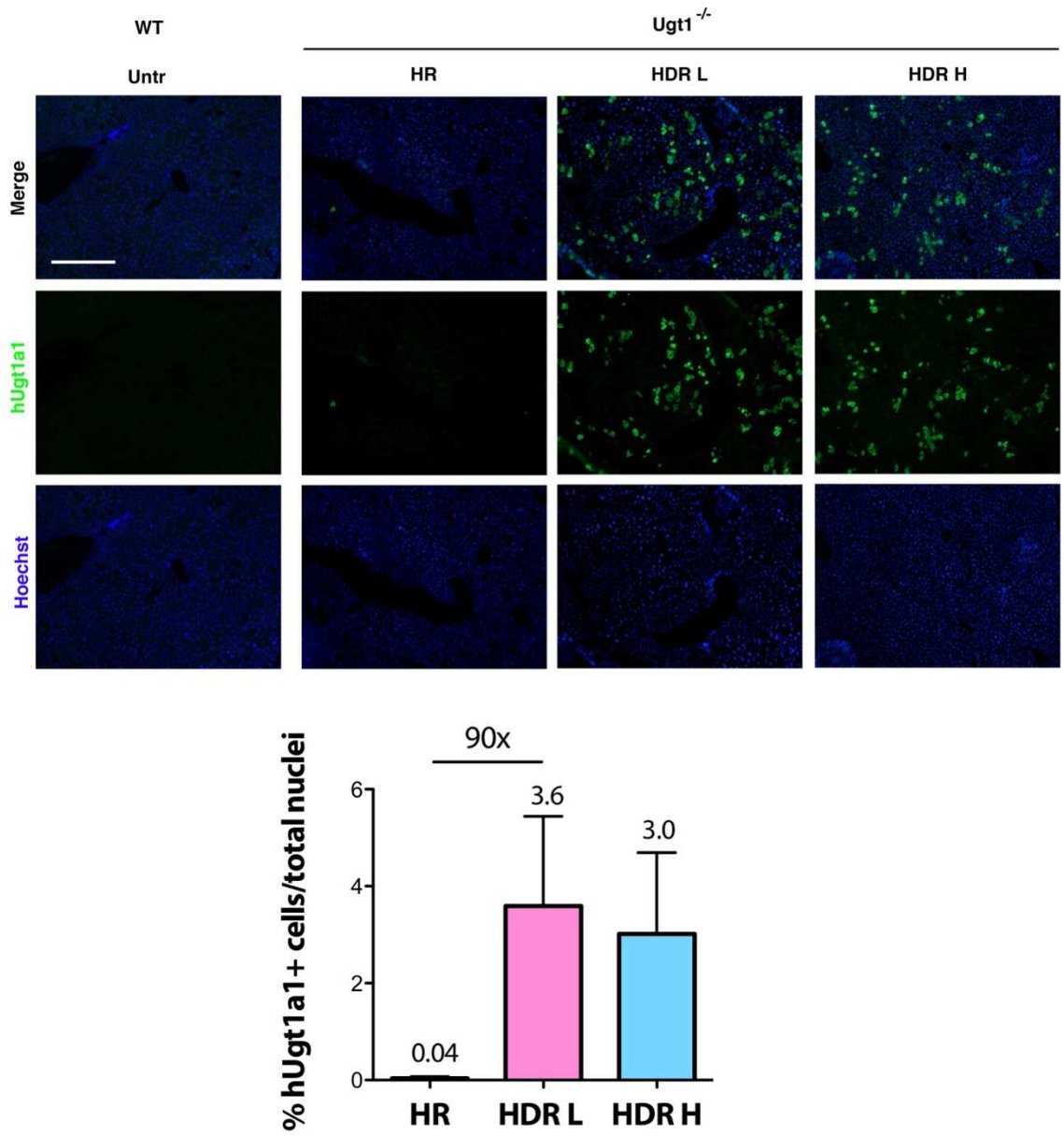

Fig. 45. GeneRide and CRISPR/*Sa*Cas9 combined strategies enhanced the percentage of recombinant hepatocytes up to 90 times in CNSI mice. Immunofluorescence analysis of liver sections of Ugt1$^{-/-}$ mice treated with rAAV8-donor-hUGT1a1 alone (HR) or in combination with two different doses of rAAV8-*Sa*Cas9-sgRNA8 (HDR L and HDR H). About 3.0-3.6% of hepatocytes were hUGT1A1-positive, with cluster localization, consistent with early recombination events and clonal proliferation of the targeted cells. Sections were stained with a human-specific anti-UGT1A1 antibody. Nuclei were counterstained with Hoechst. Lower panel: Quantification of hUgt1a1 positive hepatocytes of liver sections. Student's *t*-test, HR versus HDR, *, P = 0.0129; n = 3 per HR, n = 5 per HDR. HDR L and HDR H are joined together for the statistical analysis.

3.11.4 Treated mice have normal brain architecture and dendritic arborisation

As previously discussed, neonatal lethality of CNSI mice is due to neurological damage induced by prolonged unconjugated hyperbilirubinemia. Since all rAAV8-treated mice had plasma TB levels that were life-compatible and, moreover, those of mice treated with coupled GeneRide and CRISPR/*Sa*Cas9 platforms were comparable to WT littermate ones, even 10 months after the vector administration, I expected normal cerebellar and brain architecture, without neurological damage. In order to verify this hypothesis, I evaluated cerebellar layer thickness in WT untreated and Ugt1$^{-/-}$ rAAV8-treated mice. The analysis of brain sections confirmed the hypothesis, showing no significant differences in brain architecture between rAAV8-treated and -untreated mice (Fig. 46).

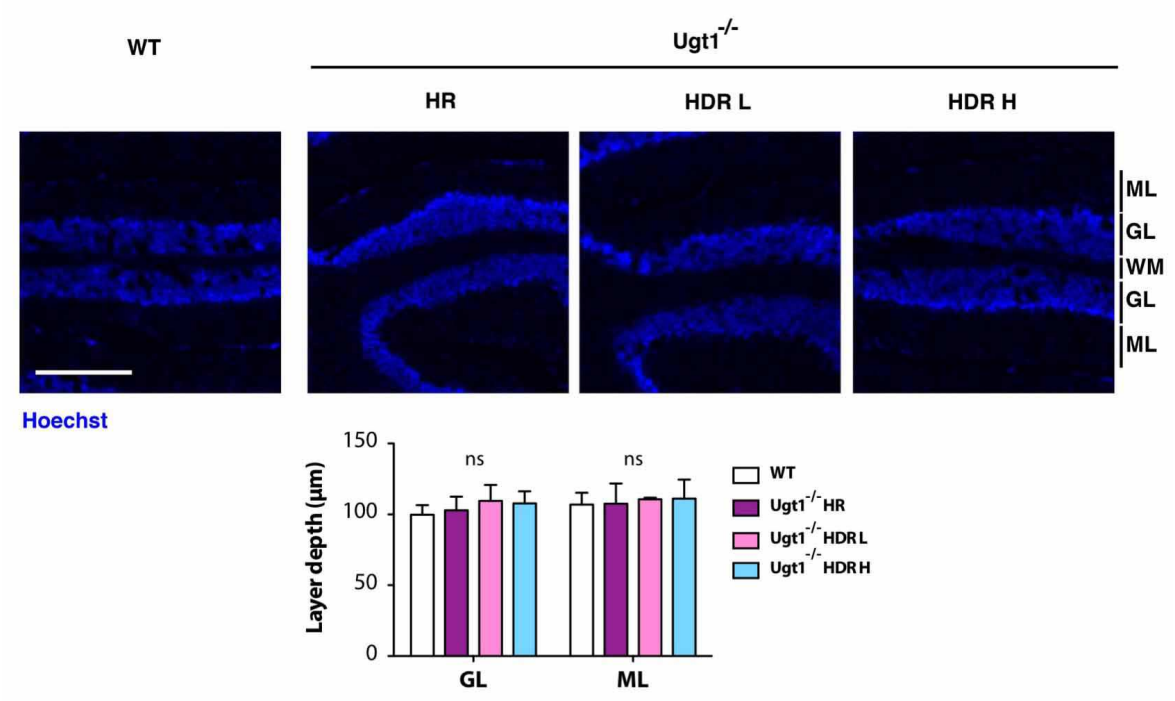

Fig. 46. Ugt1$^{-/-}$ rAVV8-treated mice showed normal cerebellar layer thickness. Cerebellar layer thickness was determined in WT untreated (Untr) and Ugt1$^{-/-}$ rAAV8-treated mice at 10 months of age with the hUGT-donor DNA alone (HR) or in combination with two different *Sa*Cas9 doses (low, HDR L; or high, HDR H), using Hoechst-stained brain sections. Representative images are shown. ML, molecular layer; GL, granular layer; WM, white matter. Scale bar = 480 µm. Two-way ANOVA: interaction, ns, P = 0.9721; treatment, ns, P = 0.6803; layer, ns, P = 0.3966; n = 3 per WT, HR and HDR H, n = 2 per HDR L.

In addition, to more finely determine potential bilirubin-induced damage in the cerebellum, I performed immunofluorescence analysis of brain sections with an anti-calbindin antibody to count the number of Purkinje cells and measure their arborisation. I counted about 6 to 8 Purkinje cells per mm, finding no variations between rAAV8-treated and -untreated WT mice (Fig. 47). The normal tissue architecture and dendritic arborisation confirmed the

absence of damage in the cerebellum of treated mice, and the life-long therapeutic efficiency of the developed strategy.

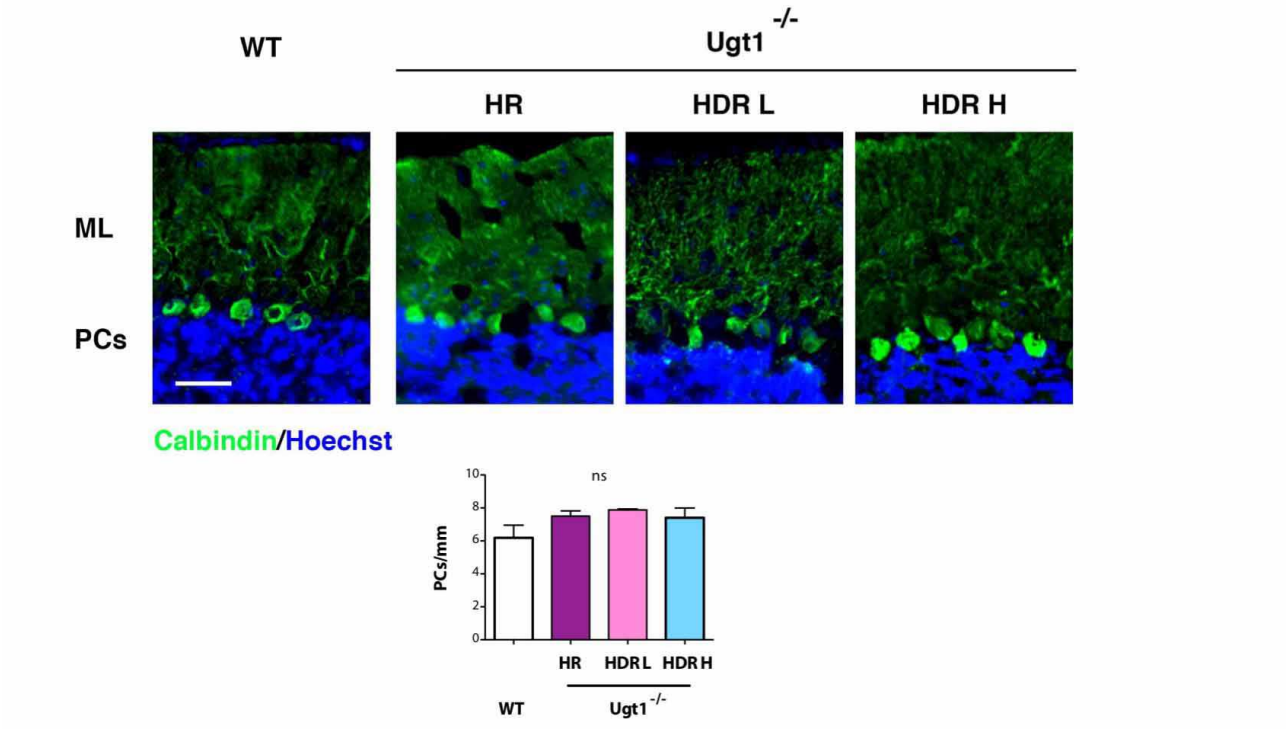

Fig. 47. Ugt1$^{-/-}$ rAVV8-treated mice showed normal Purkinje cells numbers. Purkinje cells immunofluorescence analysis of cerebellar sections using an anti-Calbindin specific antibody. Nuclei were counterstained with Hoechst. Scale bar 50 μm. ML, molecular layer; PCs, Purkinje cells. Quantification of PCs density. One-way ANOVA, ns, P = 0.0368. N = 3 per WT, HR and HDR H; N = 2 per HDR L.

3.11.5 Treated mice presented normal liver histology with no inflammatory response

Since the supra-physiological levels of the therapeutic protein produced by the hepatocytes of CNSI mice treated could have adverse effects and undesired consequences in the health of the animals, I evaluated liver histology by performing Hematoxylin and Eosin (H&E) and Masson's trichrome stainings (Fig. 48). No abnormalities such as fibrosis and leukocyte infiltration were found in all rAAV8-treated mice, whose liver sections were comparable to age-matched WT ones.

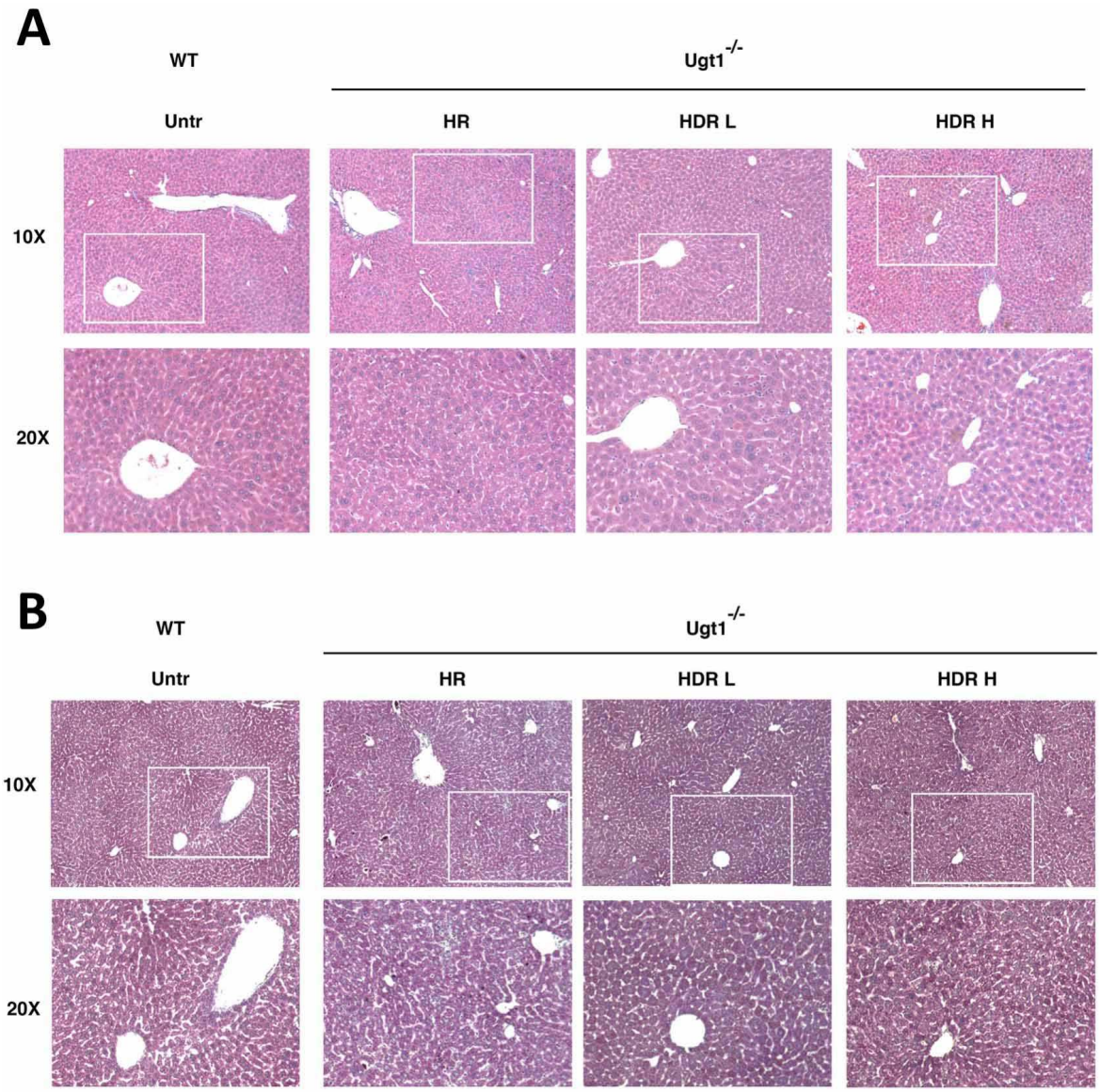

Fig. 48. Ugt1$^{-/-}$ rAVV8-treated mice showed normal liver histology. (**A**) (**B**) Haematoxylin-Eosin (H&E) (A) and Masson's trichrome (B) stainings of liver sections from WT untreated (Untr) and Ugt1$^{-/-}$ rAAV8-treated mice (M10) with the donor-hUGT alone (HR) or in combination with two different *Sa*Cas9 doses (low, HDR L; or high, HDR H). 10 x and 20 x magnifications are shown.

In order to investigate the safety of the strategy, I evaluated the expression of some of the most important inflammatory markers: TNFα, CD8, CD4 and INFγ. The mRNA levels of all mentioned genes were determined by quantitative RT-PCR analysis, showing no significantly change between untreated and treated animals (Fig. 49). These results confirmed the normal liver conditions of treated mice, already suggested by liver histology (Fig. 48).

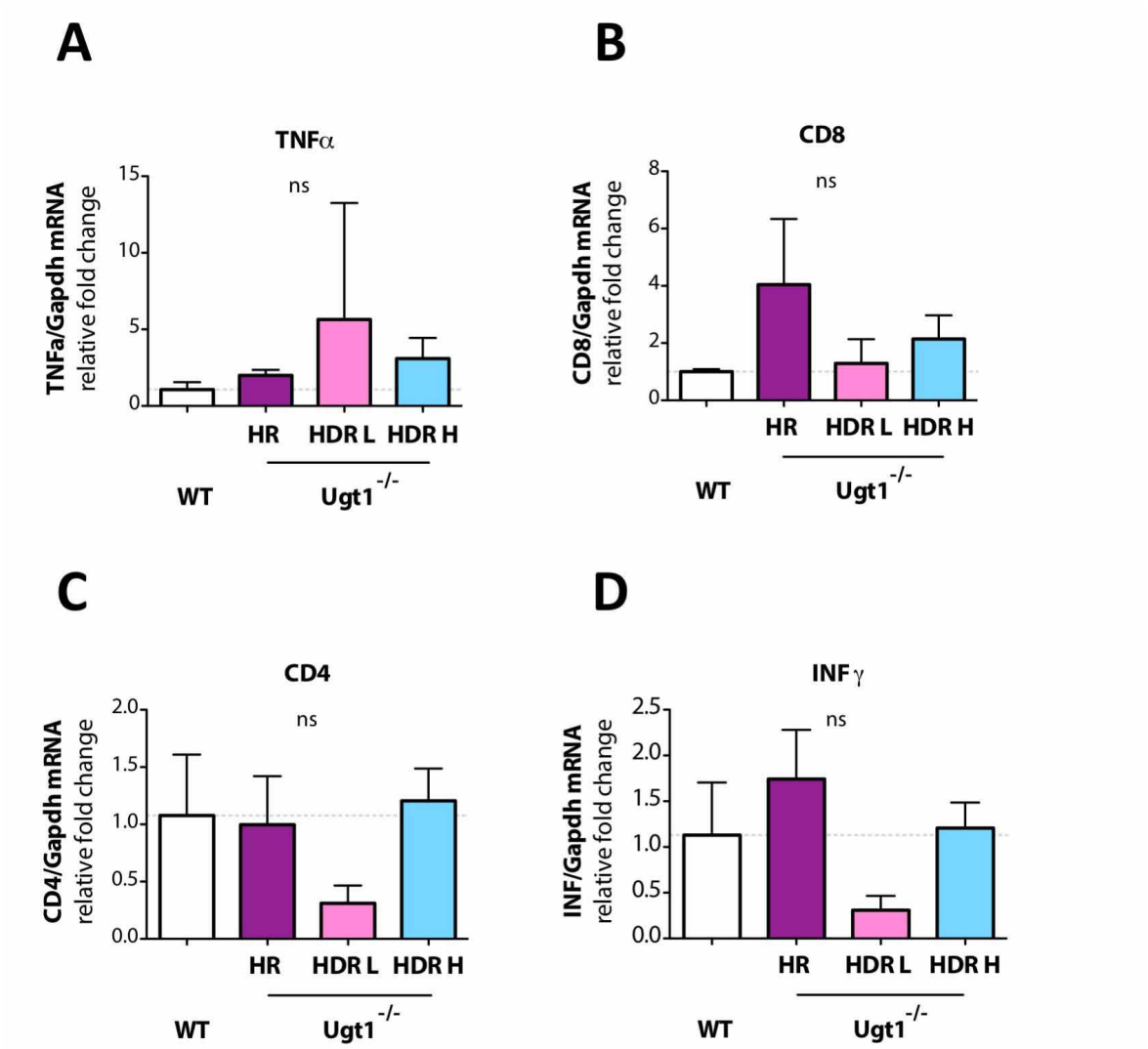

Fig. 49. Ugt1$^{-/-}$ rAVV8-treated mice showed no evidence of inflammation. (**A-D**) Evaluation of the mRNA levels by qRT-PCR of TNFα (A), CD8 (B), CD4 (C) and INFγ (D) of WT untreated and Ugt1$^{-/-}$ rAAV8-treated mice with the hUGT-donor DNA alone (HR) or in combination with two different *Sa*Cas9 doses (low, HDR L; or high, HDR H), at 10 months of age. Gapdh was used to normalize all inflammatory markers levels. One-way ANOVA: TNFα, ns, P = 0.4394; CD8, ns, P = 0.1054; CD4, ns, P = 0.1688; INFγ, ns, P = 0.0575. n = 2 per HDR L, n = 3 per WT, HR and HDR H.

3.12 Coupling GeneRide to CRISPR/*Sa*Cas9 results in a reassuring safety profile

3.12.1 Albumin expression was not affected by gene targeting

With the aim of verifying whether targeting the albumin locus after its coding sequence could affect gene expression, I determined plasma albumin levels of all experimental groups in the eGFP-, hFIX-, and UGT1A1-editing experiments. I observed that neither at 3 weeks nor at 10 months after rAAV8 vector administrations, plasma albumin levels were affected (Fig. 50).

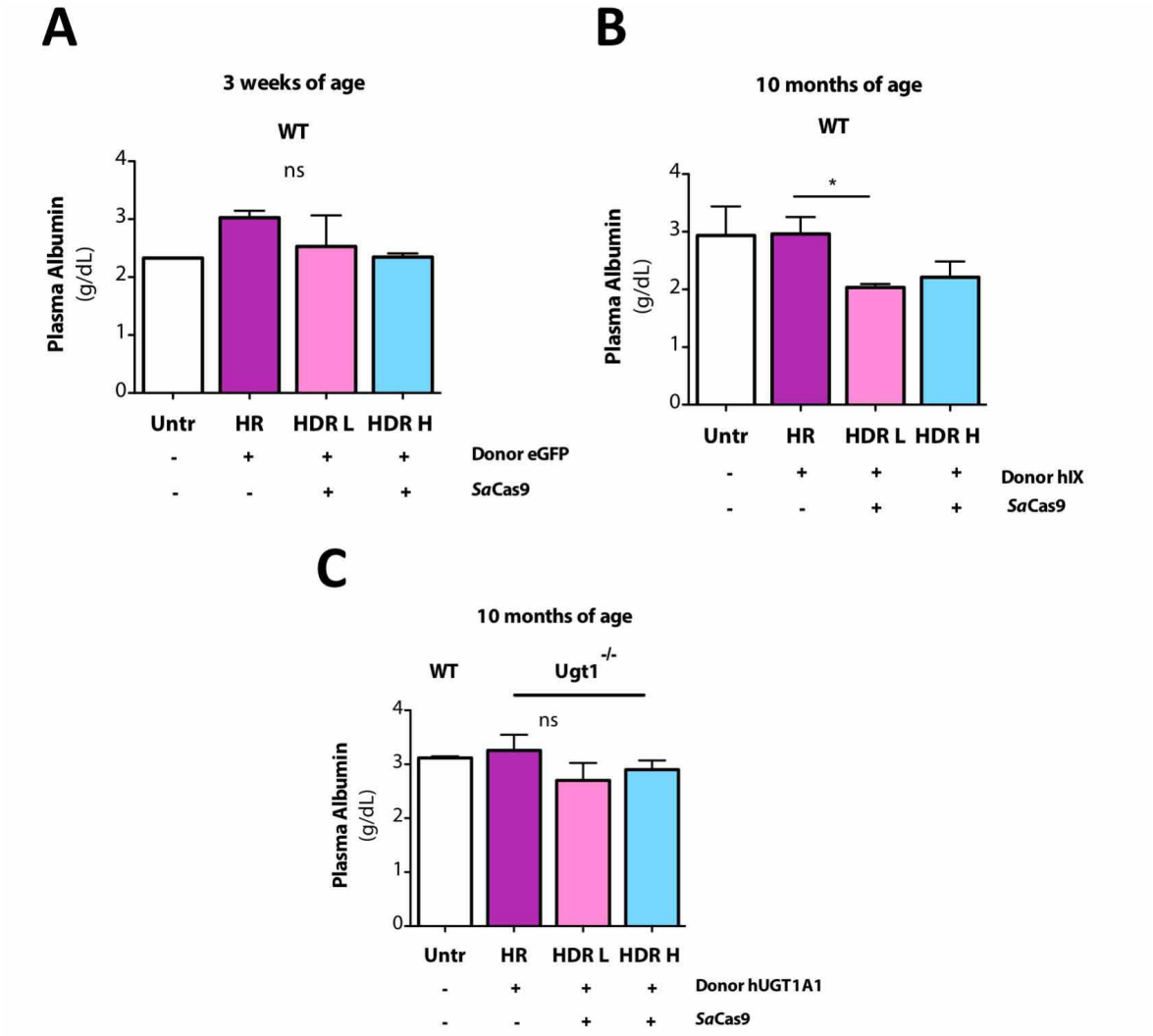

Fig. 50. Normal protein levels of albumin after *Sa*Cas9 administration. (**A**) Plasma albumin evaluation of WT mice untreated and treated at P4 with the eGFP-donor DNA vector (HR) alone or in combination with the *Sa*Cas9-sgRNA8 vector, at low (HDR L) or high *Sa*Cas9 dose (HDR H). N = 5 per experimental group. (**B**) Plasma albumin evaluation of WT mice untreated and treated at P2 with the hFIX-donor DNA vector (HR) alone or in combination with the *Sa*Cas9-sgRNA8 AAV8 vector, at low (HDR L) or high *Sa*Cas9 dose (HDR H). N = 3 per experimental group One way ANOVA, *, P = 0.0149. Bonferroni's Multiple Comparison Test, HR versus HDR L, *. (**C**) Plasma albumin evaluation of WT untreated and Ugt1$^{-/-}$ treated mice at P2 with hUGT-donor DNA (HR) alone or in combination with *Sa*Cas9-sgRNA vector, at low (HDR L) or high *Sa*Cas9 dose (HDR H). N = 3 per Untr, HR and HDR; N = 2 per HDR L. One way ANOVA, ns. Bonferroni's Multiple Comparison Test, ns.

I also evaluated albumin mRNA levels in WT mice treated only with *Sa*Cas9-sgRNA8 encoding vector whose liver was collected at different post-natal days after rAAV8 administration and in Ugt1$^{-/-}$ treated mice. qRT-PCR analysis did not highlight any significant difference between untreated and treated animals (Fig. 51), demonstrating that albumin expression, neither at protein nor at mRNA levels, was affected.

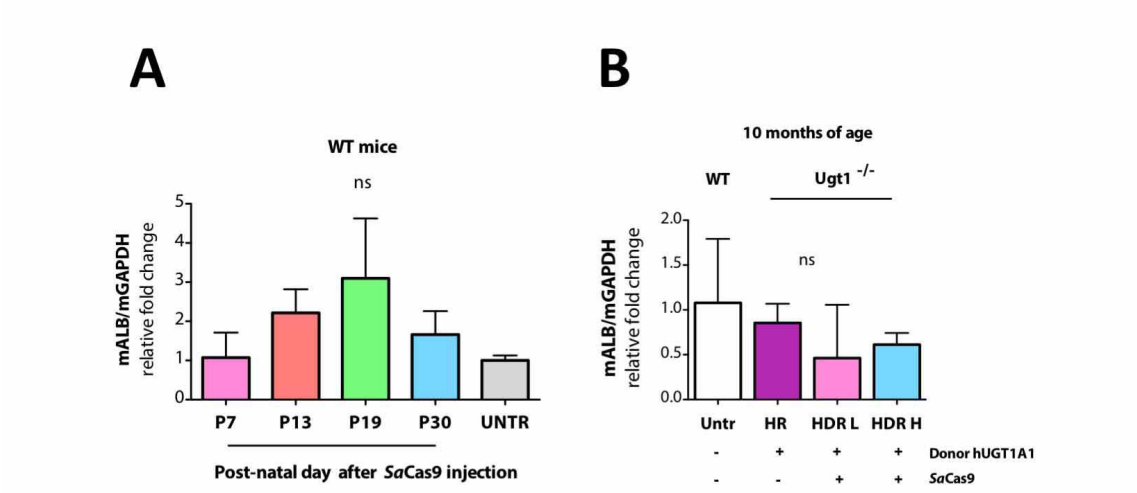

Fig. 51. Normal mRNA levels of albumin after *Sa*Cas9 administration. (**A**) Albumin mRNA levels of WT mice untreated (UNTR) and treated with only rAAV8-*Sa*Cas9-sgRNA8 (2.0E+11 vg/mouse) at P2. Mice were sacrificed at different post-natal days (P7, P13, P19, and P30) and the livers analyzed. One-way ANOVA, ns, P = 0.0979. N = 2 per UNTR; N = 3 per P7, P13, P19 and P30. (**B**) Albumin mRNA levels of WT mice untreated (Untr) and Ugt1$^{-/-}$ rAAV8-treated mice with hUGT-donor DNA (HR), or with hUGT1-donor DNA and *Sa*Cas9 encoding AAV8 vectors, at low (HDR L) or high *Sa*Cas9 dose (HDR H). One-way ANOVA, ns, P = 0.4923. Bonferroni's Multiple Comparison Test, ns, N = 3 per Untr, HR and HDR H, N = 2 per HDR L.

3.12.2 Analysis of time-persistence of *Sa*Cas9 in the transduced liver

3.12.2.1 Experimental plan

Since one of the most important concerns of the use of the CRISPR/Cas9 platform is represented by its potential unspecific activity, which may be further increased as a consequence of its long-term persistence in the target tissue, I evaluated *Sa*Cas9 expression at different post-natal days in WT mice that were treated at P2. I intravenously injected WT mice at post-natal day 2 (P2) with a dose of 2.0E+11 vg/mouse of rAAV8-*Sa*Cas9-sgRNA8 and collected the livers at P7, P13, P19 and P30 (Fig. 52).

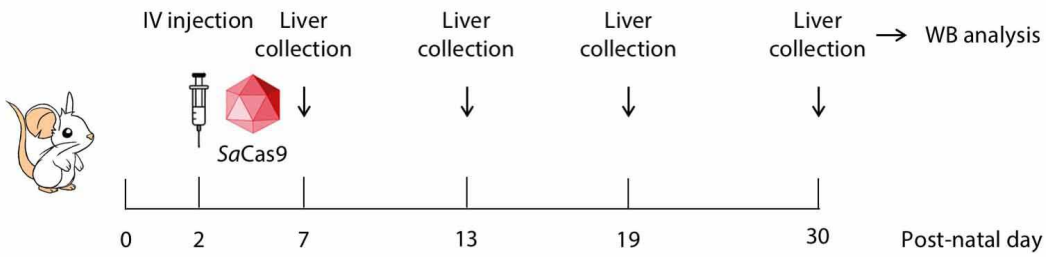

Fig. 52. *Sa*Cas9 time-long persistence. WT newborn mice were intravenously transduced with rAAV8-*Sa*Cas9-sgRNA8 (2.0E+11 vg/mouse) at post-natal day 2. Livers were collected at post-natal days 7, 13, 19 and 30 and analyzed by WB. IV, intravenous; *Sa*Cas9, rAAV8-*Sa*Cas9-sgRNA8.

3.12.2.2 The SaCas9 protein levels decrease shortly after vector administration

WB analysis of liver protein extracts showed that *Sa*Cas9 protein levels decreased after rAAV-administration, reaching undetectable levels at post-natal day 30 (Fig. 53).

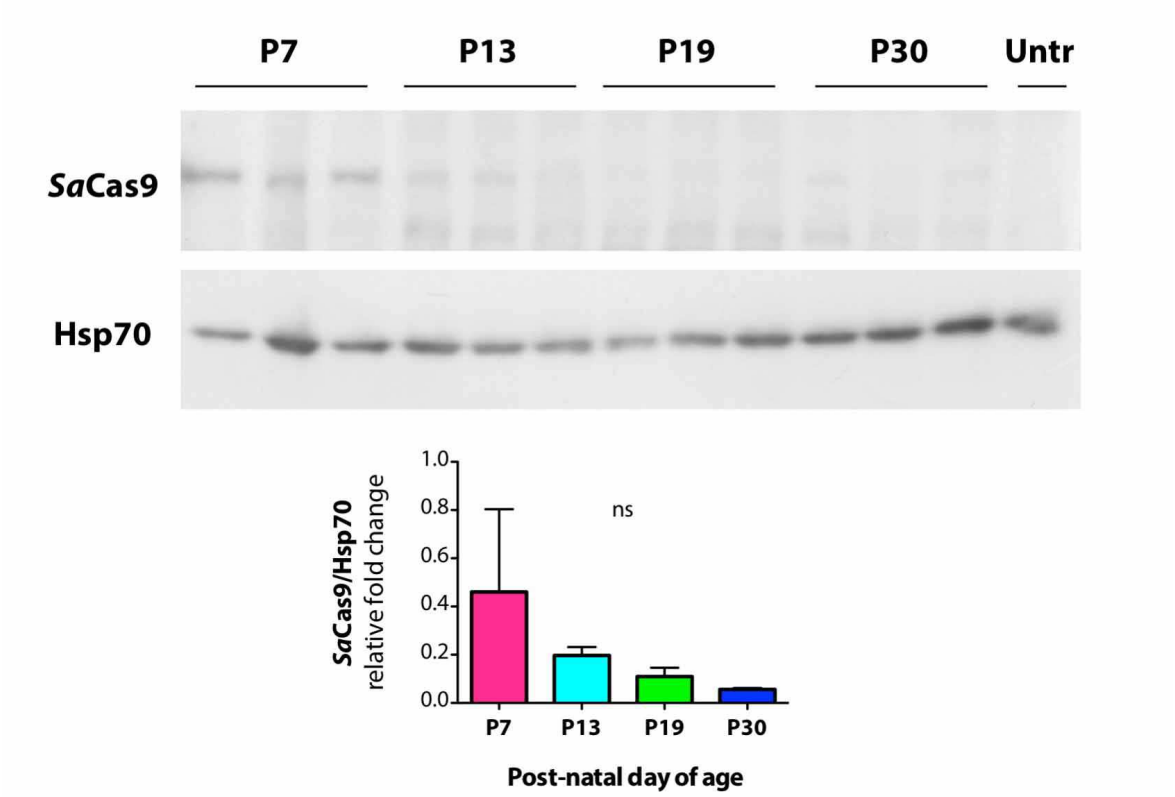

Fig. 53. *Sa*Cas9 protein levels decreased to undetectable ones 30 days after its administration. WB analysis of liver protein extracts of WT untreated and treated with rAAV8-*Sa*Cas9-sgRNA8 collected at different post-natal days. Hsp70 was used as loading control. The quantification of the WB is shown in the lower panel. One-way ANOVA, ns, P = 0.0847, n = 3 per group.

I also evaluated *Sa*Cas9 expression at mRNA level, by performing qRT-PCR analysis. I observed that mRNA levels increased soon after the vector infusion, reached a maximum at post-natal day 30 and significantly decreased at 10 months of age, the longest analyzed time point (Fig. 54).

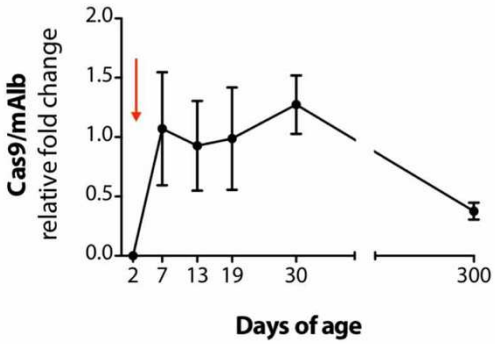

Fig. 54. *Sa*Cas9 mRNA levels. *Sa*Cas9 mRNA levels of WT mice treated with only rAAV8-*Sa*Cas9-sgRNA8 (2.0E+11 vg/mouse) at P2. Mice were sacrificed at different post-natal days, (P7, P13, P19, and P30) and the livers analyzed.

Then, I evaluated the number of viral genome particles per cell (vgp/cell) by qPCR of the liver genomic DNA. Quantitative analysis showed an important decrease in viral genome particles over time, probably consequent to episomal vector degradation and dilution during hepatocyte duplication in the context of a growing organ, since vector administration was performed at P2 (Cunningham et al., 2009) (Fig. 55). At 10 months of age I detected 1.5 vgp/cell, justifying the detected mRNA expression levels.

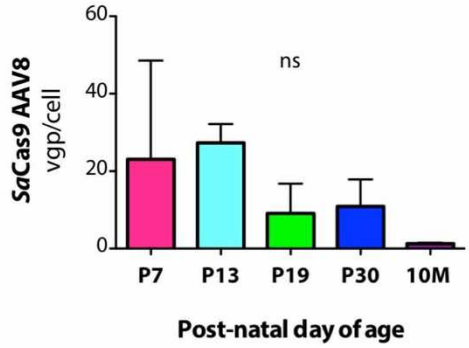

Fig. 55. Vector loss of *Sa*Cas9-sgRNA8 encoding rAAV8 vector. Viral genome particle (vgp) determination of *Sa*Cas9-sgRNA8 encoding rAAV8 vector at different post-natal days of age.

3.12.3 No changes were detected in predicted *Sa*Cas9-sgRNA8 off-target sites

3.12.3.1 In silico prediction analysis

The unspecific activity of the Cas9 nuclease can result in off-targets activity with undesired consequences such as deregulation of genes involved in the cell cycle regulation, with the potential risk of generating tumors. In order to assess the specificity of the *Sa*Cas9-sgRNA8,

I performed an *in silico* prediction analysis of potential off-target sites using the bioinformatics software Cas-Offinder (http://www.rgenome.net/cas-offinder/) Previous studies of the *Sa*Cas9 nuclease reported the absence of INDELs in target sequences containing 5 or more nucleotide mismatches with the corresponding sgRNA (Ran et al., 2015). Therefore, I focused the attention to off-target sites having a maximum of 4 mismatches in the target sequence. Based on genome location within actively transcribed regions and their functional importance, we selected TUBGCP2, KIF21A and Gm29874 genes as possible off-targets loci. While TUBGCP2 and KIF21A are protein-coding genes, Gm29874 is, instead, a long non-coding RNA gene. TUBGCP2 and KIF21A are protein-coding genes, whereas Gm29874 is a long non-coding RNA gene. I excluded from the analysis the fourth possible off-target site (Nmf420) as it corresponds to an intergenic, non-coding region, with an unknown function.

3.12.3.2 Sequencing analysis of on- and off-target sites

In order to evaluate the presence of INDELs in on-target and off-target sites, I amplified the on-target and potential off-target sites from liver DNA of mice treated with the highest dose of rAAV8-*Sa*Cas9-sgRNA8 (1.0E+12 vg/mouse; Fig. 28). The amplified PCR products were deep sequenced with an Illumina platform. Positional sequencing mutation analysis showed the precise location of INDELs in the expected albumin target site (Fig. 56), and gap-length frequency analysis highlighted a median length of the deletions, longer or equal to 2 bases, between 5 and 7 nucleotides (Tab. 15). Furthermore, positional frequency analysis showed that the median number of reads with gaps in each nucleotide position was 3 to 4.5%, up to 15% at the albumin target site, with no signal above noise levels (Fig. 57; Tab. 16).

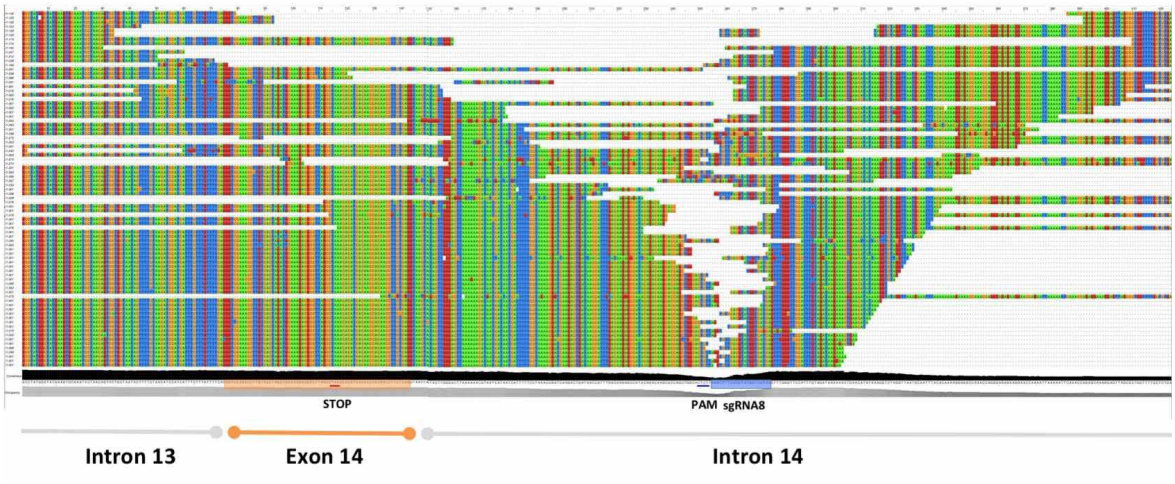

Fig. 56. Positional sequencing mutation analysis at the albumin on-target site after sgRNA8-*Sa*Cas9 transduction. Representative nucleotide sequences of the targeted albumin locus of one treated mice with sgRNA8-*Sa*Cas9 presented in Fig. 28. Sequences shown represent gap length diversity rather than the actual frequency distribution. The analysis showed the precise location of INDELs in the expected target site.

	Sample ID	Target sequence	N. of Reads	N. of gapped reads (≥2)	Percentage of reads with gaps	Maximum gap length	Mean gap length	Median gap length
1	Mouse 4 (+)	Albumin	54986	10463	**19.0**	306	**18.7**	**7**
2	Mouse 5 (+)	Albumin	16967	3115	**18.4**	239	**10.4**	**5**
3	Mouse 6 (+)	Albumin	19176	2712	**14.1**	237	**12.0**	**6**
4	Mouse (-)	Albumin	40676	78	**0.2**	69	**9.6**	**4**
5	Mouse 4 (+)	Albumin	137469	27215	**19.8**	395	**13.7**	**7**
6	Mouse (-)	Albumin	41468	111	**0.3**	97	**20.6**	**5**

Tab. 15. Gap-length frequency analysis at the albumin on-target site after sgRNA8-*Sa*Cas9 transduction. The genomic DNA of the albumin on-target site of mice treated with sgRNA8-*Sa*Cas9 presented in Fig. 28 was PCR amplified and sequenced by NGS approach. The obtained reads were aligned and noise filtered. The % of reads containing gaps ≥ 2 bases was determined. Lines 5 and 6 show the data of independent duplicate PCR reaction of Lines 1 and 4. The analysis highlighted a median length of the deletions, longer or equal to 2 bases, between 5 and 7 nucleotides.

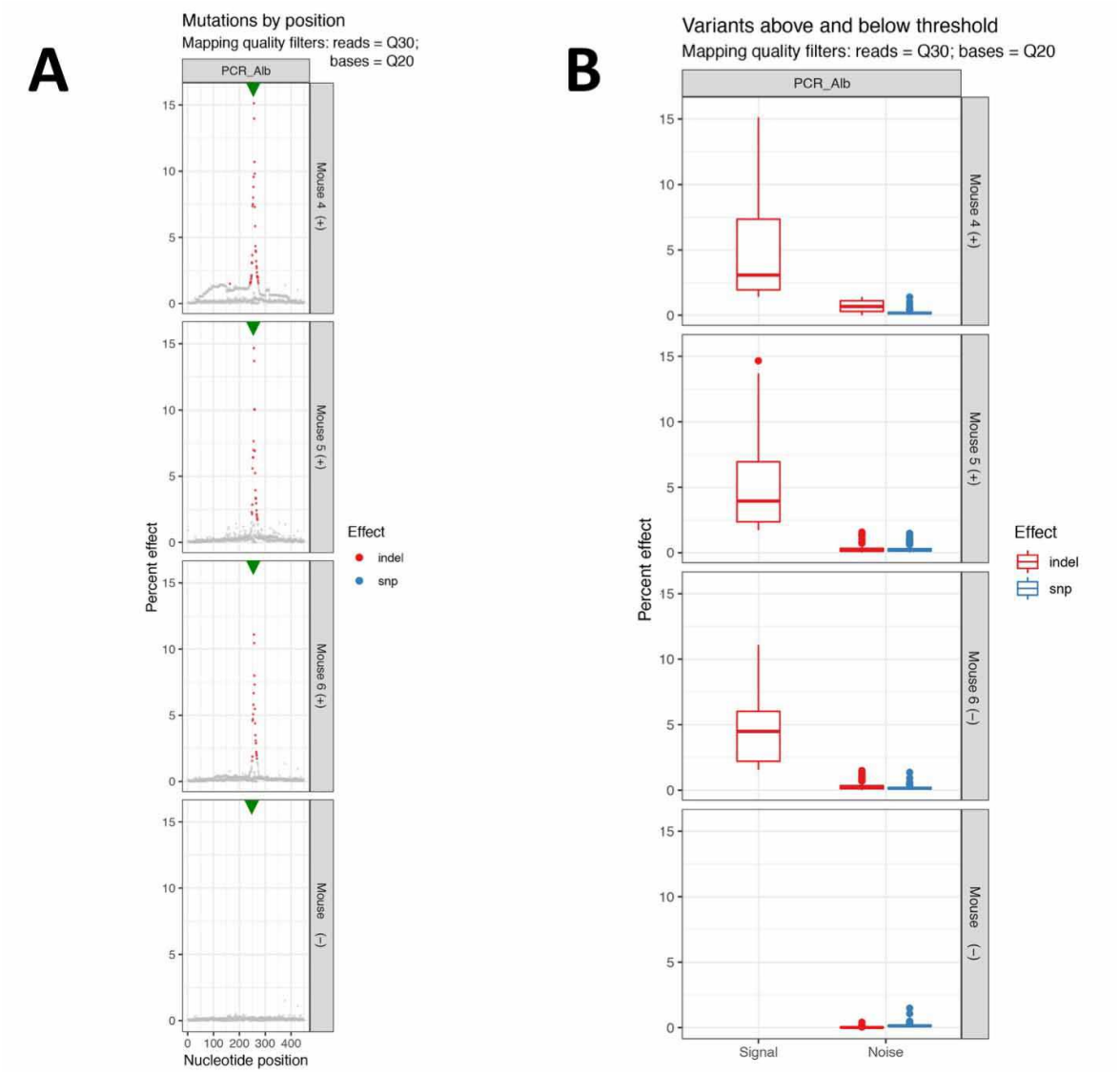

Fig. 57. sgRNA8 efficiently targets the albumin locus in neonatal treated mice. (A) Mutation frequency analysis at the albumin target site by sgRNA8. The dots represent the percentage of reads with bases different from the original sequence at each base position. The colored dots indicate variants above noise levels; the grey dots represent levels predicted as sequencing noise. The *Sa*Cas9-sgRNA8 on-target site is indicated by green arrowheads. The analysis was performed in the same animals analyzed in Fig. 28. The analysis showed that the median number of reads with gaps in each nucleotide position was 3 to 4.5%, up to 15% at the target site, with no signal above noise levels. **(B)** Box plots of the distributions of the data shown in (A), with indicated median values. Signal and noise distributions are plotted separately. Indels are represented in red and snps in blue. The analysis was performed in the same animals analyzed in Fig. 28.

Sample ID	Variant	Filter	Min	Max	Mean	Median
Mouse 4 (+)	indel	Signal	1.4194	15.1237	4.7122	**3.0840**
Mouse 4 (+)	indel	Noise	0.0020	1.4289	0.7274	**0.6702**
Mouse 4 (+)	snp	Signal	ND	ND	ND	**ND**
Mouse 4 (+)	snp	Noise	0.0146	1.4183	0.1843	**0.1649**
Mouse 5 (+)	indel	Signal	1.7169	14.6754	5.4194	**3.9463**
Mouse 5 (+)	indel	Noise	0.0074	1.5674	0.2395	**0.1945**
Mouse 5 (+)	snp	Signal	ND	ND	ND	**ND**
Mouse 5 (+)	snp	Noise	0.0121	1.4958	0.2571	**0.1812**
Mouse 6 (+)	indel	Signal	1.5569	11.0928	4.7255	**4.4905**
Mouse 6 (+)	indel	Noise	0.0056	1.5054	0.2466	**0.2070**
Mouse 6 (+)	snp	Signal	ND	ND	ND	**ND**
Mouse 6 (+)	snp	Noise	0.0105	1.3542	0.1656	**0.1453**
Mouse (-)	indel	Noise	0.0026	0.4294	0.0243	**0.0101**
Mouse (-)	snp	Signal	ND	ND	ND	**ND**
Mouse (-)	snp	Noise	0.0149	1.4904	0.1492	**0.1342**

Tab. 16. Positional-frequency analysis at the albumin on-target site after sgRNA8-*Sa*Cas9 transduction. The genomic DNA of the albumin on-target site of mice treated with sgRNA8-*Sa*Cas9 presented in Fig. 28 was PCR amplified and sequenced by NGS approach. The median values were plotted in Fig. 57B. ND, not detected

By applying conservative filters in order to keep as many false positives as possible, no INDELs or SNPs were detected above background levels at any of the predicted off-target sites in the samples from treated animals (Fig. 58; Tab. 17, 18).

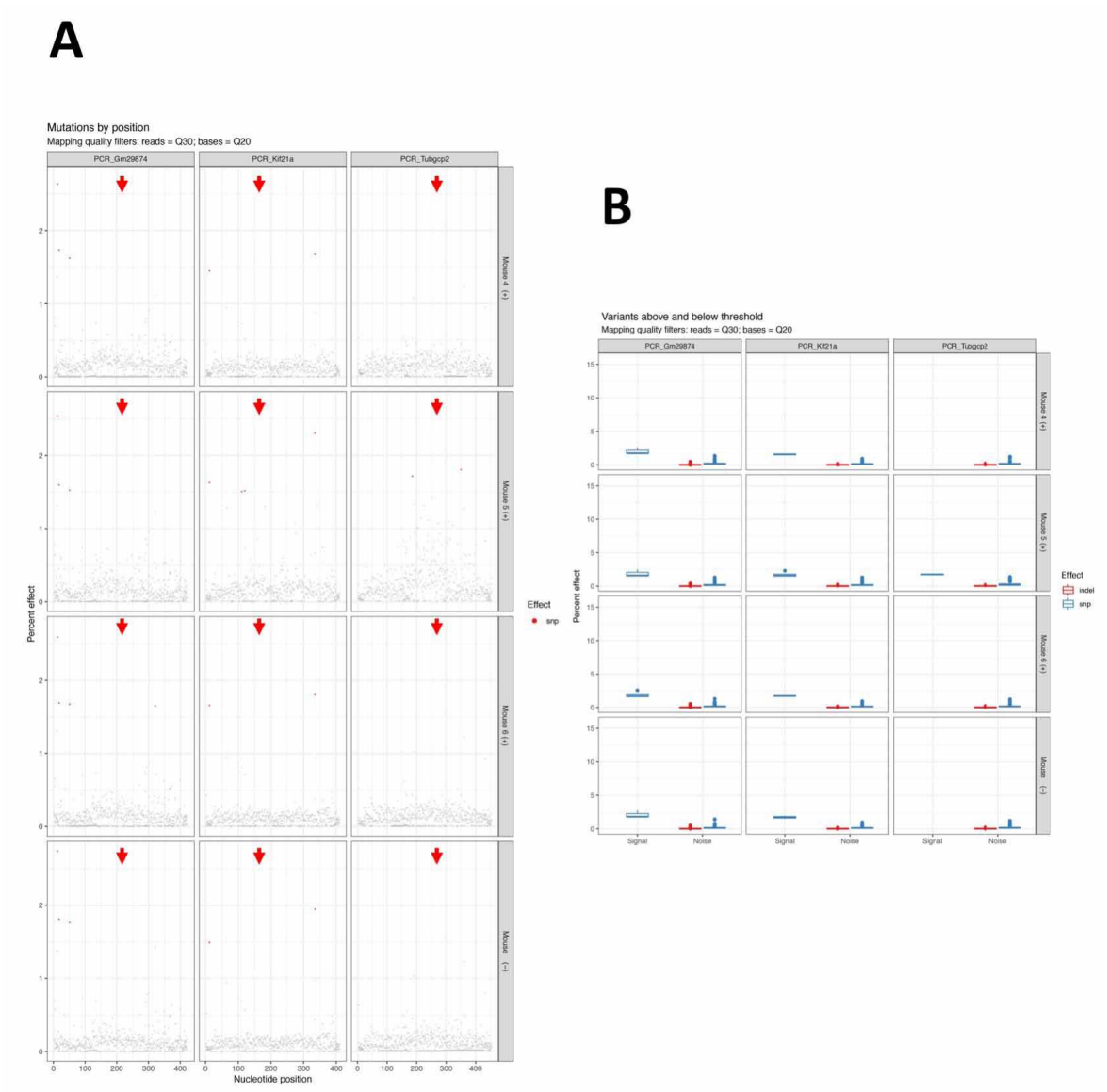

Fig. 58. Analysis of *Sa*Cas9 off-target activity. (**A**) Mutation frequency analysis of the predicted potential off-target sites by sgRNA8. The dots represent the percentage of reads with bases different from the original sequence at each base position. The red and blue dots indicate variants above noise levels. Grey dots indicate variants below threshold levels (noise). The location of the predicted *Sa*Cas9 off-target sites is indicated by a red arrow. The analysis was performed in the same animals used in Fig. 28. (**B)** Box plots of the distributions of the data shown in (A), with indicated median values. Signal and noise distributions are plotted separately. Indels are represented in red and snp in blue. The analysis was performed in the same animals used in Fig. 28.

			Kif21a				Tubgcp2			
Sample ID	Variant	Filter	Min	Max	Mean	**Median**	Min	Max	Mean	**Median**
Mouse 4 (+)	indel	Signal	ND	ND	ND	**ND**	ND	ND	ND	**ND**
Mouse 4 (+)	indel	Noise	0.001	0.168	0.019	**0.006**	0.003	0.244	0.024	**0.006**
Mouse 4 (+)	snp	Signal	1.450	1.678	1.564	**1.564**	ND	ND	ND	**ND**
Mouse 4 (+)	snp	Noise	0.014	0.948	0.149	**0.133**	0.011	1.234	0.177	**0.157**
Mouse 5 (+)	indel	Signal	ND	ND	ND	**ND**	ND	ND	ND	**ND**
Mouse 5 (+)	indel	Noise	0.002	0.246	0.026	**0.010**	0.006	0.234	0.042	**0.022**
Mouse 5 (+)	snp	Signal	1.508	2.309	1.741	**1.574**	1.718	1.808	1.763	**1.763**
Mouse 5 (+)	snp	Noise	0.014	1.324	0.194	**0.164**	0.009	1.419	0.274	**0.199**
Mouse 6 (+)	indel	Signal	ND	ND	ND	**ND**	ND	ND	ND	**ND**
Mouse 6 (+)	indel	Noise	0.001	0.179	0.018	**0.005**	0.002	0.224	0.021	**0.006**
Mouse 6 (+)	snp	Signal	1.657	1.804	1.730	**1.730**	ND	ND	ND	**ND**
Mouse 6 (+)	snp	Noise	0.015	0.957	0.136	**0.122**	0.017	1.228	0.163	**0.148**
Mouse (-)	indel	Noise	0.001	0.199	0.017	**0.004**	0.004	0.221	0.017	**0.013**
Mouse (-)	snp	Signal	1.489	1.945	1.717	**1.717**	ND	ND	ND	**ND**
Mouse (-)	snp	Noise	0.016	0.968	0.131	**0.116**	0.006	1.224	0.156	**0.135**

			Gm29874			
sample_id	sindel	pass	Min	Max	Mean	**Median**
Mouse 4 (+)	indel	Noise	0.001	0.477	0.019	**0.003**
Mouse 4 (+)	snp	Signal	1.624	2.637	2.000	**1.737**
Mouse 4 (+)	snp	Noise	0.023	1.368	0.208	**0.173**
Mouse 5 (+)	indel	Noise	0.001	0.408	0.030	**0.005**
Mouse 5 (+)	snp	Signal	1.528	2.540	1.889	**1.600**
Mouse 5 (+)	snp	Noise	0.012	1.319	0.205	**0.153**
Mouse 6 (+)	indel	Noise	0.001	0.528	0.027	**0.004**
Mouse 6 (+)	snp	Signal	1.648	2.592	1.900	**1.681**
Mouse 6 (+)	snp	Noise	0.012	1.311	0.174	**0.141**
Mouse (-)	indel	Noise	0.001	0.499	0.027	**0.005**
Mouse (-)	snp	Signal	1.761	2.739	2.103	**1.810**
Mouse (-)	snp	Noise	0.016	1.431	0.155	**0.120**

Tab. 17. Positional-frequency analysis of predicted off-target sites after sgRNA8-*Sa*Cas9 transduction. The genomic DNA of the predicted off-target site of mice treated with sgRNA8-*Sa*Cas9 presented in Fig. 28. was PCR amplified and sequenced by NGS approach. The median values were plotted in Fig. 58B. ND, not detected.

	Sample ID	Target sequence	N. of Reads	N. of gapped reads (≥2)	Percentage of reads with gaps	Maximum gap length	Mean gap length	Median gap length
1	Mouse 4 (+)	Kif21a	69776	146	0.2	367	105.0	2
2	Mouse 4 (+)	Tubgcp2	37900	99	0.3	414	56.3	3
3	Mouse 5 (+)	Kif21a	43506	78	0.2	368	82.1	2
4	Mouse 5 (+)	Tubgcp2	22151	74	0.3	164	17.1	5
5	Mouse 6 (+)	Kif21a	79425	88	0.1	366	70.5	2
6	Mouse 6 (+)	Tubgcp2	48061	84	0.2	59	8.7	3
7	Mouse (-)	Kif21a	110129	192	0.2	370	76.3	2
8	Mouse (-)	Tubgcp2	32617	67	0.2	230	14.1	3
9	Mouse 4 (+)	Gm29874	135024	1136	0.8	385	201.908	378
10	Mouse 5 (+)	Gm29874	86507	410	0.5	385	88.146	4
11	Mouse 6 (+)	Gm29874	109815	840	0.8	386	168.298	21
12	Mouse (-)	Gm29874	171007	1186	0.7	385	161.003	4

Tab. 18. Gap-length frequency analysis at predicted off-target sites after sgRNA8-*Sa*Cas9 transduction. The genomic DNA of the predicted off-target site of mice treated with sgRNA8-*Sa*Cas9 presented in Fig. 28 was PCR amplified and sequenced by NGS approach. The obtained reads were aligned and noise filtered. The % of reads containing gaps ≥ 2 bases was determined.

4. DISCUSSION

4.1 The liver directed gene transfer mediated by AAV vectors

AAV-mediated gene transfer to the liver has shown efficacy and safety in adult patients and several clinical trials in subjects with hemophilia A and B are ongoing [ClinicalTrials.gov number, NCT02484092, (George et al., 2017); ClinicalTrials.gov number, NCT02576795, (Rangarajan et al., 2017); ClinicalTrials.gov number, NCT00979238, (Nathwani et al., 2014)]. The potential of liver directed gene therapy in the clinic is under evaluation also for Crigler-Najjar type I syndrome. Indeed, a European network (CureCN), to which our group participates, is evaluating the safety and efficacy of an intravenous injection of an AAV vector expressing the UGT1A1 transgene in CNSI patients requiring phototherapy aged ≥ 10 years by an open label, escalating-dose phase I/II study (ClinicalTrials.gov number, NCT03466463). Furthermore, in the United States, Audentes Therapeutics has been recruiting patients to evaluate the safety and preliminary efficacy of an AAV8-delivered gene transfer therapy in CNSI subjects aged 1 year and older (ClinicalTrials.gov number, NCT03223194). However, the potential of liver directed gene transfer in neonatal/pediatric settings, where liver is immature and the hepatocytes proliferation triggers episomal DNA loss (Cunningham et al., 2009), is still a challenge, suggesting that more effective therapeutic strategies should be developed to cure many monogenic liver diseases that require treatment early in life.

Liver-directed gene therapy mediated by rAAV vectors has already been applied to correct very severe neonatal hyperbilirubinemia in a lethal mouse model of Crigler-Najjar type I syndrome (CNSI) (Bortolussi et al., 2012). These animals mimic the main features of the human disorder, such as neonatal lethality. rAAV8-mediated liver delivery of the therapeutic hUGT1A1 cDNA, whose expression was controlled by a strong liver-specific promoter (Mingozzi, Liu et al., 2003), resulted in the rescue of neonatal lethality with a therapeutic efficacy that lasted up to 17-months post-injection (Bortolussi et al., 2014b). Even if gene therapy succeeded in rescuing CNSI mice from neonatal lethality, a very high dose of the therapeutic AAV8 vector was required (Bockor, Bortolussi et al., 2017, Bortolussi et al., 2014b), raising important concerns regarding the safety of the procedure, since rAAV vectors can be genotoxic. Furthermore, transgene expression and, thereby, therapeutic efficacy decreased over time, as a consequence of the progressive loss of episomal AAV viral genomes during hepatocyte proliferation (Bortolussi et al., 2014b, Cunningham et al., 2009), and a second re-administration of the therapeutic gene was necessary (Bockor et al., 2017). However, while re-infusion of the beneficial AAV vector in mice is effective, it is not possible in

a clinical setting due to the presence of neutralizing antibodies against the AAV-capsid antigens, presenting potential cross-reaction among the genotypes, generated after the first vector infusion (Calcedo & Wilson, 2016). Two of the most important limits of AAV-mediated gene therapy observed in the CNSI treatment, the episomal vector loss in actively dividing cells and the development of an immune response against the gene therapy tools used, represent major obstacles for the success of AAV-mediated gene transfer to cure liver-based monogenic diseases with neonatal/pediatric onset. The concerns and limitations of non-integrative AAV-mediated gene therapy approaches stimulated researchers to find alternative therapies to cure liver inherited pediatric disorders.

4.2 The potential of AAV-mediated liver gene editing

Gene editing is a promising approach to treat rare monogenic diseases by the permanent modification of the genome, overcoming non-integrative AAV-mediated gene therapy limitations. Indeed, the possibility to permanently modify a genomic sequence and the ability of the targeted cells to transmit the introduced modification to daughter one result in long-term therapeutic efficacy of the gene transfer treatment. Two main strategies can be selected for a genome editing therapeutic approach: 1) correct the specific mutation responsible of the diseased phenotype, or 2) insert a functional copy of the therapeutic gene into a "safe harbour locus" (Sadelain, Papapetrou et al., 2011). Even if several studies demonstrated the efficacy of targeting and repairing *in vivo* the specific sequence of the genomic locus involved in the pathogenesis of the disorder (Li et al., 2011, Paulk et al., 2010, Yang et al., 2016, Yin et al., 2014), the clinical potential of the approach is limited by the existence of multiple disease causing mutations (Canu et al., 2013, Kadakol et al., 2000) and by the gene editing rate, which may not be sufficient to reach therapeutic levels of the involved protein. Many liver monogenic diseases, indeed, result from mutations that could be located in different regions of the gene, requiring the development of specific experimental strategies for each of the disease-causing mutations, with time-consuming and expensive procedures. This limit is highlighted by the 130 reported mutations of the UGT1A1 gene responsible of both Gilbert syndrome (GS) and Crigler-Najjar syndrome (CNS) (Canu et al., 2013) and the 417 disease-causing mutations counted leading to ornithine transacarbamylase deficiency (OCTD) (Caldovic, Abdikarim et al., 2015) On the contrary, targeting a functional copy of the therapeutic gene into a "safe-harbour" locus corrects most existing mutations, avoiding the need of

setting up specific approaches for each specific disease-causing mutation. Furthermore, the selection of a highly-transcribed locus whose modification does not affect the phenotype may result in high levels of therapeutic gene expression, even with low targeting rate, leading to the permanent correction of the dysfunction. Various studies selected the endogenous albumin gene to target the therapeutic cDNA due to its high transcription rate, ensuring high levels of transgene expression to correct the mutated phenotype (Barzel et al., 2015, Porro et al., 2017, Sharma, Anguela et al., 2015). Furthermore, the albumin gene was selected as a genomic "safe harbour locus" for many additional reasons: it is highly expressed in the liver, an organ in which gene delivery and gene editing can be easily determined; it is possible to target the first intron since its first exon codes for the secretory peptide that is cleaved from the mature protein; the normal levels of albumin in plasma present a wide range, assuring that the potential inactivation of a low proportion of albumin alleles by the targeting approach may not result in undesired side effects. Consequently, the albumin gene can be considered as a targeting locus of choice for liver-directed gene replacement therapies.

4.3 The limited therapeutic efficacy of GeneRide

The GeneRide approach is a genome editing strategy without nucleases (Barzel et al., 2015) which exploits the recombination capacity of rAAV vectors (Russell & Hirata, 1998). It was developed by Barzel and colleagues and it ameliorated disease in a mouse model of hemophilia B (Barzel et al., 2015). When we applied GeneRide to a mouse model of the Crigler-Najjar type I syndrome (Porro et al., 2017) by inserting the promoterless hUGT1A1 cDNA into albumin locus, we rescued neonatal lethality and all biochemical and functional abnormalities in CNI mice with a therapeutic efficacy that lasted up to 12 months after the administration (Porro et al., 2017). The observed targeting rate, around 0.033 % (Porro et al., 2017), was lower than the one determined by Barzel *et al*, which was about 0.5% (Barzel et al., 2015), however, it can be explained by important differences related to the specific construct used, albumin zonal expression (Poliard, Bernuau et al., 1986) and AAV8 transduction patterns (Bell, Wang et al., 2011). Considering vector differences, the length of the hUGT1A1 cDNA was larger than that of the hFIX, and, as a consequence, the hUGT1A1 donor construct was in the upper limit of the normal AAV cargo capacity, probably resulting in a lower quality of the virus preparation. Importantly, while the FIX experiment was performed in P2 mice, the UGT1A1 delivery was done at P4. The different post-natal delivery could contribute to

explain the observed lower targeting rate, since I have seen that spontaneous homologous recombination at P2 is about 5-fold higher than at P4. These considerations may explain, at least partially, the targeting rate differences between the two GeneRide applications (Barzel et al., 2015, Porro et al., 2017). The few edited hepatocytes were, however, able to produce functional UGT1A1 enzyme in levels that were sufficient to convert a very severe phenotype into a mild one, with life-long therapeutic efficacy. These results support the potential of GeneRide, since 5-10 % of WT activity reduces plasma bilirubin to safe levels in human and mice (Bortolussi et al., 2014b, Fox et al., 1998, Sneitz et al., 2010) and 12-22 % of functional total liver mass solves completely the metabolic defect in Gunn rat (Asonuma, Gilbert et al., 1992). The long-lasting efficiency of the approach resulted from the site-specific and permanent integration of the therapeutic cDNA into the highly-transcribed albumin locus, avoiding the episomal DNA loss observed in gene replacement strategies (Bortolussi et al., 2014b, Cunningham et al., 2009, Wang et al., 2012), which limits their potential for diseases with an early onset. Since GeneRide adopts a promoterless AAV vector, the risk to develop hepatocellular carcinoma (HCC) is limited, since unspecific integration will not result in the transactivation of nearby genes, as observed with some potent liver-specific and viral promoters (Chandler, LaFave et al., 2015, Donsante et al., 2007). Even if total plasma bilirubin levels of all mice treated with GeneRide were below the toxic range and avoided the otherwise derived brain damage, they were still too high for a potential clinical application. In addition, a high dose of AAV vector was administrated to the animals, which was much higher than the one used in hemophilia B clinical trials (Nathwani, Cochrane et al., 2009, Nathwani et al., 2014, Nathwani et al., 2011b) while no selective advantage was present in recombinant or WT hepatocytes.

4.4 Compounds and siRNAs based strategies failed to enhance homologous recombination rate

Aiming to a potential application of the approach into clinic, we looked for experimental strategies able to enhance the low integration rate obtained with GeneRide (Porro et al., 2017). One possible approach relies on the use of more efficient vectors and/or transgenes, by using AAV serotypes that more efficiently transduce the liver and/or by adopting a codon-optimized cDNA of the therapeutic gene, increasing mRNA translatability and, thus, the overall levels of enzyme (Ronzitti, Bortolussi et al., 2016). Conferring a selective advantage of gene-modified hepatocytes could be another key strategy. Nygaard *et al.* co-expressed the therapeutic gene and a short hairpin RNA

(shRNA) that confers edited hepatocytes with resistance to drug-induced toxicity. Using this approach, they were able to select gene-targeted cells and to increase transgene expression 10- to 100-fold in mice (Nygaard, Barzel et al., 2016). However, since the drug used by the authors is hepatotoxic, its potential clinical application raises many safety concerns, together with the log time necessary to obtain FDA approval, limiting the translation of the approach into a clinical setting. Other strategies to increase therapeutic efficacy could be interfering with mechanisms that cells normally use to repair DNA DSBs. Since GeneRide takes advantage of HR to target the insertion of the therapeutic cDNA into albumin locus, blocking NHEJ or enhancing HDR could boost transgene precise integration. In spite that several compounds have been reported to interfere with DNA DSBs repair pathways *in vitro* (Chu et al., 2015, Jayathilaka et al., 2008, Vartak & Raghavan, 2015) and *in vivo* (Maruyama et al., 2015, Paulk et al., 2012, Srivastava et al., 2012), we did not observe any increase in recombination rate after testing most of them *in vitro* and *in vivo*. Another promising strategy aimed to increase the efficiency of site-specific integration could be enhancing AAV transduction, since increasing amounts of donor template used by the cells to repair DNA DSBs result in higher HDR rate. Thereafter, we tested two siRNAs identified by Mano *et al*. that significantly increased viral transduction *in vivo* (Mano et al., 2015) by coupling them to GeneRide but we did not observe the expected increase in recombination rate. The differences between the two experimental strategies, such as the age and strain of mice, and the administration routes, could explain, at least, partially, the discrepancies of data. Consequently to these negative results and to the fact that silencing genes could result in undesired and unpredictable effects, we analyzed other alternative strategies to increase the recombination rate and therapeutic efficacy.

4.5 Promising genome editing tools: the engineered endonucleases

The use of genome editing approaches has been increasing very fast since researchers discovered that, by inducing specific DNA double strand breaks (DSBs), it is possible to enhance gene targeting rate by several orders of magnitude (Jasin, 1996) (Rouet et al., 1994). Many engineered endonucleases, such as ZFNs and TALENs, have been developed to generate DNA DSBs in a site-specific manner. ZFNs have been successfully adopted to correct hemophilia A and B in mouse models using AAV vectors (Sharma et al., 2015). The approach used by Sharma *et al*. is based in the targeted integration of the therapeutic cDNA (hFVIII and hFIV cDNAs for hemophilia A and B,

respectively) into the albumin locus, resulting in long-term expression of both secreted factors. Thus, we considered the use of nucleases to enhance targeting rate. However, the potential of genome editing tools such as ZFNs is limited by their time-consuming and expensive design and production. Nowadays many genome-editing strategies rely on the use of the CRISPRII/Cas9 platform, which is promising in targeting any genomic locus of choice. Indeed, the sgRNA can be easily designed to guide the Cas9 nuclease to almost any desired sequence of the genome (Jinek et al., 2012). Among different engineered endonucleases, the CRISPRII/Cas9 platform has demonstrated high efficacy in editing genes both *in vitro* and *in vivo* (Pankowicz, Barzi et al., 2016, Xue, Chen et al., 2014, Yang et al., 2016, Yin et al., 2014). Gene editing mediated by CRISPRII/Cas9 system has been successfully adopted *in vivo* to correct OTC and HTI mouse models (Yang et al., 2016, Yin et al., 2014). From the discovery of the bacterial CRISPRII/Cas9 subtype as a powerful genome editing tool, many nucleases variants have been identified, such as *Staphylococcus pyogenes* (*Sp*) and *Staphylococcus aureus* (*Sa*) Cas9 (Esvelt et al., 2013, Ran et al., 2015). However, the *Sa*Cas9 nuclease represents a safer variant for *in vivo* genome editing since its longer and more complex PAM sequence could result in higher cleavage specificity and lower off-target activity (Ran et al., 2015).

4.6 The enhanced GeneRide efficiency by CRISPRII/*Sa*Cas9 coupling in neonatal mice

Therefore, we reasoned that the combination of GeneRide with the CRISPRII/*Sa*Cas9 platform could result in enhanced gene targeting rate. In fact, when we tested the strategy in neonatal WT mice using the eGFP reporter cDNA we were able to enhance gene targeting rate up to 26-fold, reaching in some mice up to 24 % of recombinant hepatocytes. When we adopted the hFIX cDNA in neonatal WT mice, we increased the targeting efficiency more than 100-fold compared to the group without nucleases. This high integration rate resulted in plasma hFIX values that corresponded to 100-200 % of normal human ones, even 10 months after the vector administration. Combining GeneRide to CRISPRII/*Sa*Cas9 in Ugt1$^{-/-}$ mice resulted in the rescue from neonatal lethality of all treated animals with total plasma bilirubin levels that were comparable to WT littermates even 10 month after AAV-vector infusion. The edited hepatocytes, up to 3.6 %, produced an amount of UGT1 protein that was up to 6-fold higher than that produced by the same amount of liver extract from WT mice. Metabolic disorders are a heterogeneous class of monogenic diseases in which the level of therapeutic protein necessary to convert the diseased phenotype with a life-compatible one varies among

them. Hemophilia and Crigler-Najjar type I syndrome are excellent examples of liver inherited diseases that can successfully be treated with gene editing approaches since low levels of enzyme or factor activity are enough to guarantee a normal life in the treated patients. In fact, just 2-5 % or 5-10 % of normal activity of the involved protein, respectively, are needed to convert a severe phenotype into a mild one (Bortolussi et al., 2014b, White, Rosendaal et al., 2001). Other metabolic diseases, such as OTC deficiency (Briand, Francois et al., 1982), are more severe and higher levels of WT activity are necessary to correct the diseased phenotype (Cunningham, Kok et al., 2013). Considering that edited hepatocytes with this approach produced an amount of therapeutic protein that was much higher than WT one, GeneRide coupled to CRISPRII/*Sa*Cas9 could be potentially applied to correct more sever liver diseases. Furthermore, for diseases in which a lower functional activity is needed, it could be possible to further decrease the dose of rAAV vectors, which is a major concern of gene therapy and editing strategies due to potential genotoxicity of the viral DNA. The successful targeting into the albumin locus of three cDNAs, encoding for three different proteins forms with different cellular/extracellular localization, cytoplasmatic, secreted and ER transmembrane, for the eGFP, the hFIX and the hUGT1A1, respectively, supports the therapeutic potential of the strategy to treat different liver-inherited disorders in which the involved proteins may have different localization and function. One important advantage of the approach is represented by the possibility to treat different liver inherited disorders by just replacing the therapeutic cDNA in the donor AAV vector and using the same *Sa*Cas9 and sgRNA encoding AAV vector. Furthermore, the same genome editing tools can be used to treat different disease-causing mutations.

4.7 The efficiency of genome editing approaches in adults

In this study, we coupled GeneRide to CRISPRII/*Sa*Cas9 platform to develop a therapeutic strategy useful to treat diseases with early onset and looking at this aim, only neonatal mice were transduced. Considering that highly proliferative cells use preferentially HDR mechanism to repair DNA DSBs (Ceccaldi, Rondinelli et al., 2016), whereas quiescent ones adopt NHEJ, which is error-prone, we speculated that if applied to adult mice, the proposed approach result in lower correction rate than the one obtained in newborns. Yang *et al*. supported our hypothesis demonstrating that the correction of the single point mutation in OTC mice differs if they are treated during the neonatal period or in adulthood (Yang et al., 2016). Contrary to those results, Barzel *et al*. applied

GeneRide to adult mice obtaining the same correction rate achieved with neonatal administration (Barzel et al., 2015). Further experiments should be performed to determine the gene targeting efficiency with the proposed approach in adult CNSI mice.

4.8 The safe profile of GeneRide coupled to CRISPRII/*Sa*Cas9 platform

With this study, we demonstrated how GeneRide coupled to CRISPRII/*Sa*Cas9 platform can lead to increased targeting rates, resulting, thereby, in higher levels of transgene expression with life-long therapeutic efficacy. As previously mentioned, the potential off-target activity of the nucleases is a major concern in the gene-editing field. The selection of *Sa*Cas9 nuclease, instead of *Sp*Cas9, should result in the reduction of the potential off-target sites since the required PAM sequence, NNGRRT, is more complex than the one of *Sp*Cas9 (Ran et al., 2015). In order to confirm the safety of *Sa*Cas9, we first predicted potential off-target sites using the bioinformatics software Cas-Offinder. No off-target activity was detected by deep-sequencing with Illumina-seq technology in the selected sites, which had 4 mismatches, and no sites with less than 4 mismatches were detected, supporting the concept that the more complex *Sa*Cas9 PAM may result in reduced off-target sites.

To further evaluate the specificity of the approach, we analyzed in detail the *Sa*Cas9 on-target activity. The *Sa*Cas9 nuclease, guided by the sgRNA8, targets a sequence located 100 bp downstream the albumin stop codon. The induced DNA DSBs may be repaired by HDR in the presence of a donor template. However, we could not rule out the possibility that cells use the NHEJ mechanism to repair the DNA damage, leading to INDELs and, if they are large enough, to the consequent inactivation of a high number of targeted alleles. To assess this risk, we evaluated albumin expression, both at mRNA and protein levels, and we did not find any significant difference between rAAV8-treated and -untreated mice, supporting the hypothesis that the developed approach does not disrupt albumin gene expression. These results are supported by the bioinformatics analysis of the Illumina data obtained from the targeted albumin sequence, showing that the great majority of deletions were shorter than seven nucleotides, with a very low proportion of longer gaps.

As already mentioned before, the choice to target a therapeutic transgene into albumin locus is also shared by Sharma *et al.* (Sharma et al., 2015). Contrary to our strategy, they targeted a promoterless therapeutic cassette containing a splice acceptor site into the first intron of the albumin gene, thereby, inactivating the targeted allele (Sharma et al., 2015).

Our approach differs from the one of Sharma *et al.* also in terms of efficiency of targeting, which can be related to differences in the adopted strategies. Indeed, they used ZFNs in adult mice, and a different donor template (Sharma et al., 2015).

Additionally, since the long-term persistence of the nuclease in the target tissue could result in adverse effects, we evaluated *Sa*Cas9 expression at different days after rAAV administration in WT mice. We could appreciate that *Sa*Cas9 levels decreased over time, being undetectable 30 days after the vector infusion. However, we found a relevant number of AAV-*Sa*Cas9 genomes per cell at 10 months of age, which was in line with evaluated mRNA expression, suggesting that the sensitivity of the anti-*Sa*Cas9 antibody was not high enough to detect the nuclease when present at lower levels. Therefore, in order to further improve the safety profile of the approach, we may limit the time-window in which the nuclease is active by using a self-inactivating system (Merienne, Vachey et al., 2017, Petris, Casini et al., 2017) or by delivering the nuclease as mRNA or protein, taking advantage of lipid nanoparticles (Kim, Kim et al., 2014, Liang, Potter et al., 2015).

CONCLUSIONS

In this study, we aimed at enhancing gene targeting rate of GeneRide by combining it with the CRISPRII/*Sa*Cas9 platform, and testing the therapeutic efficacy in a relevant and severe animal model of a liver inherited disease.

We provided the proof-of-concept that shows the enhanced efficacy and normal safety parameters of the proposed approach to cure severe liver diseases with neonatal onset. The developed platform can be applied to different liver monogenic disorders and be considered for a potential application into the clinic. However, further pre-clinical studies will be required to fully assess long-term safety of the nuclease-based approach for the treatment for CNSI and other inherited liver diseases.

BIBLIOGRAPHY

Adam R, Karam V, Delvart V, O'Grady J, Mirza D, Klempnauer J, Castaing D, Neuhaus P, Jamieson N, Salizzoni M, Pollard S, Lerut J, Paul A, Garcia-Valdecasas JC, Rodriguez FS, Burroughs A, All contributing c, European L, Intestine Transplant A (2012) Evolution of indications and results of liver transplantation in Europe. A report from the European Liver Transplant Registry (ELTR). J Hepatol 57: 675-88

Addiego J, Kasper C, Abildgaard C, Hilgartner M, Lusher J, Glader B, Aledort L (1993) Frequency of inhibitor development in haemophiliacs treated with low-purity factor VIII. Lancet 342: 462-4

Al-Dhalimy M, Overturf K, Finegold M, Grompe M (2002) Long-term therapy with NTBC and tyrosine-restricted diet in a murine model of hereditary tyrosinemia type I. Mol Genet Metab 75: 38-45

American Academy of Pediatrics Subcommittee on H (2004) Management of hyperbilirubinemia in the newborn infant 35 or more weeks of gestation. Pediatrics 114: 297-316

Andrieu-Soler C, Halhal M, Boatright JH, Padove SA, Nickerson JM, Stodulkova E, Stewart RE, Ciavatta VT, Doat M, Jeanny JC, de Bizemont T, Sennlaub F, Courtois Y, Behar-Cohen F (2007) Single-stranded oligonucleotide-mediated in vivo gene repair in the rd1 retina. Mol Vis 13: 692-706

Aono S, Yamada Y, Keino H, Hanada N, Nakagawa T, Sasaoka Y, Yazawa T, Sato H, Koiwai O (1993) Identification of defect in the genes for bilirubin UDP-glucuronosyl-transferase in a patient with Crigler-Najjar syndrome type II. Biochem Biophys Res Commun 197: 1239-44

Aponte JL, Sega GA, Hauser LJ, Dhar MS, Withrow CM, Carpenter DA, Rinchik EM, Culiat CT, Johnson DK (2001) Point mutations in the murine fumarylacetoacetate hydrolase gene: Animal models for the human genetic disorder hereditary tyrosinemia type 1. Proc Natl Acad Sci U S A 98: 641-5

Arias IM (1962) Chronic unconjugated hyperbilirubinemia without overt signs of hemolysis in adolescents and adults. J Clin Invest 41: 2233-45

Askari FK, Hitomi Y, Mao M, Wilson JM (1996) Complete correction of hyperbilirubinemia in the Gunn rat model of Crigler-Najjar syndrome type I following transient in vivo adenovirus-mediated expression of human bilirubin UDP-glucuronosyltransferase. Gene Ther 3: 381-8

Asokan A, Schaffer DV, Samulski RJ (2012) The AAV vector toolkit: poised at the clinical crossroads. Mol Ther 20: 699-708

Asonuma K, Gilbert JC, Stein JE, Takeda T, Vacanti JP (1992) Quantitation of transplanted hepatic mass necessary to cure the Gunn rat model of hyperbilirubinemia. J Pediatr Surg 27: 298-301

Aubert D, Menoret S, Chiari E, Pichard V, Durand S, Tesson L, Moullier P, Anegon I, Ferry N (2002) Cytotoxic immune response blunts long-term transgene expression after efficient retroviral-mediated hepatic gene transfer in rat. Mol Ther 5: 388-96

Bae S, Park J, Kim JS (2014) Cas-OFFinder: a fast and versatile algorithm that searches for potential off-target sites of Cas9 RNA-guided endonucleases. Bioinformatics 30: 1473-5

Barzel A, Paulk NK, Shi Y, Huang Y, Chu K, Zhang F, Valdmanis PN, Spector LP, Porteus MH, Gaensler KM, Kay MA (2015) Promoterless gene targeting without nucleases ameliorates haemophilia B in mice. Nature 517: 360-4

Bell P, Wang L, Gao G, Haskins ME, Tarantal AF, McCarter RJ, Zhu Y, Yu H, Wilson JM (2011) Inverse zonation of hepatocyte transduction with AAV vectors between mice and non-human primates. Mol Genet Metab 104: 395-403

Benten D, Staufer K, Sterneck M (2009) Orthotopic liver transplantation and what to do during follow-up: recommendations for the practitioner. Nat Clin Pract Gastroenterol Hepatol 6: 23-36

Berns KI, Linden RM (1995) The cryptic life style of adeno-associated virus. Bioessays 17: 237-45

Bhutani VK, Zipursky A, Blencowe H, Khanna R, Sgro M, Ebbesen F, Bell J, Mori R, Slusher TM, Fahmy N, Paul VK, Du L, Okolo AA, de Almeida MF, Olusanya BO, Kumar P, Cousens S, Lawn JE (2013) Neonatal hyperbilirubinemia and Rhesus disease of the newborn: incidence and impairment estimates for 2010 at regional and global levels. Pediatr Res 74 Suppl 1: 86-100

Bissell DM (1975) Formation and elimination of bilirubin. Gastroenterology 69: 519-38

Bockor L, Bortolussi G, Iaconcig A, Chiaruttini G, Tiribelli C, Giacca M, Benvenuti F, Zentilin L, Muro AF (2017) Repeated AAV-mediated gene transfer by serotype switching enables long-lasting therapeutic levels of hUgt1a1 enzyme in a mouse model of Crigler-Najjar Syndrome Type I. Gene Ther 24: 649-660

Bortolussi G, Baj G, Vodret S, Viviani G, Bittolo T, Muro AF (2014a) Age-dependent pattern of cerebellar susceptibility to bilirubin neurotoxicity in vivo in mice. Dis Model Mech 7: 1057-68

Bortolussi G, Zentilin L, Baj G, Giraudi P, Bellarosa C, Giacca M, Tiribelli C, Muro AF (2012) Rescue of bilirubin-induced neonatal lethality in a mouse model of Crigler-Najjar syndrome type I by AAV9-mediated gene transfer. FASEB J 26: 1052-63

Bortolussi G, Zentillin L, Vanikova J, Bockor L, Bellarosa C, Mancarella A, Vianello E, Tiribelli C, Giacca M, Vitek L, Muro AF (2014b) Life-long correction of hyperbilirubinemia with a neonatal liver-specific AAV-mediated gene transfer in a lethal mouse model of Crigler-Najjar Syndrome. Hum Gene Ther 25: 844-55

Bosma PJ (2003) Inherited disorders of bilirubin metabolism. J Hepatol 38: 107-17

Bosma PJ, Chowdhury JR, Huang TJ, Lahiri P, Elferink RP, Van Es HH, Lederstein M, Whitington PF, Jansen PL, Chowdhury NR (1992a) Mechanisms of inherited deficiencies of multiple UDP-glucuronosyltransferase isoforms in two patients with Crigler-Najjar syndrome, type I. FASEB J 6: 2859-63

Bosma PJ, Chowdhury NR, Goldhoorn BG, Hofker MH, Oude Elferink RP, Jansen PL, Chowdhury JR (1992b) Sequence of exons and the flanking regions of human bilirubin-UDP-glucuronosyltransferase gene complex and identification of a genetic mutation in a patient with Crigler-Najjar syndrome, type I. Hepatology 15: 941-7

Bosma PJ, Seppen J, Goldhoorn B, Bakker C, Oude Elferink RP, Chowdhury JR, Chowdhury NR, Jansen PL (1994) Bilirubin UDP-glucuronosyltransferase 1 is the only relevant bilirubin glucuronidating isoform in man. J Biol Chem 269: 17960-4

Branchereau S, Ferry N, Myara A, Sato H, Kowai O, Trivin F, Houssin D, Danos O, Heard J (1993) [Correction of bilirubin glucuronyl transferase in Gunn rats by gene transfer in the liver using retroviral vectors]. Chirurgie 119: 642-8

Bray GL, Gomperts ED, Courter S, Gruppo R, Gordon EM, Manco-Johnson M, Shapiro A, Scheibel E, White G, 3rd, Lee M (1994) A multicenter study of recombinant factor VIII (recombinate): safety, efficacy, and inhibitor risk in previously untreated patients with hemophilia A. The Recombinate Study Group. Blood 83: 2428-35

Briand P, Francois B, Rabier D, Cathelineau L (1982) Ornithine transcarbamylase deficiencies in human males. Kinetic and immunochemical classification. Biochim Biophys Acta 704: 100-6

Brouns SJ, Jore MM, Lundgren M, Westra ER, Slijkhuis RJ, Snijders AP, Dickman MJ, Makarova KS, Koonin EV, van der Oost J (2008) Small CRISPR RNAs guide antiviral defense in prokaryotes. Science 321: 960-4

Brunetti-Pierri N, Lee B (2005) Gene therapy for inborn errors of liver metabolism. Mol Genet Metab 86: 13-24

Calcedo R, Wilson JM (2016) AAV Natural Infection Induces Broad Cross-Neutralizing Antibody Responses to Multiple AAV Serotypes in Chimpanzees. Hum Gene Ther Clin Dev 27: 79-82

Caldovic L, Abdikarim I, Narain S, Tuchman M, Morizono H (2015) Genotype-Phenotype Correlations in Ornithine Transcarbamylase Deficiency: A Mutation Update. J Genet Genomics 42: 181-94

Canu G, Minucci A, Zuppi C, Capoluongo E (2013) Gilbert and Crigler Najjar syndromes: an update of the UDP-glucuronosyltransferase 1A1 (UGT1A1) gene mutation database. Blood Cells Mol Dis 50: 273-80

Carroll D, Beumer KJ (2014) Genome engineering with TALENs and ZFNs: repair pathways and donor design. Methods 69: 137-41

Ceccaldi R, Rondinelli B, D'Andrea AD (2016) Repair Pathway Choices and Consequences at the Double-Strand Break. Trends Cell Biol 26: 52-64

Chandler RJ, LaFave MC, Varshney GK, Trivedi NS, Carrillo-Carrasco N, Senac JS, Wu W, Hoffmann V, Elkahloun AG, Burgess SM, Venditti CP (2015) Vector design influences hepatic genotoxicity after adeno-associated virus gene therapy. J Clin Invest 125: 870-80

Chen S, Yueh MF, Bigo C, Barbier O, Wang K, Karin M, Nguyen N, Tukey RH (2013) Intestinal glucuronidation protects against chemotherapy-induced toxicity by irinotecan (CPT-11). Proc Natl Acad Sci U S A 110: 19143-8

Chirmule N, Xiao W, Truneh A, Schnell MA, Hughes JV, Zoltick P, Wilson JM (2000) Humoral immunity to adeno-associated virus type 2 vectors following administration to murine and nonhuman primate muscle. J Virol 74: 2420-5

Chowdhury NR, Hays RM, Bommineni VR, Franki N, Chowdhury JR, Wu CH, Wu GY (1996) Microtubular disruption prolongs the expression of human bilirubin-uridinediphosphoglucuronate-glucuronosyltransferase-1 gene transferred into Gunn rat livers. J Biol Chem 271: 2341-6

Christian M, Cermak T, Doyle EL, Schmidt C, Zhang F, Hummel A, Bogdanove AJ, Voytas DF (2010) Targeting DNA double-strand breaks with TAL effector nucleases. Genetics 186: 757-61

Chu VT, Weber T, Wefers B, Wurst W, Sander S, Rajewsky K, Kuhn R (2015) Increasing the efficiency of homology-directed repair for CRISPR-Cas9-induced precise gene editing in mammalian cells. Nat Biotechnol 33: 543-8

Clarke DJ, Moghrabi N, Monaghan G, Cassidy A, Boxer M, Hume R, Burchell B (1997) Genetic defects of the UDP-glucuronosyltransferase-1 (UGT1) gene that cause familial non-haemolytic unconjugated hyperbilirubinaemias. Clin Chim Acta 266: 63-74

Conlee JW, Shapiro SM (1997) Development of cerebellar hypoplasia in jaundiced Gunn rats: a quantitative light microscopic analysis. Acta Neuropathol 93: 450-60

Coppoletta JM, Wolbach SB (1933) Body Length and Organ Weights of Infants and Children: A Study of the Body Length and Normal Weights of the More Important Vital Organs of the Body between Birth and Twelve Years of Age. Am J Pathol 9: 55-70

Crigler JF, Jr., Najjar VA (1952) Congenital familial nonhemolytic jaundice with kernicterus; a new clinical entity. AMA Am J Dis Child 83: 259-60

Cunniff C, Carmack JL, Kirby RS, Fiser DH (1995) Contribution of heritable disorders to mortality in the pediatric intensive care unit. Pediatrics 95: 678-81

Cunningham SC, Dane AP, Spinoulas A, Alexander IE (2008) Gene Delivery to the Juvenile Mouse Liver Using AAV2/8 Vectors. Mol Ther 16: 1081-1088

Cunningham SC, Kok CY, Spinoulas A, Carpenter KH, Alexander IE (2013) AAV-encoded OTC activity persisting to adulthood following delivery to newborn spf(ash) mice is insufficient to prevent shRNA-induced hyperammonaemia. Gene Ther 20: 1184-7

Cunningham SC, Spinoulas A, Carpenter KH, Wilcken B, Kuchel PW, Alexander IE (2009) AAV2/8-mediated correction of OTC deficiency is robust in adult but not neonatal Spf(ash) mice. Mol Ther 17: 1340-6

Daly TM, Ohlemiller KK, Roberts MS, Vogler CA, Sands MS (2001) Prevention of systemic clinical disease in MPS VII mice following AAV-mediated neonatal gene transfer. Gene Ther 8: 1291-8

Danko I, Jia Z, Zhang G (2004) Nonviral gene transfer into liver and muscle for treatment of hyperbilirubinemia in the gunn rat. Hum Gene Ther 15: 1279-86

Dobbs RH, Cremer RJ (1975) Phototherapy. Arch Dis Child 50: 833-6

Donsante A, Miller DG, Li Y, Vogler C, Brunt EM, Russell DW, Sands MS (2007) AAV vector integration sites in mouse hepatocellular carcinoma. Science 317: 477

Ehrenforth S, Kreuz W, Scharrer I, Linde R, Funk M, Gungor T, Krackhardt B, Kornhuber B (1992) Incidence of development of factor VIII and factor IX inhibitors in haemophiliacs. Lancet 339: 594-8

Emi Y, Ikushiro S, Iyanagi T (1995) Drug-responsive and tissue-specific alternative expression of multiple first exons in rat UDP-glucuronosyltransferase family 1 (UGT1) gene complex. J Biochem 117: 392-9

Erles K, Sebokova P, Schlehofer JR (1999) Update on the prevalence of serum antibodies (IgG and IgM) to adeno-associated virus (AAV). J Med Virol 59: 406-11

Erlinger S, Arias IM, Dhumeaux D (2014) Inherited disorders of bilirubin transport and conjugation: new insights into molecular mechanisms and consequences. Gastroenterology 146: 1625-38

Esvelt KM, Mali P, Braff JL, Moosburner M, Yaung SJ, Church GM (2013) Orthogonal Cas9 proteins for RNA-guided gene regulation and editing. Nat Methods 10: 1116-21

Fagiuoli S, Daina E, D'Antiga L, Colledan M, Remuzzi G (2013) Monogenic diseases that can be cured by liver transplantation. J Hepatol 59: 595-612

Fox IJ, Chowdhury JR, Kaufman SS, Goertzen TC, Chowdhury NR, Warkentin PI, Dorko K, Sauter BV, Strom SC (1998) Treatment of the Crigler-Najjar syndrome type I with hepatocyte transplantation. N Engl J Med 338: 1422-6

Friedland AE, Baral R, Singhal P, Loveluck K, Shen S, Sanchez M, Marco E, Gotta GM, Maeder ML, Kennedy EM, Kornepati AV, Sousa A, Collins MA, Jayaram H, Cullen BR, Bumcrot D (2015) Characterization of Staphylococcus aureus Cas9: a smaller Cas9 for all-in-one adeno-associated virus delivery and paired nickase applications. Genome Biol 16: 257

Fu Y, Foden JA, Khayter C, Maeder ML, Reyon D, Joung JK, Sander JD (2013) High-frequency off-target mutagenesis induced by CRISPR-Cas nucleases in human cells. Nat Biotechnol 31: 822-6

Fujiwara R, Nguyen N, Chen S, Tukey RH (2010) Developmental hyperbilirubinemia and CNS toxicity in mice humanized with the UDP glucuronosyltransferase 1 (UGT1) locus. Proc Natl Acad Sci U S A 107: 5024-9

Garby L, Lammert O, Kock KF, Thobo-Carlsen B (1993) Weights of brain, heart, liver, kidneys, and spleen in healthy and apparently healthy adult Danish subjects. Am J Hum Biol 5: 291-296

Garrick D, Fiering S, Martin DI, Whitelaw E (1998) Repeat-induced gene silencing in mammals. Nat Genet 18: 56-9

Gasiunas G, Siksnys V (2013) RNA-dependent DNA endonuclease Cas9 of the CRISPR system: Holy Grail of genome editing? Trends Microbiol 21: 562-7

George LA, Sullivan SK, Giermasz A, Rasko JEJ, Samelson-Jones BJ, Ducore J, Cuker A, Sullivan LM, Majumdar S, Teitel J, McGuinn CE, Ragni MV, Luk AY, Hui D, Wright JF, Chen Y, Liu Y, Wachtel K, Winters A, Tiefenbacher S et al. (2017) Hemophilia B Gene Therapy with a High-Specific-Activity Factor IX Variant. N Engl J Med 377: 2215-2227

Gombash Lampe SE, Kaspar BK, Foust KD (2014) Intravenous injections in neonatal mice. J Vis Exp: e52037

Gong QH, Cho JW, Huang T, Potter C, Gholami N, Basu NK, Kubota S, Carvalho S, Pennington MW, Owens IS, Popescu NC (2001) Thirteen UDPglucuronosyltransferase genes are encoded at the human UGT1 gene complex locus. Pharmacogenetics 11: 357-68

Guh S, Grosse SD, McAlister S, Kessler CM, Soucie JM (2012) Health care expenditures for Medicaid-covered males with haemophilia in the United States, 2008. Haemophilia 18: 276-83

Gunn CH (1938) HEREDITARY ACHOLURIC JAUNDICEin a New Mutant Strain of Rats. Journal of Heredity 29: 137-139

Gurlevik E, Schache P, Goez A, Kloos A, Woller N, Armbrecht N, Manns MP, Kubicka S, Kuhnel F (2013) Meganuclease-mediated virus self-cleavage facilitates tumor-specific virus replication. Mol Ther 21: 1738-48

Guschin DY, Waite AJ, Katibah GE, Miller JC, Holmes MC, Rebar EJ (2010) A rapid and general assay for monitoring endogenous gene modification. Methods Mol Biol 649: 247-56

Haagsma EB, Hagens VE, Schaapveld M, van den Berg AP, de Vries EG, Klompmaker IJ, Slooff MJ, Jansen PL (2001) Increased cancer risk after liver transplantation: a population-based study. J Hepatol 34: 84-91

Hagenbuch B, Meier PJ (2004) Organic anion transporting polypeptides of the OATP/ SLC21 family: phylogenetic classification as OATP/ SLCO superfamily, new nomenclature and molecular/functional properties. Pflugers Arch 447: 653-65

Hale CR, Zhao P, Olson S, Duff MO, Graveley BR, Wells L, Terns RM, Terns MP (2009) RNA-guided RNA cleavage by a CRISPR RNA-Cas protein complex. Cell 139: 945-56

Hansen K, Horslen S (2008) Metabolic liver disease in children. Liver Transpl 14: 713-33

Hendrie PC, Hirata RK, Russell DW (2003) Chromosomal integration and homologous gene targeting by replication-incompetent vectors based on the autonomous parvovirus minute virus of mice. J Virol 77: 13136-45

Hendrie PC, Russell DW (2005) Gene targeting with viral vectors. Mol Ther 12: 9-17

Herrero JI (2009) De novo malignancies following liver transplantation: impact and recommendations. Liver Transpl 15 Suppl 2: S90-4

Hodges PE, Rosenberg LE (1989) The spfash mouse: a missense mutation in the ornithine transcarbamylase gene also causes aberrant mRNA splicing. Proc Natl Acad Sci U S A 86: 4142-6

Hsu PD, Scott DA, Weinstein JA, Ran FA, Konermann S, Agarwala V, Li Y, Fine EJ, Wu X, Shalem O, Cradick TJ, Marraffini LA, Bao G, Zhang F (2013) DNA targeting specificity of RNA-guided Cas9 nucleases. Nat Biotechnol 31: 827-32

Huen MS, Lu LY, Liu DP, Huang JD (2007) Active transcription promotes single-stranded oligonucleotide mediated gene repair. Biochem Biophys Res Commun 353: 33-9

Inoue N, Dong R, Hirata RK, Russell DW (2001) Introduction of single base substitutions at homologous chromosomal sequences by adeno-associated virus vectors. Mol Ther 3: 526-30

Inoue N, Hirata RK, Russell DW (1999) High-fidelity correction of mutations at multiple chromosomal positions by adeno-associated virus vectors. J Virol 73: 7376-80

Iyanagi T, Emi Y, Ikushiro S (1998) Biochemical and molecular aspects of genetic disorders of bilirubin metabolism. Biochim Biophys Acta 1407: 173-84

Iyanagi T, Watanabe T, Uchiyama Y (1989) The 3-methylcholanthrene-inducible UDP-glucuronosyltransferase deficiency in the hyperbilirubinemic rat (Gunn rat) is caused by a -1 frameshift mutation. J Biol Chem 264: 21302-7

Jangi S, Otterbein L, Robson S (2013) The molecular basis for the immunomodulatory activities of unconjugated bilirubin. Int J Biochem Cell Biol 45: 2843-51

Jasin M (1996) Genetic manipulation of genomes with rare-cutting endonucleases. Trends Genet 12: 224-8

Jayathilaka K, Sheridan SD, Bold TD, Bochenska K, Logan HL, Weichselbaum RR, Bishop DK, Connell PP (2008) A chemical compound that stimulates the human homologous recombination protein RAD51. Proc Natl Acad Sci U S A 105: 15848-53

Jemnitz K, Heredi-Szabo K, Janossy J, Ioja E, Vereczkey L, Krajcsi P (2010) ABCC2/Abcc2: a multispecific transporter with dominant excretory functions. Drug Metab Rev 42: 402-36

Jia Z, Danko I (2005) Single hepatic venous injection of liver-specific naked plasmid vector expressing human UGT1A1 leads to long-term correction of hyperbilirubinemia and prevention of chronic bilirubin toxicity in Gunn rats. Hum Gene Ther 16: 985-95

Jinek M, Chylinski K, Fonfara I, Hauer M, Doudna JA, Charpentier E (2012) A programmable dual-RNA-guided DNA endonuclease in adaptive bacterial immunity. Science 337: 816-21

Johnson L, Sarmiento F, Blanc WA, Day R (1959) Kernicterus in rats with an inherited deficiency of glucuronyl transferase. AMA J Dis Child 97: 591-608

Kadakol A, Ghosh SS, Sappal BS, Sharma G, Chowdhury JR, Chowdhury NR (2000) Genetic lesions of bilirubin uridine-diphosphoglucuronate glucuronosyltransferase (UGT1A1) causing Crigler-Najjar and Gilbert syndromes: correlation of genotype to phenotype. Hum Mutat 16: 297-306

Kienstra KA, Freysdottir D, Gonzales NM, Hirschi KK (2007) Murine neonatal intravascular injections: modeling newborn disease. J Am Assoc Lab Anim Sci 46: 50-4

Kim S, Kim D, Cho SW, Kim J, Kim JS (2014) Highly efficient RNA-guided genome editing in human cells via delivery of purified Cas9 ribonucleoproteins. Genome Res 24: 1012-9

Kim YG, Chandrasegaran S (1994) Chimeric restriction endonuclease. Proc Natl Acad Sci U S A 91: 883-7

Kinosaki M, Masuko T, Sogawa K, Iyanagi T, Yamamoto T, Hashimoto Y, Fujii-Kuriyama Y (1993) Intracellular localization of UDP-glucuronosyltransferase expressed from the transfected cDNA in cultured cells. Cell Struct Funct 18: 41-51

Kobayashi H, Carbonaro D, Pepper K, Petersen D, Ge S, Jackson H, Shimada H, Moats R, Kohn DB (2005) Neonatal gene therapy of MPS I mice by intravenous injection of a lentiviral vector. Mol Ther 11: 776-89

Kren BT, Parashar B, Bandyopadhyay P, Chowdhury NR, Chowdhury JR, Steer CJ (1999) Correction of the UDP-glucuronosyltransferase gene defect in the gunn rat model of crigler-najjar syndrome type I with a chimeric oligonucleotide. Proc Natl Acad Sci U S A 96: 10349-54

Labrune P, Myara A, Hadchouel M, Ronchi F, Bernard O, Trivin F, Chowdhury NR, Chowdhury JR, Munnich A, Odievre M (1994) Genetic heterogeneity of Crigler-Najjar syndrome type I: a study of 14 cases. Hum Genet 94: 693-7

Lachmann RH (2011) Enzyme replacement therapy for lysosomal storage diseases. Curr Opin Pediatr 23: 588-93

Lanpher B, Brunetti-Pierri N, Lee B (2006) Inborn errors of metabolism: the flux from Mendelian to complex diseases. Nat Rev Genet 7: 449-60

Li H, Durbin R (2009) Fast and accurate short read alignment with Burrows-Wheeler transform. Bioinformatics 25: 1754-60

Li H, Haurigot V, Doyon Y, Li T, Wong SY, Bhagwat AS, Malani N, Anguela XM, Sharma R, Ivanciu L, Murphy SL, Finn JD, Khazi FR, Zhou S, Paschon DE, Rebar EJ, Bushman FD, Gregory PD, Holmes MC, High KA (2011) In vivo genome editing restores haemostasis in a mouse model of haemophilia. Nature 475: 217-21

Li L, Wu LP, Chandrasegaran S (1992) Functional domains in Fok I restriction endonuclease. Proc Natl Acad Sci U S A 89: 4275-9

Li Q, Murphree SS, Willer SS, Bolli R, French BA (1998) Gene therapy with bilirubin-UDP-glucuronosyltransferase in the Gunn rat model of Crigler-Najjar syndrome type 1. Hum Gene Ther 9: 497-505

Liang X, Potter J, Kumar S, Zou Y, Quintanilla R, Sridharan M, Carte J, Chen W, Roark N, Ranganathan S, Ravinder N, Chesnut JD (2015) Rapid and highly efficient mammalian cell engineering via Cas9 protein transfection. J Biotechnol 208: 44-53

Lieber MR (2010) The mechanism of double-strand DNA break repair by the nonhomologous DNA end-joining pathway. Annu Rev Biochem 79: 181-211

London IM, West R, Shemin D, Rittenberg D (1950) On the origin of bile pigment in normal man. J Biol Chem 184: 351-8

Lusher JM, Arkin S, Abildgaard CF, Schwartz RS (1993) Recombinant factor VIII for the treatment of previously untreated patients with hemophilia A. Safety, efficacy, and development of inhibitors. Kogenate Previously Untreated Patient Study Group. N Engl J Med 328: 453-9

Mackenzie PI, Owens IS, Burchell B, Bock KW, Bairoch A, Belanger A, Fournel-Gigleux S, Green M, Hum DW, Iyanagi T, Lancet D, Louisot P, Magdalou J, Chowdhury JR, Ritter JK, Schachter H, Tephly TR, Tipton KF, Nebert DW (1997) The UDP glycosyltransferase gene superfamily: recommended nomenclature update based on evolutionary divergence. Pharmacogenetics 7: 255-69

Maeder ML, Gersbach CA (2016) Genome-editing Technologies for Gene and Cell Therapy. Mol Ther 24: 430-46

Maisels MJ, McDonagh AF (2008) Phototherapy for neonatal jaundice. N Engl J Med 358: 920-8

Makarova KS, Haft DH, Barrangou R, Brouns SJ, Charpentier E, Horvath P, Moineau S, Mojica FJ, Wolf YI, Yakunin AF, van der Oost J, Koonin EV (2011) Evolution and classification of the CRISPR-Cas systems. Nat Rev Microbiol 9: 467-77

Mali P, Aach J, Stranges PB, Esvelt KM, Moosburner M, Kosuri S, Yang L, Church GM (2013) CAS9 transcriptional activators for target specificity screening and paired nickases for cooperative genome engineering. Nat Biotechnol 31: 833-8

Mannucci PM, Tuddenham EG (2001) The hemophilias--from royal genes to gene therapy. N Engl J Med 344: 1773-9

Mano M, Ippodrino R, Zentilin L, Zacchigna S, Giacca M (2015) Genome-wide RNAi screening identifies host restriction factors critical for in vivo AAV transduction. Proc Natl Acad Sci U S A 112: 11276-81

Maruyama T, Dougan SK, Truttmann MC, Bilate AM, Ingram JR, Ploegh HL (2015) Increasing the efficiency of precise genome editing with CRISPR-Cas9 by inhibition of nonhomologous end joining. Nat Biotechnol 33: 538-42

McKenna A, Hanna M, Banks E, Sivachenko A, Cibulskis K, Kernytsky A, Garimella K, Altshuler D, Gabriel S, Daly M, DePristo MA (2010) The Genome Analysis Toolkit: a MapReduce framework for analyzing next-generation DNA sequencing data. Genome Res 20: 1297-303

McMillan CW, Shapiro SS, Whitehurst D, Hoyer LW, Rao AV, Lazerson J (1988) The natural history of factor VIII:C inhibitors in patients with hemophilia A: a national cooperative study. II. Observations on the initial development of factor VIII:C inhibitors. Blood 71: 344-8

Meech R, Mackenzie PI (1997) UDP-glucuronosyltransferase, the role of the amino terminus in dimerization. J Biol Chem 272: 26913-7

Memon N, Weinberger BI, Hegyi T, Aleksunes LM (2016) Inherited disorders of bilirubin clearance. Pediatr Res 79: 378-86

Merienne N, Vachey G, de Longprez L, Meunier C, Zimmer V, Perriard G, Canales M, Mathias A, Herrgott L, Beltraminelli T, Maulet A, Dequesne T, Pythoud C, Rey M, Pellerin L, Brouillet E, Perrier AL, du Pasquier R, Deglon N (2017) The Self-Inactivating KamiCas9 System for the Editing of CNS Disease Genes. Cell Rep 20: 2980-2991

Miller DG, Wang PR, Petek LM, Hirata RK, Sands MS, Russell DW (2006) Gene targeting in vivo by adeno-associated virus vectors. Nat Biotechnol 24: 1022-6

Mingozzi F, Liu YL, Dobrzynski E, Kaufhold A, Liu JH, Wang Y, Arruda VR, High KA, Herzog RW (2003) Induction of immune tolerance to coagulation factor IX antigen by in vivo hepatic gene transfer. J Clin Invest 111: 1347-56

Miranda PS, Bosma PJ (2009) Towards liver-directed gene therapy for Crigler-Najjar syndrome. Curr Gene Ther 9: 72-82

Moghrabi N, Clarke DJ, Burchell B, Boxer M (1993) Cosegregation of intragenic markers with a novel mutation that causes Crigler-Najjar syndrome type I: implication in carrier detection and prenatal diagnosis. Am J Hum Genet 53: 722-9

Mojica FJ, Diez-Villasenor C, Garcia-Martinez J, Almendros C (2009) Short motif sequences determine the targets of the prokaryotic CRISPR defence system. Microbiology 155: 733-40

Montenegro-Miranda PS, Paneda A, ten Bloemendaal L, Duijst S, de Waart DR, Gonzalez-Aseguinolaza G, Bosma PJ (2013) Adeno-associated viral vector serotype 5 poorly transduces liver in rat models. PLoS One 8: e82597

Montenegro-Miranda PS, Pichard V, Aubert D, Ten Bloemendaal L, Duijst S, de Waart DR, Ferry N, Bosma PJ (2014) In the rat liver, Adenoviral gene transfer efficiency is comparable to AAV. Gene Ther 21: 168-74

Nakai H, Wu X, Fuess S, Storm TA, Munroe D, Montini E, Burgess SM, Grompe M, Kay MA (2005) Large-scale molecular characterization of adeno-associated virus vector integration in mouse liver. J Virol 79: 3606-14

Nathwani AC, Cochrane M, McIntosh J, Ng CY, Zhou J, Gray JT, Davidoff AM (2009) Enhancing transduction of the liver by adeno-associated viral vectors. Gene Ther 16: 60-9

Nathwani AC, Gray JT, McIntosh J, Ng CY, Zhou J, Spence Y, Cochrane M, Gray E, Tuddenham EG, Davidoff AM (2007) Safe and efficient transduction of the liver after peripheral vein infusion of self-complementary AAV vector results in stable therapeutic expression of human FIX in nonhuman primates. Blood 109: 1414-21

Nathwani AC, Reiss UM, Tuddenham EG, Rosales C, Chowdary P, McIntosh J, Della Peruta M, Lheriteau E, Patel N, Raj D, Riddell A, Pie J, Rangarajan S, Bevan D, Recht M, Shen YM, Halka KG, Basner-Tschakarjan E, Mingozzi F, High KA et al. (2014) Long-term safety and efficacy of factor IX gene therapy in hemophilia B. N Engl J Med 371: 1994-2004

Nathwani AC, Rosales C, McIntosh J, Rastegarlari G, Nathwani D, Raj D, Nawathe S, Waddington SN, Bronson R, Jackson S, Donahue RE, High KA, Mingozzi F, Ng CY, Zhou J, Spence Y, McCarville MB, Valentine M, Allay J, Coleman J et al. (2011a) Long-term safety and efficacy following systemic administration of a self-complementary AAV vector encoding human FIX pseudotyped with serotype 5 and 8 capsid proteins. Mol Ther 19: 876-85

Nathwani AC, Tuddenham EG, Rangarajan S, Rosales C, McIntosh J, Linch DC, Chowdary P, Riddell A, Pie AJ, Harrington C, O'Beirne J, Smith K, Pasi J, Glader B, Rustagi P, Ng CY, Kay MA, Zhou J, Spence Y, Morton CL et al. (2011b) Adenovirus-associated virus vector-mediated gene transfer in hemophilia B. N Engl J Med 365: 2357-65

Nguyen N, Bonzo JA, Chen S, Chouinard S, Kelner MJ, Hardiman G, Belanger A, Tukey RH (2008) Disruption of the ugt1 locus in mice resembles human Crigler-Najjar type I disease. J Biol Chem 283: 7901-11

Nguyen TH, Aubert D, Bellodi-Privato M, Flageul M, Pichard V, Jaidane-Abdelghani Z, Myara A, Ferry N (2007) Critical assessment of lifelong phenotype correction in hyperbilirubinemic Gunn rats after retroviral mediated gene transfer. Gene Ther 14: 1270-7

Nguyen TH, Bellodi-Privato M, Aubert D, Pichard V, Myara A, Trono D, Ferry N (2005) Therapeutic lentivirus-mediated neonatal in vivo gene therapy in hyperbilirubinemic Gunn rats. Mol Ther 12: 852-9

Nygaard S, Barzel A, Haft A, Major A, Finegold M, Kay MA, Grompe M (2016) A universal system to select gene-modified hepatocytes in vivo. Sci Transl Med 8: 342ra79

Pankowicz FP, Barzi M, Legras X, Hubert L, Mi T, Tomolonis JA, Ravishankar M, Sun Q, Yang D, Borowiak M, Sumazin P, Elsea SH, Bissig-Choisat B, Bissig KD (2016) Reprogramming metabolic pathways in vivo with CRISPR/Cas9 genome editing to treat hereditary tyrosinaemia. Nat Commun 7: 12642

Paques F, Duchateau P (2007) Meganucleases and DNA double-strand break-induced recombination: perspectives for gene therapy. Curr Gene Ther 7: 49-66

Parekh-Olmedo H, Ferrara L, Brachman E, Kmiec EB (2005) Gene therapy progress and prospects: targeted gene repair. Gene Ther 12: 639-46

Pattanayak V, Lin S, Guilinger JP, Ma E, Doudna JA, Liu DR (2013) High-throughput profiling of off-target DNA cleavage reveals RNA-programmed Cas9 nuclease specificity. Nat Biotechnol 31: 839-43

Paulk NK, Loza LM, Finegold MJ, Grompe M (2012) AAV-mediated gene targeting is significantly enhanced by transient inhibition of nonhomologous end joining or the proteasome in vivo. Hum Gene Ther 23: 658-65

Paulk NK, Wursthorn K, Wang Z, Finegold MJ, Kay MA, Grompe M (2010) Adeno-associated virus gene repair corrects a mouse model of hereditary tyrosinemia in vivo. Hepatology 51: 1200-8

Petris G, Casini A, Montagna C, Lorenzin F, Prandi D, Romanel A, Zasso J, Conti L, Demichelis F, Cereseto A (2017) Hit and go CAS9 delivered through a lentiviral based self-limiting circuit. Nat Commun 8: 15334

Pett S, Mowat AP (1987) Crigler-Najjar syndrome types I and II. Clinical experience--King's College Hospital 1972-1978. Phenobarbitone, phototherapy and liver transplantation. Mol Aspects Med 9: 473-82

Poliard AM, Bernuau D, Tournier I, Legres LG, Schoevaert D, Feldmann G, Sala-Trepat JM (1986) Cellular analysis by in situ hybridization and immunoperoxidase of alpha-fetoprotein and albumin gene expression in rat liver during the perinatal period. J Cell Biol 103: 777-86

Porro F, Bortolussi G, Barzel A, De Caneva A, Iaconcig A, Vodret S, Zentilin L, Kay MA, Muro AF (2017) Promoterless gene targeting without nucleases rescues lethality of a Crigler-Najjar syndrome mouse model. EMBO Mol Med 9: 1346-1355

Ran FA, Cong L, Yan WX, Scott DA, Gootenberg JS, Kriz AJ, Zetsche B, Shalem O, Wu X, Makarova KS, Koonin EV, Sharp PA, Zhang F (2015) In vivo genome editing using Staphylococcus aureus Cas9. Nature 520: 186-91

Rangarajan S, Walsh L, Lester W, Perry D, Madan B, Laffan M, Yu H, Vettermann C, Pierce GF, Wong WY, Pasi KJ (2017) AAV5-Factor VIII Gene Transfer in Severe Hemophilia A. N Engl J Med 377: 2519-2530

Ritter JK, Chen F, Sheen YY, Tran HM, Kimura S, Yeatman MT, Owens IS (1992a) A novel complex locus UGT1 encodes human bilirubin, phenol, and other UDP-glucuronosyltransferase isozymes with identical carboxyl termini. J Biol Chem 267: 3257-61

Ritter JK, Yeatman MT, Ferreira P, Owens IS (1992b) Identification of a genetic alteration in the code for bilirubin UDP-glucuronosyltransferase in the UGT1 gene complex of a Crigler-Najjar type I patient. J Clin Invest 90: 150-5

Riviere J, Hauer J, Poirot L, Brochet J, Souque P, Mollier K, Gouble A, Charneau P, Fischer A, Paques F, de Villartay JP, Cavazzana M (2014) Variable correction of Artemis deficiency by I-Sce1-meganuclease-assisted homologous recombination in murine hematopoietic stem cells. Gene Ther 21: 529-32

Rodkey FL (1965) Direct Spectrophotometric Determination of Albumin in Human Serum. Clin Chem 11: 478-87

Ronzitti G, Bortolussi G, van Dijk R, Collaud F, Charles S, Leborgne C, Vidal P, Martin S, Gjata B, Sola MS, van Wittenberghe L, Vignaud A, Veron P, Bosma PJ, Muro AF, Mingozzi F (2016) A translationally optimized AAV-UGT1A1 vector drives safe and long-lasting correction of Crigler-Najjar syndrome. Mol Ther Methods Clin Dev 3: 16049

Rouet P, Smih F, Jasin M (1994) Expression of a site-specific endonuclease stimulates homologous recombination in mammalian cells. Proc Natl Acad Sci U S A 91: 6064-8

Russell DW, Hirata RK (1998) Human gene targeting by viral vectors. Nat Genet 18: 325-30

Russell DW, Kay MA (1999) Adeno-associated virus vectors and hematology. Blood 94: 864-74

Sadelain M, Papapetrou EP, Bushman FD (2011) Safe harbours for the integration of new DNA in the human genome. Nat Rev Cancer 12: 51-8

Schmid R, McDonagh AF (1975) The enzymatic formation of bilirubin. Ann N Y Acad Sci 244: 533-52

Schwank G, Koo BK, Sasselli V, Dekkers JF, Heo I, Demircan T, Sasaki N, Boymans S, Cuppen E, van der Ent CK, Nieuwenhuis EE, Beekman JM, Clevers H (2013) Functional repair of CFTR by CRISPR/Cas9 in intestinal stem cell organoids of cystic fibrosis patients. Cell Stem Cell 13: 653-8

Schwartz RS, Abildgaard CF, Aledort LM, Arkin S, Bloom AL, Brackmann HH, Brettler DB, Fukui H, Hilgartner MW, Inwood MJ, et al. (1990) Human recombinant DNA-derived antihemophilic factor (factor VIII) in the treatment of hemophilia A. recombinant Factor VIII Study Group. N Engl J Med 323: 1800-5

Seppen J, Bakker C, de Jong B, Kunne C, van den Oever K, Vandenberghe K, de Waart R, Twisk J, Bosma P (2006) Adeno-associated virus vector serotypes mediate sustained correction of bilirubin UDP glucuronosyltransferase deficiency in rats. Mol Ther 13: 1085-92

Seppen J, Bosma PJ, Goldhoorn BG, Bakker CT, Chowdhury JR, Chowdhury NR, Jansen PL, Oude Elferink RP (1994) Discrimination between Crigler-Najjar type I and II by expression of mutant bilirubin uridine diphosphate-glucuronosyltransferase. J Clin Invest 94: 2385-91

Sharma R, Anguela XM, Doyon Y, Wechsler T, DeKelver RC, Sproul S, Paschon DE, Miller JC, Davidson RJ, Shivak D, Zhou S, Rieders J, Gregory PD, Holmes MC, Rebar EJ, High

KA (2015) In vivo genome editing of the albumin locus as a platform for protein replacement therapy. Blood 126: 1777-84

Shibata A, Jeggo PA (2014) DNA double-strand break repair in a cellular context. Clin Oncol (R Coll Radiol) 26: 243-9

Sinaasappel M, Jansen PL (1991) The differential diagnosis of Crigler-Najjar disease, types 1 and 2, by bile pigment analysis. Gastroenterology 100: 783-9

Sinkunas T, Gasiunas G, Waghmare SP, Dickman MJ, Barrangou R, Horvath P, Siksnys V (2013) In vitro reconstitution of Cascade-mediated CRISPR immunity in Streptococcus thermophilus. EMBO J 32: 385-94

Slaymaker IM, Gao L, Zetsche B, Scott DA, Yan WX, Zhang F (2016) Rationally engineered Cas9 nucleases with improved specificity. Science 351: 84-8

Sneitz N, Bakker CT, de Knegt RJ, Halley DJ, Finel M, Bosma PJ (2010) Crigler-Najjar syndrome in The Netherlands: identification of four novel UGT1A1 alleles, genotype-phenotype correlation, and functional analysis of 10 missense mutants. Hum Mutat 31: 52-9

Sorrentino D, Berk PD (1988) Mechanistic aspects of hepatic bilirubin uptake. Semin Liver Dis 8: 119-36

Srivastava M, Nambiar M, Sharma S, Karki SS, Goldsmith G, Hegde M, Kumar S, Pandey M, Singh RK, Ray P, Natarajan R, Kelkar M, De A, Choudhary B, Raghavan SC (2012) An inhibitor of nonhomologous end-joining abrogates double-strand break repair and impedes cancer progression. Cell 151: 1474-87

Stevenson DA, Carey JC (2004) Contribution of malformations and genetic disorders to mortality in a children's hospital. Am J Med Genet A 126A: 393-7

Strauss KA, Robinson DL, Vreman HJ, Puffenberger EG, Hart G, Morton DH (2006) Management of hyperbilirubinemia and prevention of kernicterus in 20 patients with Crigler-Najjar disease. Eur J Pediatr 165: 306-19

Tada K, Chowdhury NR, Neufeld D, Bosma PJ, Heard M, Prasad VR, Chowdhury JR (1998) Long-term reduction of serum bilirubin levels in Gunn rats by retroviral gene transfer in vivo. Liver Transpl Surg 4: 78-88

Tenhunen R, Marver HS, Schmid R (1968) The enzymatic conversion of heme to bilirubin by microsomal heme oxygenase. Proc Natl Acad Sci U S A 61: 748-55

Tenhunen R, Marver HS, Schmid R (1970) The enzymatic catabolism of hemoglobin: stimulation of microsomal heme oxygenase by hemin. J Lab Clin Med 75: 410-21

Tenhunen R, Ross ME, Marver HS, Schmid R (1970) Reduced nicotinamide-adenine dinucleotide phosphate dependent biliverdin reductase: partial purification and characterization. Biochemistry 9: 298-303

Tiribelli C, Ostrow JD (1993) New concepts in bilirubin chemistry, transport and metabolism: report of the Second International Bilirubin Workshop, April 9-11, 1992, Trieste, Italy. Hepatology 17: 715-36

Vajdic CM, van Leeuwen MT (2009) Cancer incidence and risk factors after solid organ transplantation. Int J Cancer 125: 1747-54

van der Wegen P, Louwen R, Imam AM, Buijs-Offerman RM, Sinaasappel M, Grosveld F, Scholte BJ (2006) Successful treatment of UGT1A1 deficiency in a rat model of Crigler-Najjar disease by intravenous administration of a liver-specific lentiviral vector. Mol Ther 13: 374-81

Vartak SV, Raghavan SC (2015) Inhibition of nonhomologous end joining to increase the specificity of CRISPR/Cas9 genome editing. FEBS J 282: 4289-94

Vasileva A, Jessberger R (2005) Precise hit: adeno-associated virus in gene targeting. Nat Rev Microbiol 3: 837-47

Vasquez KM, Narayanan L, Glazer PM (2000) Specific mutations induced by triplex-forming oligonucleotides in mice. Science 290: 530-3

Vitek L, Carey MC (2003) Enterohepatic cycling of bilirubin as a cause of 'black' pigment gallstones in adult life. Eur J Clin Invest 33: 799-810

Vodret S, Bortolussi G, Schreuder AB, Jasprova J, Vitek L, Verkade HJ, Muro AF (2015) Albumin administration prevents neurological damage and death in a mouse model of severe neonatal hyperbilirubinemia. Sci Rep 5: 16203

Vouillot L, Thelie A, Pollet N (2015) Comparison of T7E1 and surveyor mismatch cleavage assays to detect mutations triggered by engineered nucleases. G3 (Bethesda) 5: 407-15

Wang L, Wang H, Bell P, McMenamin D, Wilson JM (2012) Hepatic gene transfer in neonatal mice by adeno-associated virus serotype 8 vector. Hum Gene Ther 23: 533-9

White G, Shapiro A, Ragni M, Garzone P, Goodfellow J, Tubridy K, Courter S (1998) Clinical evaluation of recombinant factor IX. Semin Hematol 35: 33-8

White GC, 2nd, Courter S, Bray GL, Lee M, Gomperts ED (1997) A multicenter study of recombinant factor VIII (Recombinate) in previously treated patients with hemophilia A. The Recombinate Previously Treated Patient Study Group. Thromb Haemost 77: 660-7

White GC, 2nd, Rosendaal F, Aledort LM, Lusher JM, Rothschild C, Ingerslev J, Factor V, Factor IXS (2001) Definitions in hemophilia. Recommendation of the scientific subcommittee on factor VIII and factor IX of the scientific and standardization committee of the International Society on Thrombosis and Haemostasis. Thromb Haemost 85: 560

Wu Y, Liang D, Wang Y, Bai M, Tang W, Bao S, Yan Z, Li D, Li J (2013) Correction of a genetic disease in mouse via use of CRISPR-Cas9. Cell Stem Cell 13: 659-62

Wu Z, Asokan A, Samulski RJ (2006) Adeno-associated virus serotypes: vector toolkit for human gene therapy. Mol Ther 14: 316-27

Wu Z, Yang H, Colosi P (2010) Effect of genome size on AAV vector packaging. Mol Ther 18: 80-6

Xue W, Chen S, Yin H, Tammela T, Papagiannakopoulos T, Joshi NS, Cai W, Yang G, Bronson R, Crowley DG, Zhang F, Anderson DG, Sharp PA, Jacks T (2014) CRISPR-mediated direct mutation of cancer genes in the mouse liver. Nature 514: 380-4

Yang Y, Wang L, Bell P, McMenamin D, He Z, White J, Yu H, Xu C, Morizono H, Musunuru K, Batshaw ML, Wilson JM (2016) A dual AAV system enables the Cas9-mediated correction of a metabolic liver disease in newborn mice. Nat Biotechnol 34: 334-8

Yin H, Xue W, Chen S, Bogorad RL, Benedetti E, Grompe M, Koteliansky V, Sharp PA, Jacks T, Anderson DG (2014) Genome editing with Cas9 in adult mice corrects a disease mutation and phenotype. Nat Biotechnol 32: 551-3

Yohannan MD, Terry HJ, Littlewood JM (1983) Long term phototherapy in Crigler-Najjar syndrome. Arch Dis Child 58: 460-2

You L (2004) Steroid hormone biotransformation and xenobiotic induction of hepatic steroid metabolizing enzymes. Chem Biol Interact 147: 233-46

Zhang J, Rouillon C, Kerou M, Reeks J, Brugger K, Graham S, Reimann J, Cannone G, Liu H, Albers SV, Naismith JH, Spagnolo L, White MF (2012) Structure and mechanism of the CMR complex for CRISPR-mediated antiviral immunity. Mol Cell 45: 303-13

Università degli Studi di Ferrara

Sezioni

Dottorati di ricerca

Il tuo indirizzo e-mail

alessia.decaneva@student.unife.it

Oggetto:

Dichiarazione di conformità della tesi di Dottorato

Io sottoscritto Dott. (Cognome e Nome)

De Caneva Alessia

Nato a:

Udine

Provincia:

Udine

Il giorno:

04.11.1989

Avendo frequentato il Dottorato di Ricerca in:

Scienze Biomediche e Biotecnologiche

Ciclo di Dottorato

31

Titolo della tesi:

Coupling AAV-mediated promoterless gene-targeting to SaCas9 nuclease to efficiently correct liver metabolic diseases

Titolo della tesi (traduzione):

Sviluppo di una terapia di "gene targeting" per curare in modo permanente malattie metaboliche del fegato mediante la combinazione delle tecnologie GeneRide e CRISPR/SaCas9

Tutore: Prof. (Cognome e Nome)

Muro Andrés

Settore Scientifico Disciplinare (S.S.D.)

BIO/10

Parole chiave della tesi (max 10):

Gene editing; CRISPR/SaCas9; AAV vectors; liver metabolic disorders; pediatric diseases; homology directed repair; Crigler-Najjar syndrome

Consapevole, dichiara

CONSAPEVOLE: (1) del fatto che in caso di dichiarazioni mendaci, oltre alle sanzioni previste dal codice penale e dalle Leggi speciali per l'ipotesi di falsità in atti ed uso di atti falsi, decade fin

dall'inizio e senza necessità di alcuna formalità dai benefici conseguenti al provvedimento emanato sulla base di tali dichiarazioni; (2) dell'obbligo per l'Università di provvedere al deposito di legge delle tesi di dottorato al fine di assicurarne la conservazione e la consultabilità da parte di terzi; (3) della procedura adottata dall'Università di Ferrara ove si richiede che la tesi sia consegnata dal dottorando in 2 copie, di cui una in formato cartaceo e una in formato pdf non modificabile su idonei supporti (CD-ROM, DVD) secondo le istruzioni pubblicate sul sito : http://www.unife.it/studenti/dottorato alla voce ESAME FINALE – disposizioni e modulistica; (4) del fatto che l'Università, sulla base dei dati forniti, archivierà e renderà consultabile in rete il testo completo della tesi di dottorato di cui alla presente dichiarazione attraverso l'Archivio istituzionale ad accesso aperto "EPRINTS.unife.it" oltre che attraverso i Cataloghi delle Biblioteche Nazionali Centrali di Roma e Firenze. DICHIARO SOTTO LA MIA RESPONSABILITA': (1) che la copia della tesi depositata presso l'Università di Ferrara in formato cartaceo è del tutto identica a quella presentata in formato elettronico (CD-ROM, DVD), a quelle da inviare ai Commissari di esame finale e alla copia che produrrà in seduta d'esame finale. Di conseguenza va esclusa qualsiasi responsabilità dell'Ateneo stesso per quanto riguarda eventuali errori, imprecisioni o omissioni nei contenuti della tesi; (2) di prendere atto che la tesi in formato cartaceo è l'unica alla quale farà riferimento l'Università per rilasciare, a mia richiesta, la dichiarazione di conformità di eventuali copie. PER ACCETTAZIONE DI QUANTO SOPRA RIPORTATO

Dichiarazione per embargo

12 mesi

Richiesta motivata embargo

1. Tesi in corso di pubblicazione

Liberatoria consultazione dati Eprints

Consapevole del fatto che attraverso l'Archivio istituzionale ad accesso aperto "EPRINTS.unife.it" saranno comunque accessibili i metadati relativi alla tesi (titolo, autore, abstract, ecc.)

Firma del dottorando

Ferrara, li 24.01.2019 (data) Firma del Dottorando

Firma del Tutore

Visto: Il Tutore Si approva Firma del Tutore